Aston University

Some pages of this thesis may have been removed for copyright restrictions.

If you have discovered material in Aston Research Explorer which is unlawful e.g. breaches copyright, (either yours or that of a third party) or any other law, including but not limited to those relating to patent, trademark, confidentiality, data protection, obscenity, defamation, libel, then please read our Takedown policy and contact the service immediately (openaccess@aston.ac.uk)

DEVELOPMENT AND EVALUATION OF AN ION INDUCED X-RAY EMISSION SYSTEM FOR THE ANALYSIS OF LIGHT AND MEDIUM WEIGHT ELEMENTS

JOGINDER SINGH PHULL

Doctor of Philosophy

THE UNIVERSITY OF ASTON IN BIRMINGHAM

1988

~~October 1987~~

This copy of the thesis has been supplied on condition that anyone who consults it is understood to recognise that its copyright rests with the author and that no quotation from the thesis and no information derived from it may be published without the author's prior, written consent.

THE UNIVERSITY OF ASTON IN BIRMINGHAM

DEVELOPMENT AND EVALUATION OF AN ION INDUCED X-RAY EMISSION SYSTEM FOR THE ANALYSES OF LIGHT AND MEDIUM WEIGHT ELEMENTS

by
Joginder Singh Phull

Submitted for the Degree of
Doctor of Philosophy
OCTOBER 1987

SUMMARY

The present work describes the development of a proton induced X-ray emission (PIXE) analysis system, especially designed and built for routine quantitative multi-elemental analysis of a large number of samples. The historical and general developments of the analytical technique and the physical processes involved are discussed.

The philosophy, design, constructional details and evaluation of a versatile vacuum chamber, an automatic multi-sample changer, an on-demand beam pulsing system and ion beam current monitoring facility are described.

The system calibration using thin standard foils of Si, P, S, Cl, K, Ca, Ti, V, Fe, Cu, Ga, Ge, Rb, Y and Mo was undertaken at proton beam energies of 1 to 3 MeV in steps of 0.5 MeV energy and compared with theoretical calculations. An independent calibration check using bovine liver Standard Reference Material was performed.

The minimum detectable limits have been experimentally determined at detector positions of 90^{0} and 135^{0} with respect to the incident beam for the above range of proton energies as a function of atomic number Z. The system has detection limits of typically 10^{-7} to 10^{-9}g for elements $14<Z<42$ for $10\mu C$ of charge.

Computer programmes have been written for data analysis and calculations of areal density of thin foils using Rutherford backscattering data.

Amniotic fluid samples supplied by South Sefton Health Authority were successfully analysed for their low base line elemental concentrations. A pre-concentration technique developed for this work is described.

In conclusion the findings of this work are discussed with suggestions for further work.

KEYWORDS

Proton Induced X-rays, PIXE system, Calibration, Minimum detectable limits, Amniotic fluids.

Dedicated

to

My Wife and Family

ACKNOWLEDGEMENTS

I am indebted to my academic supervisor, Dr D. Crumpton for his guidance, encouragement and useful discussions throughout this work and to my associate supervisor Dr P.E. Francois for his invaluable advice and help. The head of department, Professor J.E. Flood, Emeritus Professor S.E. Hunt, Emeritus Professor W.E.J. Neal and Dr N.W. Grimes are thanked for their support of this work. Professor T. Mulvey is thanked for his constant encouragement and interest. Members of the PIXE group are thanked for their assistance and companionship.

The staff at the Birmingham Radiation Centre are thanked in particular Dr L.G. Earwaker and Dr R.S. Sokhi for being most helpful.

I would like to express my appreciation to the following persons: my son Sukhvinder for helping me type this thesis; Narsim Murthy for assistance with the AAS analyses; Barry Brooks for the production of the photographs; Beverley Parker and Parvinder Sihra for expertly drafting the figures and drawings.

The University of Aston is acknowledged for funding this research work.

Finally I would like to thank my wife and family for their un-ending support and having to put up with my midnight oil burning.

CONTENTS

TABLES

FIGURES

CHAPTER II

CHAPTER III

CHAPTER I

INTRODUCTION.

Ion-induced X-ray emission involves the removal of electrons from the inner shells of atoms, followed by the rapid de-excitation of the excited atoms to lower energy states through the emission of radiation. This emission, except for the lightest elements, is in the X-ray region of the electromagnetic spectrum. Since atoms of each element have unique atomic levels, the observation of the emitted X-rays forms a method of identification of the elements present in a specimen.

The inner shell ionization of the atoms in any sample to be analysed can be brought about by charged particles such as electrons, protons, other heavy ions or photons. The latter technique is called X-ray fluorescence emission. Most of the applied work in ion-excited X-ray emission has been involved with protons as projectiles. Protons being more massive than electrons produce far less bremsstrahlung resulting in a better signal-to-noise ratio. However interaction with sample material of protons of energies greater than 3 MeV and heavy ions may produce γ-radiations which gives an undesirable continuous Compton

distribution in the detector. Thus at present 1-3 MeV protons are generally considered more useful as regards their analytical capabilities. Hence throughout the present work, the discussion is concentrated upon proton induced X-ray emission (PIXE).

PIXE exhibits some very desirable features sought after by analysts seeking an ideal elemental analysis technique. Among the inherent features, are its;

(a) high sensitivity over a wide range of elements
(b) simultaneous multi-elemental analysis in a single run
(c) non-destructive method able to work with a very small quantities of material
(d) possibility of high degree of automation.

The application of PIXE is hence most suitable for a situation calling for the simultaneous analysis of 15 - 20 elements in trace concentrations (ppm) in small samples, down to 1 μg and analysis of a large batch of samples, where conventional methods become rather laborious.

Consequently PIXE is becoming well established among analysts in almost every field, particularly in medical, biochemical and environmental studies, as a reliable and highly efficient analytical technique as

has been demonstrated at the proceedings of three international conferences on PIXE, published in Nuclear Instruments and Methods in Physics Research 1977, 1981 and 1984.

Quantitative analysis is generally performed using K X-rays for elements with atomic numbers $Z<55$, while L X-rays are used for heavier elements. Detection limits for trace elements are typically as low as 0.1 to 1 ppm and are nearly the same order of magnitude for all elements with atomic number greater than 14. The detection limit for light elements is governed by the absorption of the low energy characteristic X-rays from these elements in the beryllium window and the silicon dead layer of the Si(Li) detectors employed for the measurement of X-rays and their energy. The main factor which effects the analytical sensitivity of the PIXE system at the lower end of the energy spectrum, is the competing processes of bremsstrahlung background and the fall-off of the fluorescence yield. At high Z the decrease in sensitivity is mainly due to the lower X-ray cross sections. However, with due care and attention to the proper selection of the experimental parameters such as detector-target geometry and position, sample type and preparation, use of filters etc, the system sensitivity can be optimised. Generally one finds that PIXE sensitivity is more than adequate for an extensive range of important applications.

The availability of improved electronic data handling, processing and data storage systems at reasonable cost has contributed towards the high degree of automation of most PIXE analytical system.

The tireless effort made by so many workers in developing PIXE is reflected in the numerous publications found in many different journals, relating to the applications, capabilities and the limitations of this technique, Valkovic 1973; Folkmann 1975; Deconnick et al 1975; Johansson et al 1976; Campbell 1977; Valkovic 1980; Mitchell and Barfoot 1981; Khan and Crumpton 1981.

The over-riding impression left by the activity of the past two decades, since the early work of Johansson et al, 1970, is of a steady improvement in the quality of the experiments and the refinement of their interpretation. Different laboratories may well have different experimental arrangements but there is now a very good consensus on the grounds of technical requirements as to what constitutes an efficient analytical system.

The present work describes the development and evaluation of an experimental PIXE system specifically designed for routine analysis of a variety of samples.

The system was re-designed around an already existing set-up first installed in the mid-seventies at the Radiation Centre, Birmingham University.

The main object of the present development work was to:

(a) make routine analysis more cost effective
(b) improve the over all system sensitivity
(c) improve the accuracy of the beam current measurement
(d) include innovative features such as beam pulsing and RBS spectroscopy to improve system performance.

In this thesis the main historical developments are reviewed in chapter II. It gives some idea of the illustrious pedigree of PIXE and the span of time from the discovery of X-rays to the application of X-ray emission methods. For completeness the chapter also discusses, albeit very briefly, the various physical processes associated with the production of characteristic X-rays. Background production processes and its angular distribution are discussed in detail as the sensitivity of a system depends to a very large extent on the background continuum in the spectrum.

The development and deployment of the system is

described in chapter III. Economical factors are discussed, followed by the design description and constructional details of the scattering chamber, automatic sample changer, on-demand beam pulsing, beam monitoring and beam transportation systems. The detection of X-rays and detection systems together with general instrumentation and data acquisition systems are also described. Details of the vacuum system and external beam PIXE are included.

The complete system evaluation is discussed in chapter IV. System response is evaluated using thin targets and the calibration curves obtained are compared to the ones calculated for the previous system. Photon continuum background measured experimentally at 90^0 and 135^0 are compared to study angular distribution effects at these angles. System sensitivity for different elements at energies of 1.0, 1.2, 1.5, 2.0, 2.5 and 3.0 MeV are calculated. Improved target charge measurements are discussed.

Several interesting biomedical and general PIXE applications are outlined in Chapter V. Trace and major elements are surveyed in amniotic fluids. A different approach to sample concentration and preparation for amniotic fluid is described. The results of analysis are compared to those obtained using the Atomic Absorption technique and to those published recently by

other workers.

Finally conclusions and suggestions for further work are given in chapter VI.

CHAPTER II

2.1 Historical Developments and Physical Processes.

Before proceeding with historical developments and the processes involved in proton induced X-ray emission a brief experimental overview of the PIXE analysis technique is given as it may serve as a useful reference frame for the discussions which follow.

2.2 A Basic PIXE Arrangement.

Figure (2.1) shows a basic PIXE analysis system. A proton beam strikes a sample which is normally positioned at 45° to the beam. X-rays generated by the interaction of the incident particles with sample atoms are detected by a Si(Li) solid state detector, which converts the X-ray photons into electrical pulses. The train of pulses from the detector, after amplification, are coupled to a multi-channel analyser which sorts the pulses according to their heights (amplitude) into discrete energy channels , thus generating a spectrum of X-ray counts verses channel number as shown in Figure (2.2). The X-ray spectrum provides both qualitative and quantitative results. Since the channel number corresponds to the input pulse height voltage

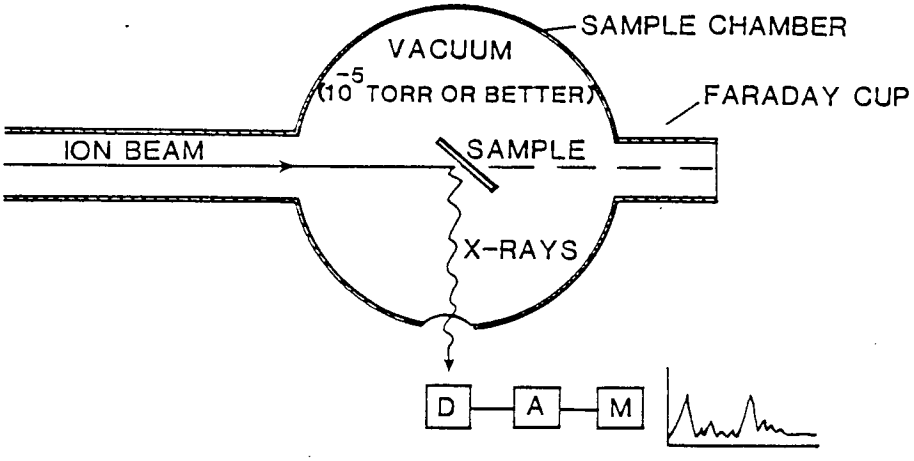

D X-RAY DETECTOR

A AMPLIFIER

M MULTI-CHANNEL ANALYSER

FIGURE 2.1

A Basic PIXE Arrangement

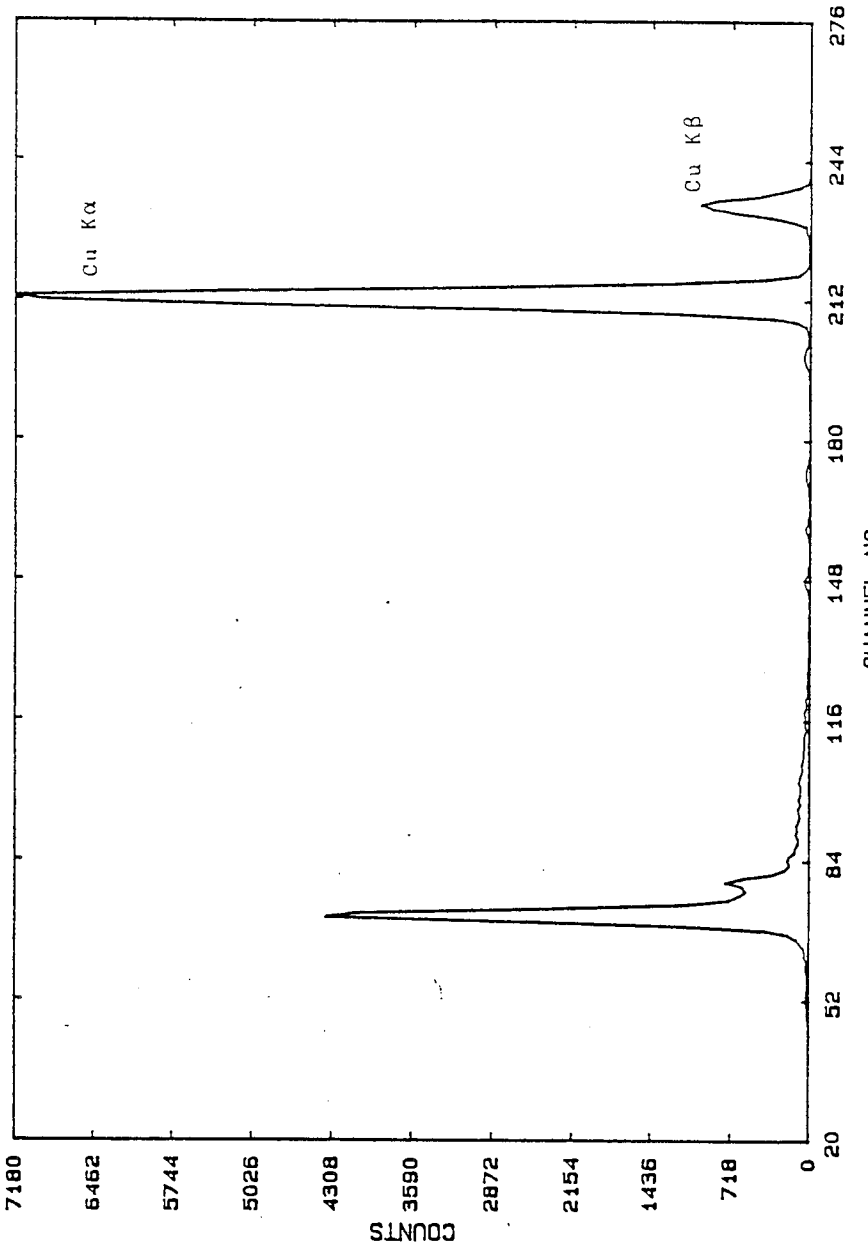

FIGURE 2.2 Typical Energy Spectrum for PIXE

and this voltage corresponds to the X-ray energy, one can thus determine the X-ray energy and thus the element. Quantitative data is readily obtained from the corresponding X-ray peak area if the total proton charge accumulated on the sample and systems efficiency calibrations are known.

2.3 General and Main Historical Developments.

In 1895, W.C.Rontgen while working with cathode-ray tubes, discovered a new electromagnetic radiation. He called his discovery of 'a new kind of ray', X-ray. A flurry of research activity followed this announcement and many investigators vigorously pursued the problem of "solving for X, the unknown in X-ray".

C.G.Barkla and his co-workers in 1901 made an important study of the characteristic X-rays. They devised the nomenclature used to this day and also identified the K and L X-rays. Chadwick 1912, first reported the use of charged particles to induce X-ray emission. He studied and identified the X-rays emitted from several elements, using alpha particles from a radium source.

Although development work in the field of X-rays progressed quite rapidly the basic understanding of the

physical origin and nature of X-rays was still unclear. It was not until Bohr 1913, proposed his theory of atomic spectra and atomic studies could some light be shed on the physical aspects of X-ray emission. He used with dramatic success, the quantum laws given by Planck and the atomic model of J.J.Thomson in explaining the theory of characteristics of X-ray spectra. His model of the hydrogen atom though no longer considered as very satisfactory also played a very useful role in the understanding of atomic spectra and coupled with Rutherford's work laid the foundations for later progress in X-ray theory. The early work on interpreting X-ray spectra in terms of Bohr's atom model is mainly due to Kossel, 1917.

The nature of X-rays too remained a mystery until 1912, since there was no satisfactory method of evaluating X-ray spectra in terms of wavelength or energy. Von Laue's experimental proof of the diffraction of X-rays by crystals, explained the fundamental nature of radiation. It also opened the door to a vast new area of crystallography and spectrometric analysis of elemental composition. Using crystal diffraction technique suggested by W.H.Bragg and W.L.Bragg, for obtaining X-ray spectrum, Moseley,1913, first related the atomic number of an element with the wavelength of the elements characteristic X-ray emission. He also demonstrated

that an X-ray spectrum of a brass sample was made up of the spectra of Cu and Zn elements, and thus established the basis of the elemental identification and analysis via its characteristic X-ray emission.

The use of characteristic X-rays for chemical analysis was studied by Van Hevesy and other workers during the 1920's. The existence of the element hafnium 72, predicted on the basis of Bohr's theory to be associated with zirconium, was confirmed by Coster and Van Hevesy, 1923, from the X-ray emission spectrum of Norwegian zircon sample. This work firmly established wavelength dispersive X-ray spectroscopy as an analytical technique in its own right.

As all ready indicated, although Chadwick, 1912, had demonstrated charged particle induced X-ray emission, it was about 25 years later that the subject featured again in the literature. Bothe & Franz, 1928, published their work on cross-section measurements for K, L and M-shell X-rays of the different elements. Again alpha particles from radioactive source were used for inducing X-rays, but they employed a Gieger counter to measure the X-ray yields.

X-ray emission by proton excitation, was first reported by Gerthsen and Russe, 1933. They used low energy protons between 30 to 150 keV to bombard Al and

Mg samples. Livingstone et al, 1937, made a quantitative study of X-rays produced by protons of 1.76 MeV energy incident on different samples. They drew the erroneous conclusion from their results that the background bremsstrahlung associated with electron excitation could be eliminated using protons, probably due to extremely low background levels normally associated with proton excitation compared to electron excitation. Cork, 1941, first reported the production of characteristic X-rays by deutron bombardment. He studied the yield of Cu K X-rays as a function of the exciting energy.

Another milestone in the history of ion induced X-ray detection technique was the perfection of scintillation counters as detectors for X-rays by Curran and Baker in 1944. Development of commercial instruments for X-ray photometry in chemical analysis in 1947 brought this technique out from the few research institutes to the general analytical laboratories round the world.

During the fifties the rapidly changing laboratory environment characterised by new applications and improved X-ray detection enabled L.S.Birks and coworkers to design a modern fluorescence spectrometer with Gieger, proportional and scintillation counters as detectors for quantitative

chemical analysis. In 1951 Castening and Gunier devised the first 'point by point' electron probe microanalyser.

Lewis et al, 1953, studied characteristic X-rays produced by protons of 1.7 to 3.0 MeV energy incident on different targets, using a NaI(Tl) scintillation detector to measure K and L radiation. In the same year C.Simane, 1953, used 750 keV protons to produce characteristic X-rays from Cu and confirmed the results previously obtained by Livingstone et al, 1937. Bernstein and Lewis, 1954, extended the energy range of protons from 1.5 to 4.25 MeV and presented a set of absolute cross-sections for X-ray production. Hansteen and Messelt, 1956, and later Messelt, 1958, contributed to the data on K-shell X-ray cross-sections for different elements at proton energies of 0.14 to 1.30 MeV. In the same year Merzbacher and Lewis, 1958, published their most referenced paper on the theoretical aspects of X-rays produced by charged particles.

Khan et al, 1966, used protons of 0.1 to 1.7 MeV energy to measure experimentally the X-ray cross sections. Christenseen et al, 1967, a year later also contributed to cross section data for 0.1 MeV protons.

The concept of proton induced X-ray emission as a

means of elemental analysis was reported by Birks et al, 1964. They studied proton excitation of characteristic X-rays for X-ray spectrochemical analysis and suggested that a considerable advantage could be obtained with proton excitation compared to electron excitation because of the reduction of background interference. It was experimentally shown by Johansson et al, 1970, that a combination of X-ray excitation by protons and detection by a silicon detector constitutes a powerful analytical method of high sensitivity. The simultaneous detection of 13 elements in a sixty minute analysis of a carbon foil exposed to air demonstrated the potential and sensitivity of the method. Watson et al, 1971, and Flocchini et al, 1972, showed that α-particles could also be used with advantage.

During the seventies proton induced X-ray emission analysis began commanding considerable interest, some 20 to 30 laboratories in the world became engaged in PIXE research. Apart from a very large number of important research papers, many in depth review articles were published which include those of Volkovic, 1973, Folkmann, 1975, Deconnick, 1975, Johansson et al, 1976, and Khan and Crumpton, 1981. Several books are now available dealing with the subject of PIXE.

The first 'International Conference on Particle Induced X-ray Emission and its Analytical Applications' was held in Sweden in 1976 and since then two more have taken place, the last one being held in Germany in 1983. In his closing address at this conference Johansson, 1984, stated that PIXE has already established it self as an analytical technique.

The PIXE studies at Aston were started in the mid seventies at the Radiation Centre as a joint venture between the universities of Aston and Birmingham. A commercial trace elemental analytical service using the PIXE system developed in the present work is one of the main services currently provided by Radiation Centre Material Analysis group for Industry.

2.4 Physical Processes.

The theory behind most of the physical processes involved in proton induced X-ray emission, especially the production of X-rays, is very well known and hence they will be mentioned only very briefly.

2.4.1 Production of X-rays.

Following the removal of an inner-shell electron the excited atom returns to its ground state via

electron transitions from higher shells or sub-shells to the inner shells, resulting in the emission of characteristic X-rays. The emission consists of K, L, M....lines produced by electron transitions to the K, L, M.... shells of the atom. Figure 2.3 , is a simplified diagram of the energy levels in an atom showing the transitions which give rise to the K- and L- X-ray series. Figure 2.4 , from Valkovic, 1975, gives all possible transition and energy levels.

Each transition in the de-excitation process of an atom returning to its ground state lowers the energy of the excited atom, and this energy loss must be accounted for elsewhere in the system, for the conservation of energy. Three main possibilities exist to satisfy the requirement, that energy be conserved.

2.4.2 Fluorescence.

When an inner vacancy is filled by an electron from a higher shell this may result in the emission of an X-ray photon, the energy of which is equal to the difference between the final and initial electron energy states. The energy of this photon is characteristic of the element and the shells or sub-shells of the atom between which the transitions take place. This effect is the desired interaction and

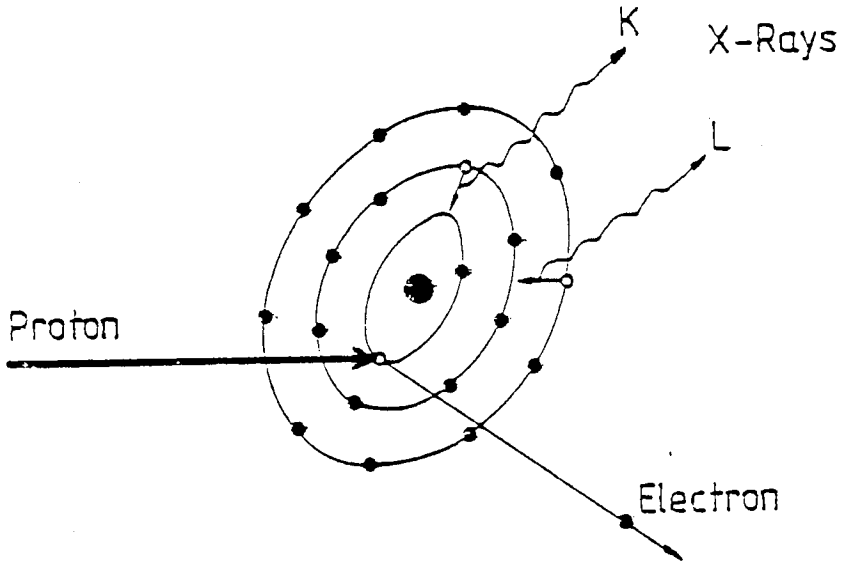

FIGURE 2.3

Simplified Schematic representation of K and L X-ray production

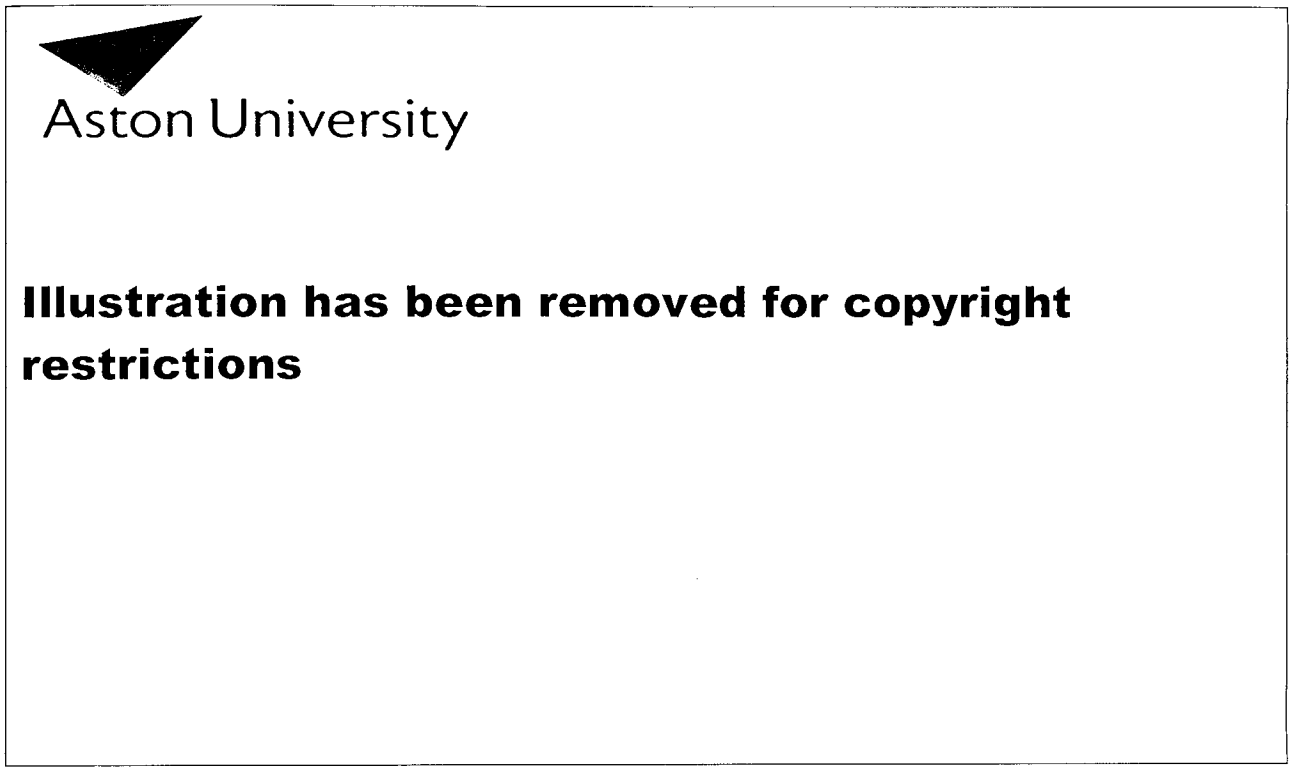

Figure 2.4 Representation of Energy Levels for X-ray emission and their possible transition (Volkovic,1975)

is of greatest importance for the purposes of inducing characteristic X-rays.

2.4.3 Auger Electrons

This radiationless transition is an alternative to the emission of photons and leads to the emission of Auger electrons. The inner shell vacancy is filled by an electron transition from a higher level, as in the previous case, and the energy available as a result of this transition results in the emission of an outer electron, Auger electron. This effect occurs mostly in low Z elements, where the fraction of vacancies producing X-ray photons may be less than 10%, Burhop and Asaad, 1972. Chattarji, 1976, have reviewed the mechanism of the Auger process. The energy spectra of the electrons produced in this process can be used to obtain analytical information. The technique and applications of Auger electron spectroscopy, AES, for surface analysis are given in the review articles by Holloway, 1980 and Grant, 1982.

The spectrum of Auger electrons is superimposed on the bremmstrahlung background produced by secondary electrons and the effect that these Auger electrons have on the X-ray background depends on their energy and yield. For very light elements, $Z < 8$, although the

yield is very high, the Auger electron energy is about 500 eV and does not effect the energy region of the X-ray lines of heavier elements. However for light elements, $13 \leqslant Z \leqslant 17$ in medium Z matrix, Ca to Zn, Auger electrons have sufficient energy to contribute to the X-ray background in the region of interest.

2.4.4 Coster-Kronig Transitions.

Radiationless Coster-Kronig transitions take place only for the L-shell and higher shells in which the primary inner-shell vacancy is removed by a transition from a sub-shell within the same atomic shell. By this process, a primary vacancy may be moved to higher sub-shell, altering the distribution, of vacancy of the sub-shell. Suppose an initial vacancy is in the L_1 subshell, then this is filled by an L_2 or L_3 electron leaving a vacancy in L_2 or L_3 subshell. The energy released by this vacancy "move" is transferred to an electron in M_4 or M_5 subshell via Coulomb interaction. Consequently the electron in M_4 or M_5 subshell will be knocked out, leaving the atom in a state of double ionization, Chattarji, 1976.

2.4.5 Fluorescence Yield.

The above processes show that only a proportion

of the ionized atoms will emit characteristic X-rays. The ratio of the number of primary vacancies filled giving rise to X-ray emission, to the number of initial vacancies created is termed the fluorescence yield of the atom. Conveniently the fluorescence yield (ω), can also be expressed as the ratio of the X-ray production cross-section to the ionization cross-section and is given by:

$$\omega = \sigma x/\sigma i \quad \ldots\ldots \quad (2.1)$$

where σx is the X-ray production cross-section and σi the ionization cross-section. This definition as it stands is applicable to the K-shell only. For the other shells, which exhibit sub-shells, the primary vacancy distribution may change due to Coster-Kronig transition, making the situation more complex. K-shell fluorescence yield(ω_k) as function of atomic number Z has been calculated by various authors. Figure 2.5 is reproduced from Krause, 1979.

2.4.6 Cross Sections.

In order to evaluate the yields of X-rays produced by charged particles at different bombarding energies, it is essential to have an accurate knowledge

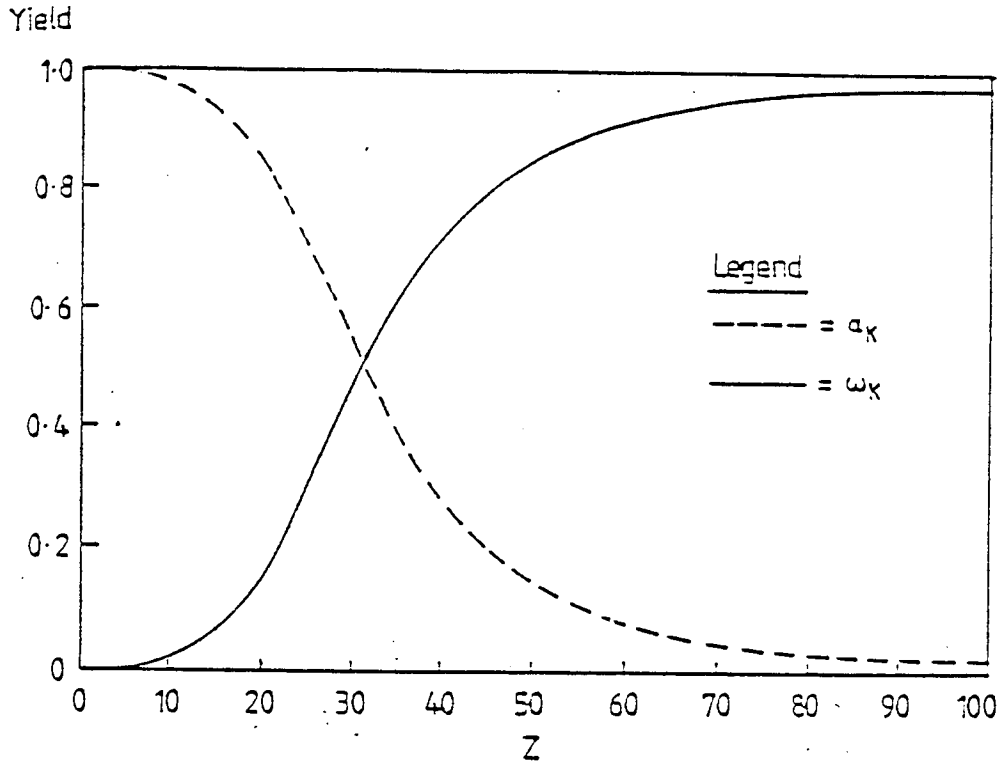

FIGURE 2.5 K-shell Fluorescence and Auger Yield as a Function of Atomic Number Z (From Krause, 1979).

of the production cross-section. This measure of probability of X-ray production for a particular energy of the projectile is obtained either theoretically or experimentally.

2.4.6.1 Theoretical.

There are three main theoretical models from which ionization cross-sections and their variation with energy can be calculated. These are, the plane wave born approximation (PWBA) of Merzbacher and Lewis, 1958; the binary encounter approximation (BEA) put forward by Gryzinski, 1965 and later developed by Garcia, 1970a,b and the semi-classical approximation (SCA) due to Bang et al, 1959.

(a)The Plane Wave Born Approximation (PWBA):

In this approximation the incident charged particles are treated as plane waves and the target electrons with which it interacts are described by hydrogenic wave functions. The Coulomb interaction between the bound electron and the incident proton is responsible for vacancy production.

Results using PWBA calculations agree with experiments except in the case of very heavy

target atoms and where the projectile energies are low as shown by Hansteen, 1975.

The use of the PWBA for evaluating cross sections for light positively charged particles have been fully discussed by Merzbacher and Lewis, 1958; Basbas, 1973; Rice et al, 1977; and Briggs and Taulbjerg, 1978.

Brandt and Lapicki, 1979 and Mukoyama and Sarkadi, 1983, while working within the PWBA theory included additional factors, both for the K-Shell and the L-shell, to take into account corrections for the binding energy (B), Coulomb deflection (C), polarisation (P), relativistic effect (R) and perturbed stationary states approach (PSS). Brandt and Lapicki, 1981, added an energy loss correction factor (E). The complete theory is commonly known as the ECPSSR theory. The theory of Mukoyama and Sarkadi, 1983, employing relativistic target electron wave functions within the PWBA model is usually referred to as the RPWBA-BC.

(b) The Binary Encounter Approximation (BEA):

In the binary encounter approximation the interactions between projectile and a free electron is treated classically. The results

obtained are the same as the PWBA under certain conditions as discussed by Gracia et al, 1973 and Hansen, 1973.

Madison and Merzbacher, 1975, and Taulbjerg, 1976, have shown that the BEA can be obtained from PWBA theory by suitable choice of the representation of the emitted electron.

However, the BEA fails at low impact velocities when it is applied to the ionization of a specific sub-shell.

(c)The Semi-Classical Approximation (SCA):

In this collision process, the motion of the incident projectile in the field of the target nucleus is treated classically and the transition of the inner-shell electron to the continuum is described quantum mechanically.

Hansteen et al, 1975, has given detailed discussion of this model. Taulbjerb, 1977, has shown that the total cross-sections obtained from SCA and PWBA are similar.

Laegsgaard et al, 1978, added corrections for binding, Coulomb repulsion and relativistic effects to the SCA theory. Their results for medium to high Z elements show acceptable agreement with measured cross-section data.

2.4.6.2 Experimental.

With the aid of above approximations it is possible to calculate values for the cross-section for X-ray production as a function of incident particle energy. Khan and Crumpton, 1981, point out the ease with which ionisation cross-sections may be evaluated, using empirical polynomial expressions formulated by Khan et al, 1977, and Johansson and Johansson, 1976, based upon their experimental measurements.

Experimentally, the cross-sections are normally measured using thin samples of known thickness and density. A sample is bombarded by an incident ion beam and the characteristic X-rays emitted are detected. The ionisation cross section σi is given by:

$$\sigma i = ((Yx.A.4\pi)/(Np.N.(\rho t).\omega.T.d)) \quad ...(2.4)$$

and may then be evaluated,
where

Yx = number of X-rays detected

A = Atomic weight of the element

ω = the fluorescence yield

Np = number of bombarding protons

N = Avogadro's Number

(ρt) = areal density of the sample

T = detector efficiency including

the various absorption effects

$d\Omega$ = solid angle

A number of difficulties are encountered in evaluating precise values of the various parameters in the above equation, hence variations are found in results obtained by different workers.

Another method is to measure backscattered protons using an SSB detector, at the same time as X-rays, as described by Deconnick et al, 1975.

A number of authors have published data of their experimental measurements. Gardener and Grey, 1978, has made this data available in the form of tables, for K-shell ionisation cross-sections.

The polynomials of Khan et al, were used for K X-ray ionisation cross-sections for theoretical calculations of F(xz) values for elements of atomic number $Z > 20$, and is given by:

$$\sigma i = (41.16 - 37.32E + 8.448E^2) - (12.212 - 21.242E + 4.864E^2) \ln Z - (0.0107 + 2.737 E - 0.6551E^2) \ln Z^2 \ldots\ldots\ldots (2.3)$$

2.5 Inner-shell cross-sections and projectile energy.

The dependence of the inner shell ionization cross-section (σi) on the proton energy (Ep) and on the

the atomic number of the sample element (Z_K) is given by Merzbacher and Lewis, 1958. They have shown that for the values of $T_m << I_K$, where T_m is the maximum energy that can be transferred by a heavy particle to a free electron and I_K is the binding energy of the K electrons. σ_i the ionization cross section is proportional to T_m^4 and inversely proportional to I_K^6. Since I_K is proportional to Z^2, the effective atomic number for the K-shell electron, and T_m is proportional to Ep.

$$\sigma_i \propto E_p^4 \; / \; Z_K^{12} \qquad \ldots 2.5$$

The behaviour of X-ray production cross-section (σ_X) as a function of the projectile energy E_p is very important in optimising the experimental parameters for maximum sensitivity in the elemental region of interest.

2.6 BACKGROUND RADIATION.

2.6.1 Introduction.

During the charged particle bombardment of a

target, in addition to the characteristic X-rays emission a continuous background radiation spectrum also appears. The sources of this background radiation are primarily the same basic processes that produce the X-rays.

Figure 2.6 shows a typical ion induced X-ray spectrum displaying a series of discrete characteristic X-ray peaks superimposed on a broad continuum background which has a maximum at low energies. The decrease in the continuum at the very low end of the spectrum is due to absorption of X-rays in the Be window in front of the Si(Li) detector employed for dispersive energy measurements. The very high background in the low energy region presents a problem for easy and accurate analysis of the light elements in the spectrum, mainly due to the difficulties in assesing the correct area under the characteristic X-ray peaks of light elements as these are are normally superimposed on the high bremmstahlung region.

The background radiation is a major factor which influences the sensitivity of a PIXE system. In order to measure characteristic X-rays from trace elements in a sample it is essential to know the background against which the characteristic peaks are to be seen. The following section presents a review of the major contributions to background radiation and discusses

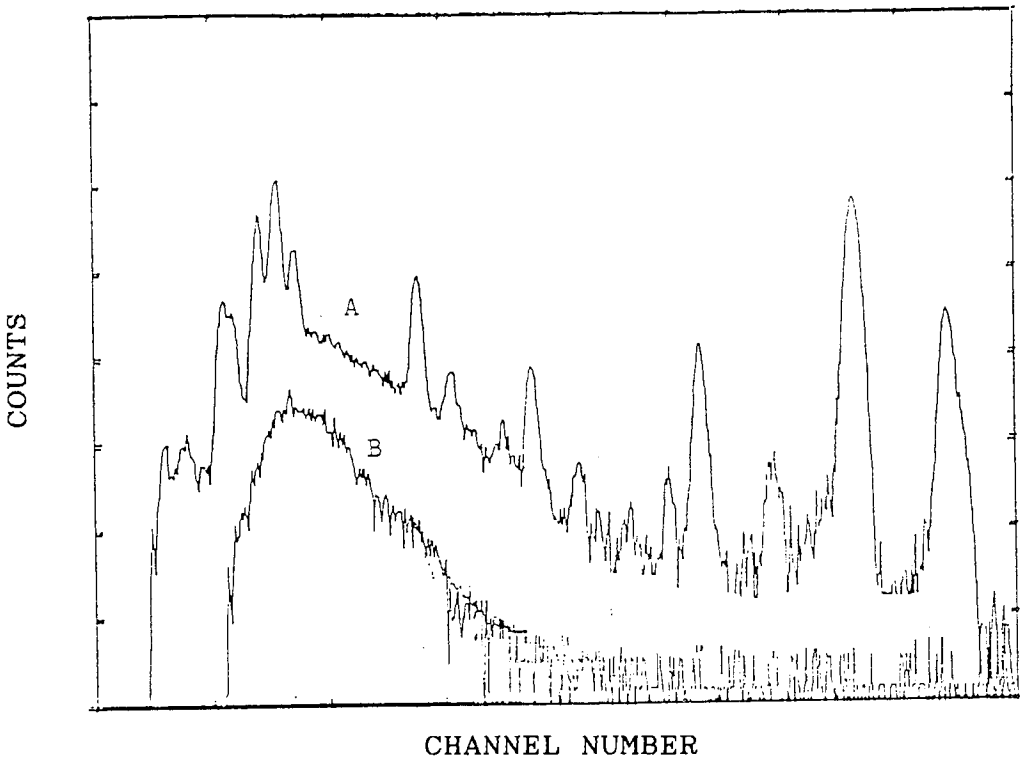

Figure 2.6 Characteristic X-ray Peaks Superimposed on Typical Background Continuum

Background levels :

A: Sample and a substrate.
B::Blank substrate.

attempts made at minimising this background in the present system. Results of practical work undertaken are illustrated in Chapter IV under system evaluation.

Bremsstrahlung radiation is a continuous spectrum of electro-magnetic radiation and results from both acceleration and deceleration of charged particles in the presence of electric fields. Bremsstrahlung from secondary electrons is dominant at low energies while other processes dominate at higher energies. However the actual experimentally observed level of bremsstrahlung background depends on a number of considerations such as target composition and thickness and the projectiles and their energies.

The discussion of proper selection of parameters for optimising the sensitivity of a system is discussed later. The spectral background in a PIXE analysis can be attributed to the following possible sources as given by Katsanos, 1980:

(a) Secondary electron bremsstrahlung.
(b) Incident projectile bremsstrahlung.
(c) Compton scattering of gamma rays.
(d) Target charging and discharging.
(e) Nuclear reactions.
(f) Quasi molecular radiation.(g) Low energy tails of the characteristic lines.

(h) Room background and background associated with detector and the pulse processing electronics.

These processes have been discussed fully by a number of authors such as Folkmann et al, 1974, 1984; Ishii et al, 1975, 1984; Tawara et al, 1976; Ward and Dyson, 1979 and others. Some of the more dominant processes that affect PIXE sensitivity in the present study are discussed in the following sections and also (h) is discussed in Chapter III under the heading of X-ray detection.

2.6.2 Secondary Electron Bremsstrahlung.

The secondary electron bremsstrahlung is generally the dominant continuum radiation at low X-ray energies. It is believed to be largely due to the bremsstrahlung caused by the secondary electrons ejected from the target atoms, by the primary ion beam during the collision process and extends up to an energy (Tm) given by:

$$Tm = 4(Mm/(M+m)^2).E \quad \ldots\ldots(2.7)$$

where, E and M are the energy and mass of a heavy projectile and m is the electron mass, and decreases

rapidly as the energy of the radiation exceeds Tm, the maximum energy a projectile can transfer to free electron. For excitation by protons Tm = (E/460), from the above equation. For example protons of energy 3 MeV give electrons of approximately 6 keV energy. It follows that characteristic X-ray lines from trace elements with energies less than 6 keV have to be measured against this low energy bremsstrahlung.

The secondary electron bremsstrahlung is produced by a two step process where the first is the ejection of secondary electrons by the incident projectiles and the second is the deceleration of such electrons as they interact with target nuclei. Most electrons loose their energy in numerous unequal steps rather than in one single step, thus generating a continuous background spectrum. Tseng and Pratt, 1971, and Pratt et al, 1979, calculated the intensity and angular distribution of secondary electron bremsstrahlung expressing their angular shape function as :

$$S(E_r, E_e, \theta_{er}) = \frac{A}{4\pi} \frac{\left(1 + \sum_{i=1}^{N} B_i(E_r, E_e) P_i(\cos\theta_{er})\right)}{(1 - \beta_e \cos\theta_{er})^m} \qquad 2\cdot8$$

where, E_e is the kinetic energy of the electron, β_e its velocity divided by the velocity of light, θ_{er} the angle between the electron and the emission of radiation of energy E_r, Pi is the Legendre polynomial.

Folkmann et al, 1974, have calculated the intensity of this bremsstrahlung and their results are reproduced in Figure 2.5, for 2.0 MeV protons on carbon foil. They initially treated the two stages separately and then combined these to integrate over the all possible energy exchanges.

They first employed the binary encounter approximations to calculate the probability that a projectile with energy E_1 will produce an electron of energy E in the energy range E_e to $E_e + dE_e$. The probability that an electron ejected with a kinetic energy E produce a bremsstrahlung photon of energy between E_r and $E_r + dE_e$, is given by:

$$dY(E_1, E_r) = \int_{E_r}^{E_3} d\sigma_r(E_e, E_r) \frac{dE_e}{S_M(E_e) A_M M} \qquad 2.9$$

where $dE_e/S_M(E_e)A_mM)$¿ is equivalent to the number of atoms per unit area corresponding to the energy loss dE_e of the electrons moving in the matrix of atoms with mass number A_m.

They then calculated the cross-section for an electron of energy E to produce a photon of energy E_r to $E_r + dE_r$. Their results showed that the cross-section for the production of bremsstrahlung is proportional to E_1^4 and decreases as E_r^{-8}.

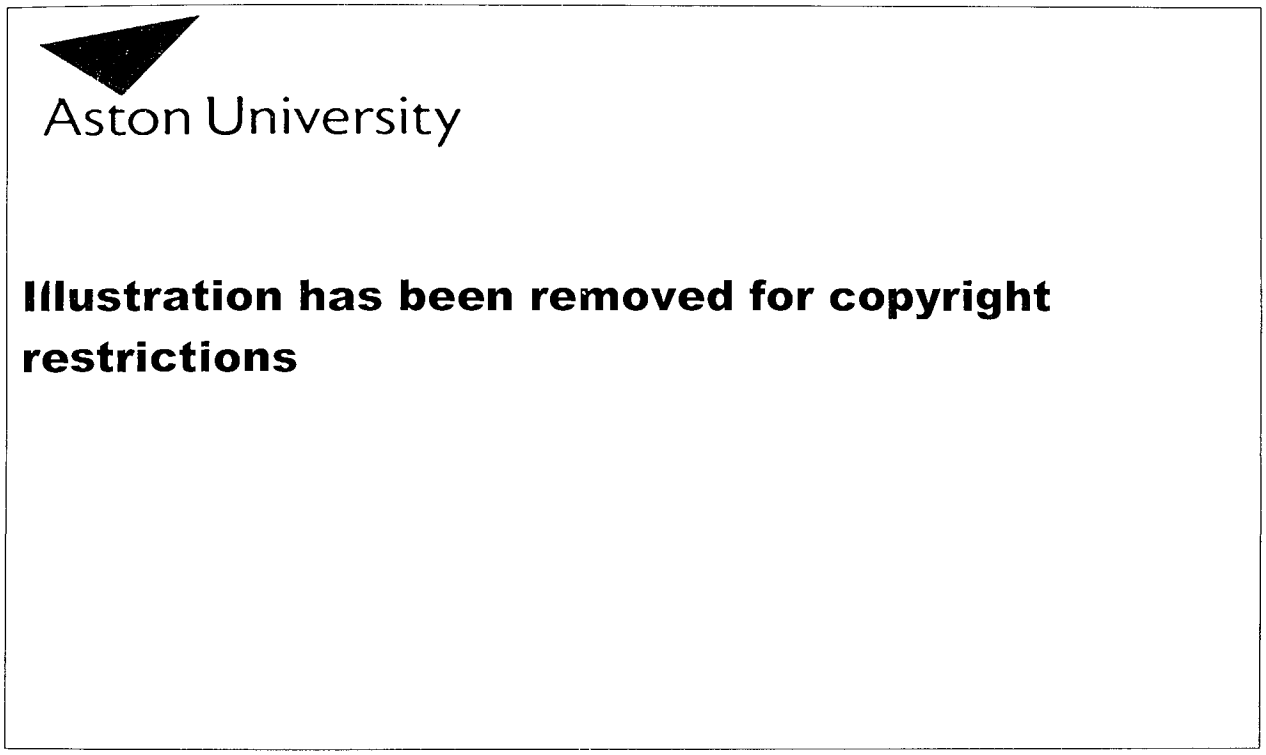

E_r in KeV

Figure 2.7

Experimental and Theoretical Background. Radiation Cross-Sections for Thin Carbon Foil (Folkmann et al 1974a).

Hence the probability for the production of high energy photons by an indirect process is negligible whereas probability for direct production of bremsstrahlung radiation varies as E_1^{-1} and E_r^{-1} making the contribution of higher energy radiation along the spectrum very flat.

The coulomb interaction of an incoming ion with an orbital bound electron will cause the electron to be accelerated and bremsstrahlung radiation to be emitted. Ogier et al, 1966, and Guy and Leyge, 1978, have calculated the bremsstrahlung produced indirectly from electrons accelerated in the incident protons field. Their results show that this bremsstrahlung is greater for higher energies (>3 MeV) than has been previously reported.

2.6.3 Incident Projectile Bremsstrahlung.

The deceleration of incident projectiles as they undergo collisions with target atoms may also result in the emission of bremsstrahlung X-rays. It appears to be a primary contribution to the background at the high energy end of the X-ray spectrum.

For a projectile of charge (Z_1) mass (A_1) and energy (E_1) incident on a target (Z_2, A_2), the cross-section for the production of projectile bremsstrahlung of energy E_r is given by Alder et al, 1956, as:

$$\frac{d\sigma_{\gamma}^{B}}{dE_r} = C.\ \frac{A_1 Z_1^2 Z^2}{E_1 E_r}\ \left[\ \frac{Z_1}{A_1} - \frac{Z_2}{A_2}\right] \quad + \text{higher multipolarities}$$

where C is approximately constant. The term $[Z_1/A_1 - Z_2/A_2]$ arises from the interference between the radiation of the projectile and the recoiling nucleus. Hence it suggests that electric dipole radiation could be minimised by a suitable choice of projectile target configuration, i.e where $[(A_1/Z_1)=(A_2/Z_2)]$. In these cases, higher multipolarities become important, but according to Folkmann et al, 1974, are of much less intensity.

2.6.4 Compton Scattering of Gamma Rays.

Gamma rays are frequently produced when energetic heavy ions have sufficient energy to induce excited nuclear state in the target atom. These γ-rays generate a high energy tail in the spectrum due to Compton scattering in the detector. Moreover the γ-rays may themselves lie in the X-ray region, and be detected by the detector as discrete peaks which may be mistaken for characteristic X-ray peaks. The production of γ-rays increase with increasing incident ion energy. The number of γ-rays produced also depends on the composition of the target because some nuclei such as ^{19}F and ^{23}Na have a high cross-section for γ-ray

emission. The design of collimators, target chamber and its contents may also provide sources for γ -ray scattering and thus aid the production of this background, by causing γ-ray back scattering. Folkmann et al, 1974a,b, have found this background to be dominant at high radiation energies and higher projectile velocities. They showed that for 3 - 5 MeV the background due to Compton scattering of γ-rays was much more important than the background due to proton bremsstrahlung. Hence to minimise this background, the beam energy should be kept as low practicable while still providing sufficient characteristic X-rays. For the proton beam energies, 1.00 - 3.00 MeV, the target and matrix compositions used in the present work, this bremsstrahlung presented no real problems.

2.6.5 Background due to Charge Build Up.

The accumulation of charge in the case of non-conducting samples from the incident charged particles leads to a build up of large background in the spectrum. This results from the frequent discharges of the sample due to the bremsstrahlung of the electrons in the discharge. This discharge produces a continous background radiation up to 15 or 20 keV with incident proton energy of 2 MeV, Valkovic, 1980. This increased background not only drastically reduces the

sensitivity of the strong X-ray lines but also completely masks a number of weaker X-ray lines in the spectrum. The electrons in the discharge apart from the bremsstrahlung may also excite characteristic X-rays from the sample, thus affecting any sample normalisation by backscattered protons.

A number of different solutions have been suggested and successfully applied to reduce or eliminate the problem by removing the charge build-up on non-conducting targets. These methods involved :

(i) Evaporation of a thin conducting layer onto the face of the sample. Papper et al, 1979, successfully employed this simple approach to reduce the charging of thick dried blood samples by evaporation of a pure carbon film onto the samples.

(ii) Applications of an electron flood-gun. This method has been described by Shabasson et al, 1973, Ahlberg et al, 1975 and Katsanos et al, 1976, Goclowski et al, 1983. A filament is placed close to the target, the glow current neutralizes the charge produced on the sample.

(iii) Mingay and Bernard, 1978, employed a magnetic field in the plane of the target extending out to the target holder. Secondary electrons are thus returned to the target without being fully accelerated by the potential developed between the sample beam spot and earth.

(iv) Mixing a pure known conducting power with the sample before pressing it into a pellet, Jepsson et al, 1962.

(v) Use of an external-beam PIXE system as discussed in chapter III, William, 1983.

(vi) Operating under non-vacuum conditions in the target chamber Ahlberg, 1975, Gollowski, 1984, but this leads to additional problems of uncertainties of beam energy contamination and limited life-time of the foil separating accelerator vacuum and target chamber pressure.

The above charge build up suppression techniques when investigated under the same experimental conditions showed similar results as reported by Godowski et al, 1983. However the use of a filament appears to be the more commonly employed method for removing charge build

up on non-conducting samples.

2.7 Angular Distribution.

The intensity of the continuum radiation has been investigated for secondary electron bremsstrahlung (SEB) by several workers - Tseng and Pratt, 1971 & 1979, Folkmann, 1974, Jitschin et al, 1983, but no real attention was paid its anisotropic emission. Tawara et al, 1976, first demonstrated that the angular distribution of secondary electron bremsstrahlung is anisotropic and generally more intense at 90°. This was confirmed by Ishii et al, 1977, who have also shown that the angular distribution of bremsstrahlung is not symmetric around 90° and that there is a marked reduction in the continuum at the backward angles relative to that at 90°. Sioshansi et al, 1976, has concluded that a reduction of over 40% is possible in the continuous background by placing a detector in a suitable backward position. They explained this behaviour by the relativistic retardation effect in bremsstrahlung production. Ranan, 1980, and more recently Folkmann, 1984, obtained results in agreement with anisotropic emission of bremsstrahlung reported by Ishii et al, 1977.

The most important continuum radiation, as

already mentioned previously, is the secondary electron bremsstrahlung (SEB). Ishii et al, have calculated the theoretical production cross-section of bremsstrahlung of secondary electrons σ^{SEB} produced by proton bombardment using the following equation:

$$\frac{d\sigma^{SEB}}{d(\hbar\omega)\,d\Omega_L} \approx (3C_2 - C_1)\sin^2\theta_L + 2(C_1 - C_2) + 4\cos\theta_L \times \left[2(C_1^R - C_2^R) + (5C_2^R - 3C_1^R)\sin^2\theta_L\right],$$

where

$$C_1 = \int dE_e \int dE'_e \int d\theta_e f,$$

$$C_2 = \int dE_e \int dE'_e \int d\theta_e f \cos^2\theta_e,$$

$$C_1^R = \int dE_e \int dE'_e \int d\theta_e f \cos\theta_e \beta,$$

and

$$C_2^R = \int dE_e \int dE'_e \int d\theta_e f \cos^3\theta_e \beta,$$

with

$$f(E'_e, E_e, \theta_e) = \frac{3}{8}\frac{d\sigma^{br}}{d(\hbar\omega)}\left(\frac{-N dx}{dE'_e}\right)\frac{d\sigma_e}{dE_e d\Omega_e}\sin\theta_e.$$

The relativistic retardation effect contributed by the last term of the equation shows that the bremsstrahlung is not symmetric around 90°. The anisotropy of bremsstrahlung $R(\theta_L)$ is expressed by :

$$R(\theta_L) = \frac{\sigma^{SEB}(\theta_L)}{\sigma^{SEB}(90^\circ)} = (3 - 4P_1)\sin^2\theta_L + 2(2P_1 - 1) + 4\left[2(P_1^R - P_2^R) + (5P_2^R - 3P_1^R)\sin^2\theta_L\right]\cos\theta_L,$$

where

$$P_1 = \frac{C_1}{C_1 + C_2}, \qquad P_2 = \frac{C_2}{C_1 + C_2}, \qquad P_1^R = \frac{C_1^R}{C_1 + C_2}, \qquad P_2^R = \frac{C_2^R}{C_1 + C_2}.$$

and (θ_L) is the observed angle with respect to the beam direction. Folkmann et al, 1984 calculated the angular distribution for (SEB) combining three separate processes, namely the bremsstrahlung of single electron, the production of secondary electron by the proton impact and the slowing down of these electrons in the solid. While their calculations for an Al target gave a useful estimate of the maximum reduction of the intensity at backward angles of 135° and 160° for energies of 4 MeV protons, the theoretical values for lower energies (3-2 MeV) for the same backward angles gave less favourable results when compared with the experimental measurements. They attributed this to possible nuclear excitation of Al and suggest that other material, such as carbon would probably follow the calculated behaviour. Both theoretical and experimental investigations by various workers and our own results described in chapter IV, demonstrate that a substantial reduction of bremsstrahlung is gained at backward angles. The consensus of opinion is firmly in favour of PIXE measurements to be made at as large a backward angle as possible.

CHAPTER III

3.0 DEVELOPMENT OF THE SYSTEM

3.1 Introduction.

The various aspects of design improvements relating to the scattering chamber, automatic sample changer, beam pulsing, and beam current monitoring and RBS facilities incorporated into the present system are described. Also the X-ray detection, beam transportation, vacuum system and external beam PIXE system are discussed in this chapter.

The design work was undertaken with a view to improving the collection of X-rays and to reduce the accelerator 'down' time, there-by making sample analysis more cost effective. Before commencing design work a study was made of the scattering chambers and target assemblies reported in the literature, see for example Feld, et al 1972; Herman, et al 1973; Mangelson, 1974; Valkovic et al 1974; Johansson et al 1976 (summarising data on several scattering

chambers); Hasselmann et al 1977; Lecomte et al 1978; Akselsson, et al 1979; Weber, et al 1980; Mitchell, et al 1980 and Budnar et al 1981.

It was concluded from this survey that a versatile and efficient vacuum chamber should allow for rapid and sensitive analysis of many types of samples. Detector-target geometry should be tight, provision for the detector to be positioned in the backward direction with respect to the incident beam and facilities for sample and absorber changing should be provided.

3.2 Economical Factors and PIXE System.

Unlike most other analytical systems, ion induced. X-ray emission. analysis. system. is accelerator based and is not generally available commercially. An accelerator is costly both in terms of initial cost and its running cost. To use an accelerator solely for analytical purposes does not make economical sense, particularly in todays highly competitive economy, when other low price analytical techniques may be available. The question then is, why invest in a costly PIXE system. The answer lies, apart. from. other. advantages of PIXE analysis, in it being a simultaneous multielemental analytical technique requiring a very small amount of sample material. When

cost per element using ion induced X-ray analysis is compared to other conventional methods of analysis ie AA, XRF and NAA, PIXE can be made very competitive. Katsanos, 1980, states that a complete PIXE system would cost between US $ 50,000 and US $ 170,000 and that the minimum number of personnel required for the operation of the the equipment and for data collection would be one accelerator operator, one electronics technician and two scientists. This gives one some idea of the running cost i.e. the operational cost in terms of salary alone. The operational cost of an accelerator at the Radiation Centre is estimated at about 1200 for two 7 hour shifts per day. This includes salaries of operators, electronic technician, computer officer and two scientists. Also included in this amount are the pro-rata accelerator and equipment costs, the overheads and computer analysis time. With this degree of expense one has to aim for analysis of around 50 samples a day, to bring the cost per element to approximately 2.50 to make PIXE analysis competitive with other conventional techniques.

3.3. PIXE System.

Since PIXE analysis systems are not available as a package a number of laboratories in the world currently applying PIXE analysis have had to develop, design and construct their own individual systems. All

these PIXE analysis systems from the very simple to most sophisticated design have the following in common:

(a) Collimated and homogeneous monoenergetic proton beam.
(b) Vacuum chamber.
(c) Target Assembly.
(d) X-ray detection system.
(e) Data collection systems.

3.3.1. Scattering Chamber.

The beam line and vacuum chamber utilized prior to this work has been fully described by other workers ie Khan, 1979; Saied, 1981 and Sokhi, 1984. The vacuum chamber, a rectangular stainless steel box of approximate dimensions 12 cm x 15 cm had a limited sample capacity and accommodated a maximum of four samples at a time. This proved prohibitively expensive in terms of time and cost, when measuring samples requiring short irradiations. A change of samples entailed letting the vacuum chamber up to air and then evacuating the 4000 cc volume again after the sample change. This operation usually took 30-45 minutes and with certain runs resulted in as much as 50% of valuable machine time being wasted. Thus a new automatic sample changer with increased target capacity of up to 80 samples was designed to go with a new

vacuum chamber.

Before finalising plans for construction of the chamber a full size model was made and found to be most useful in evaluating details of the solid state (SSB) detector positions, target assembly and various other mountings inside the chamber. It was also useful as a template for the 'graphite paper lining' for the chamber.

During planning stages of the scattering chamber careful considerations had to be given to any particular requirements of other workers in the PIXE group. Hence allowances were made in the final plan to accommodate those needs. The initial detector port size had to be increased to present 75 mm to accommodate a large Ortec detector used by another group. Another consideration which was always in the forefront was to make the design as versatile as possible for any future adaptation.

3.3.2 Chamber Design and Construction Details.

The chamber layout is shown in Figure 3.1, and detailed plans for construction of the vacuum chamber, re-entrant tube and flanges are shown in Drawing Numbers JSP/1/81 and JSP/2/81 (Figures 3.2 and 3.3)

SAMPLE CHAMBER

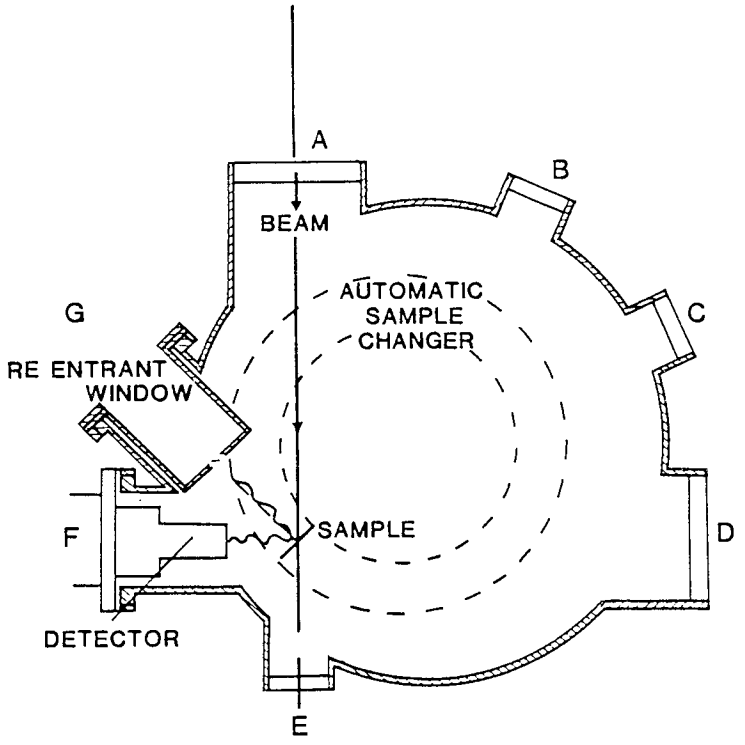

Figure 3.1

Lay Out Details of the Vacuum Chamber

A Incident Beam Port

B Electrical Connection Port

C Pumping Port

D Viewing Port

E Beam Dump/Exit Port

F Detector Port 90°

G Detector Port 135°

respectively (see backcover pocket)).

Figure 3.1, is a horizontal cross-section through the chamber at the beam axis. The target (T) is positioned at 45 degrees to the incident beam line entering from the top at A. This arrangement effectively increases the thickness of the sample by $\sqrt{2}$ as seen by the incident particles and has to be taken into account for sensitivity calculations described in Chapter IV.

Three ports B,C,D on the right are for electrical connections to the detectors, connections to the sample changer and a viewing window respectively. Port E at the bottom is for a beam dump or for taking a beam outside the chamber. Ports A and D are standard 200 mm diameter "Dependex" couplings while ports B, C and E are standard 100 mm diameter "Dependex" flanges. On the left are F and G two 75 mm diameter ports with specially designed flanges shown in Figure 3.3 (Drawing No. JSP/2/81). Also given in this figure are the details of re-entrant tubes which were designed and constructed to allow a Si(Li) detector to be used outside the vacuum but still at very nearly the same distance from the target as when maintained inside the vacuum chamber.

The chamber was constructed from helically wound

stainless steel, (schedule 10) tube of 360 mm nominal bore and 430 mm length. It was manufactured at the main workshop of the Physics Department at Birmingham University.

Six holes in the main chamber tube, to take the various ports were first machined out and then two 20 mm thick stainless steel collars of 438 mm outside diameter and 356 mm inside diameter were joined to the top by a seal welds on the inside and stitch welds on the outside.

This welding method was used with all major joints to give them strength and ensure vacuum integrity. Both collars had grooves to carry size 0459 "O" rings.

Both the cover and bottom plates were machined from 20 mm thick stainless steel plates of 438 mm diameter. Twelve holes, size number 13 drill equispaced on 388 mm pitch circle diameter were drilled in the collars and the top and bottom plates for fastening.

A special jig was constructed to hold the two angled detector ports firmly in position to avoid any distortion of the chamber walls, during the process of welding. The precision machining and welding of these three separate tubes in a precise and accurate

configuration were of utmost importance,the slightest distortion would throw the whole geometry out. This in fact did happen after attempting to cure a small vacuum leak in this region by rewelding. Luckily the damage was not too great, and the problem was overcome by re-positioning the re-entrant tube's (X-rays) exit hole very slightly.

3.3.2.1. Base Plate Mountings.

The base plate of the chamber had four 7.5 mm blind holes drilled on a 254 mm PCD to take four adjustable mounting rods for the automatic sample changer platform and clamping device. This arrangement enabled fine alignment of the target position with respect to the incident ion beam once the scattering chamber had been fixed in position.

Three further mountings were fixed to a platform inside the chamber. Two of the mounting were for the solid state (SSB) detectors (for RBS work) and were fabricated from PTFE to electrically isolate detectors from the chamber. PTFE was used as perspex and some other plastic insulating materials adversely affect the clean conditions of the accelerator vacuum. The third adjustable mounting was made of a rectangular aluminium bar to carry a beam monitoring foil, to be used in

conjunction with the second SSB detector, Figure 3.4 (photograph). Further details are given in the latter sub-section.

3.3.2.2 Chamber Stand.

A sturdy frame of 50 mm x 25 mm rectangular mild steel tubing was welded together to act as the chamber stand. To the top of the four legs of the framework were fixed 22 mm diameter threaded rods 100 mm in length. To these rods were attached 7.5 mm steel plates bolted to the bottom of the chamber. This facilitated the vertical alignment of the chamber where as horizontal alignment with respect to the ion beam was carried out by a similar arrangement at the bottom of the stand. The framework was firmly bolted to the concrete floor of the beam room, once coarse alignment of the tube was undertaken. Specially designed insulating bushes made of PTFE were used between the chamber mounting plates and threaded rods of the framework to electrically isolate the chamber from the stand.

3.3.3 Detector Positions.

The distance from the target to detector

Aston University

Content has been removed for copyright reasons

increased by 14.5 mm due to the positioning of re-entrant tubes between the target and detector in either of the two detector ports G or F, (Figure 3.1). Port F is at 45° to the target and Port G is at 90° degrees to the target or 135° degrees in the backwards direction with respect to the incoming ion beam.

With detector in Port F the distance between the target and detector is small, 5 cm, hence the solid angle (d) subtended is large. This results in higher X-ray count rate and hence reduced specimen counting time. But any inhomogeniety in the sample will affect the analytical results adversely in this position.

The arrangement is shown in Figure 3.5, where (a-b) is the target at 45° degrees to the detector face (D). The distance (a-D) is smaller than the distance (b-D), hence a count rate from or near the point (a) will be higher than a count rate from the point (b); thus detector position (F) will be ideal for a homogenous samples only. This problem is overcome using port G, since there is no tilt in the target position with respect to detector face.

3.3.4 Background Suppression.

Although the count rate at the detector port (G)

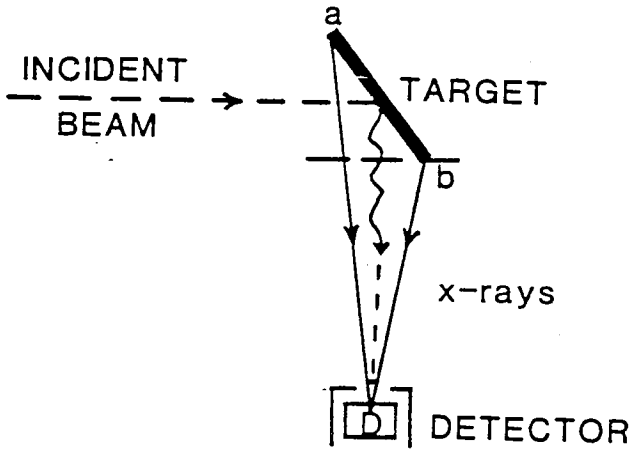

FIGURE 3.5

Target Position at 45° to the incident beam

is lower than the detector port (F), the bremsstrahlung intensity as discussed in Section 2.7, is minimised at large background angles compared to the more used position (F) of 90° degrees. This effect has been exploited in the present system.

The possibility of X-rays originating from scattered protons reaching chamber walls and seen by the Si(Li) detector is reduced to negligible proportions by lining the walls with "graphite paper". The vertical "guides" of the sample changer were covered with PTFE tape.

A Faraday cup from the previous chamber was used. It is constructed from a 405 mm long stainless steel tube of 50 mm diameter, and is attached to the scattering chamber port E, Figure 3.1, to act as a beam 'dump' for the emergent proton beam passing through the thin samples. A tantalum aperture of 7.5 mm diameter was fitted to the entrance of the Faraday cup to prevent secondary electrons escaping from the cup into the chamber and causing 'leakage' of current. The Faraday cup is placed at 115 mm behind the target.

3.4. Sample Changer.

The sample changer assembly was designed so that

a maximum number of samples could be loaded and positioned accurately with respect to the beam, using a remote controlled mechanism without opening up the scattering chamber or affecting its vacuum. As described earlier this criteria was most important to make analysis cost effective by reducing accelerator down time.

Several authors mentioned earlier, used the principle employed in an ordinary slide projector to change the samples in their multiple sample assembly. Lecomte et al, 1978, reported the use of a carousel type slide changer.

In the present work a Kodak Carousel slide projector Model S/SAV was completely modified and designed to operate inside the vacuum chamber and is shown in the photograph, Figure 3.6.

The slide projector was stripped down and the bottom half of the rectangular die cast container together with the light source, optical lens system, cooling fan, all cables, cable ties and electrical motor drive system were discarded. The two corners of the square top tray carrying the rotary magazine were carefully cut and machined, to fit the cylindrical shape of the chamber, without affecting operation of the clutch mechanism, Figure 3.7.

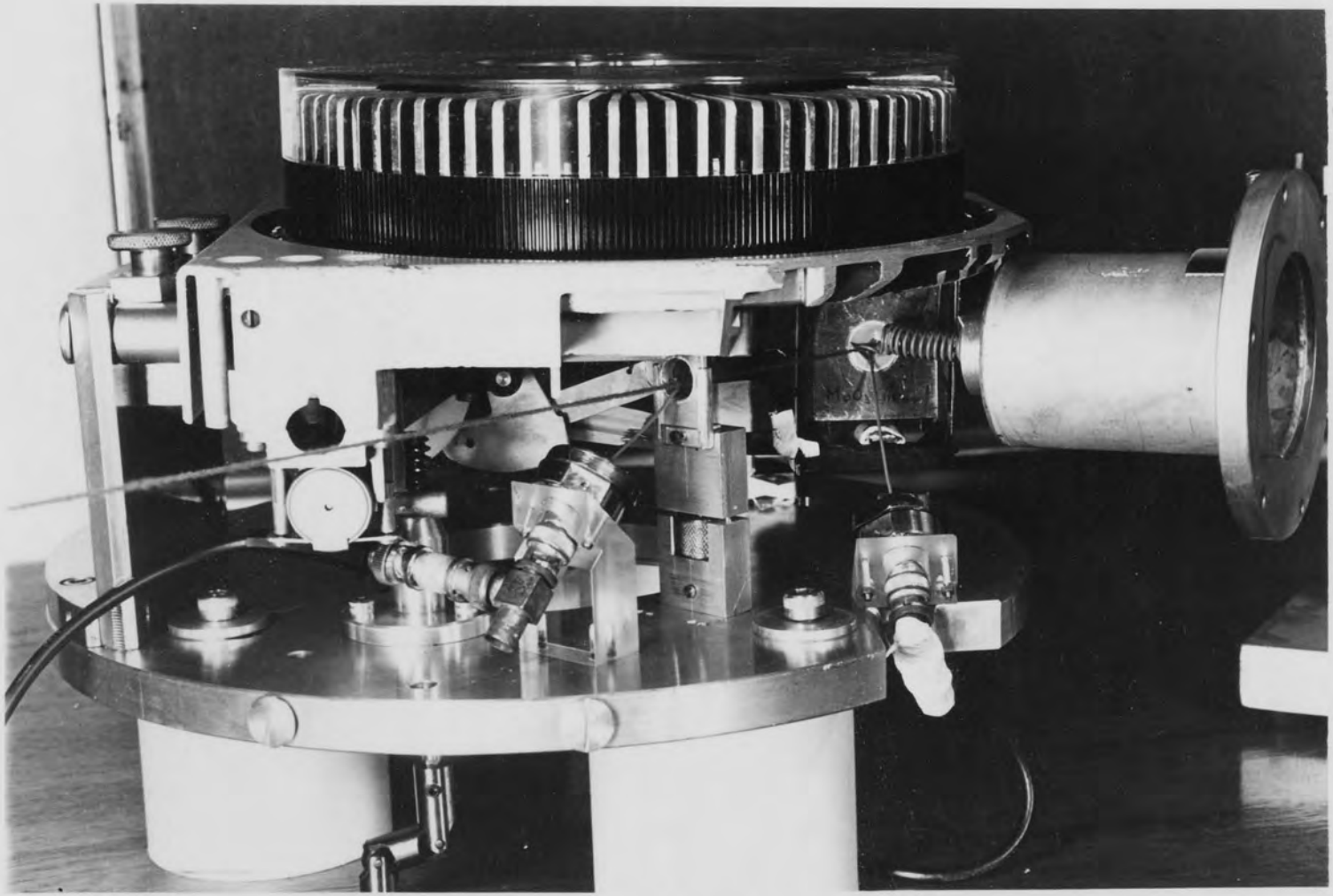

FIGURE 3.6 Sample Changer Assembly

Aston University

Content has been removed for copyright reasons

The clutch solenoids, one for the engagement of the operating drive and the other for 'forward' or 'reverse' motion of the sample tray, were re-installed after thoroughly cleaning away traces of any lubricating oil. To conform with the restrictions placed on the use of certain plastic materials inside the accelerator vacuum, the plastic drive gear was replaced with a steel gear wheel. The plastic materials used in the manufacture of the Carousel magazine were subjected to prolonged tests inside a vacuum system to check their effect on the vacuum pressure before use in the accelerator vacuum. They were found to be clean and stable.

In the most unlikely event of a sample getting stuck in the 'projector' mechanism and having to be manually retrieved it was decided to clamp the target changer to an adjustable platform rather than fix it permanently. Rigid and accurate clamping was achieved via two 15 mm diameter steel studs fixed to the side of the target system. These studs fitted into two precisely milled slots in the 10 mm thick by 100 mm x 200 mm aluminium plate. This aluminium plate was bolted edge wise onto the platform and carried two clamping fingers with hinges in one side and tightening screws on the other to clamp the studs. To support the far side of the target assembly an adjustable aluminium bar of 2 cm x 1 cm diameter was fixed.

To drive the target positioning mechanism, a Stepping Motor model FDTA/A51, Evershed Powertor, London, was employed. It was mounted underneath the chamber and connected through a Ferrifluidic Rotary Drive fixed to the bottom plate of the scattering chamber.

Special miniature flexible spindle couplings for light engineering applications made of stainless steel, by Fennel Power Transmission, Birmingham, were used to link the stepping motor, rotary drive and target positioning mechanism. The torque of a fully loaded target assembly was measured and found to be well within the specified limits of the rotary drive and stepping motor, when used in its continuous mode.

3.4.1 Sample Holder.

Pure aluminium frames 50 mm x 50 mm square by 2mm thick were designed and constructed to be used as sample holders. The sample frames had a reamed circular aperture of 15 mm diameter to take thin backing material, 5 μm thick Nuclepore or Kimfol, which was stretched and held across the hole with the aid of an aluminium ring of slightly smaller circular diameter.

Very thin samples, ie carbon films, were simply picked onto the hole after floating them in distilled water. Thick alloy steel targets and other biological

thick targets could also be easily mounted on recessed aluminium frames designed for the purpose.

The rotary slide magazine is capable of carrying up to 80 samples at a time. Any one of these targets can be positioned with a very high degree of accuracy, manually or by automatic remote control. Prolonged bench tests were carried out and sample positions checked with the aid of a travelling microscope.

Carousel rotary magazines used as sample trays are ready indexed and have a clear plastic cover which not only allows visual inspection of the sample positions but also helps to keep the targets dust and contamination free. The targets are loaded into the tray and a complete target replacement is easily done by opening the chamber, removing the magazine and replacing it with a fresh one.

3.4.2. Remote Control Unit.

The target assembly was operated by a remote control unit. This wire remote control unit was designed and built to cater for the following operations:

(a) Forward movement and sequential positioning of targets.

(b) Reverse movement of the slide magazine and target positioning.

(c) A counter to keep tally of the sample position number.

(d) Reset switch to set the counter to zero or any required number.

(e) A green LED indicator to show that target is in position.

(f) A red LED indicator to show that a target is being loaded.

Figure 3.8, shows a schematic diagram of the connections between the remote control unit and sample changer. To avoid excessive relay contact wear, usual contact suppression technique were employed. The unit was operated from a 24 volt d.c supply.

3.5 Beam Transportation and Monitoring Arrangement.

3.5.1 Introduction.

Charged particle beams, mostly protons and alpha particles of 1 to 3 MeV energy for the work described in this study, were obtained from the 3 MeV Dynamitron

CIRCUIT DIAGRAM AND CONNECTIONS BETWEEN THE REMOTE CONTROL UNIT AND THE SAMPLE CHANGER

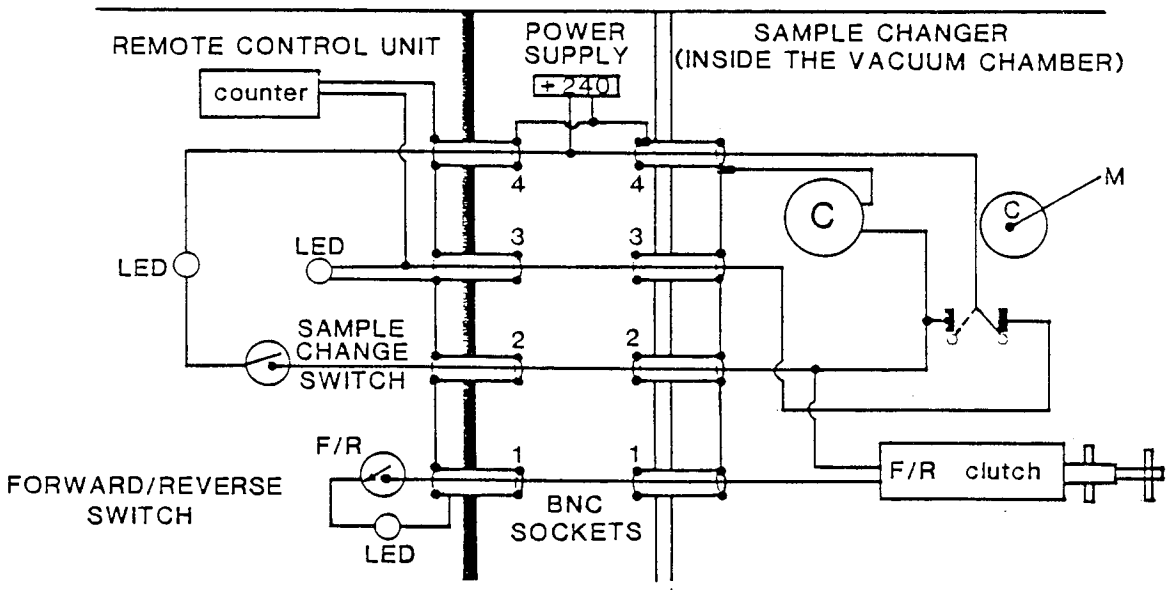

Figure 3.8

accelerator at the Birmingham Radiation Centre. The ions required for the incident beam are produced in the ion source at the head of the accelerator and then bent into the line of the accelerated column, for effective mass separation using a permanent magnet. After acceleration the vertical beam is directed into the 'Aston Beam Room', via a main bending magnet mounted on a rotatable cradle to facilitate change of the beam from one experimental room to another. The detailed beam transportation arrangement at the Centre has been described by Weaver (1980).

A further bending magnet in the Aston Beam Room is employed to deflect the beam through 45 degrees. The horizontal beam is then focused using a quadrupole pair of focusing magnets. Figure 3.9, shows a schematic diagram of the original experimental beam line and Figure 3.10 and photograph, Figure 3.11, shows the re-designed and much improved beam line arrangement incorporating the beam pulsing system and the versatile scattering chamber designed especially for this project.

3.5.2. Beam Collimation.

A set of tantalum collimators A1 and A2(Figure 3.10) with aperture diameter of 2mm and 4mm

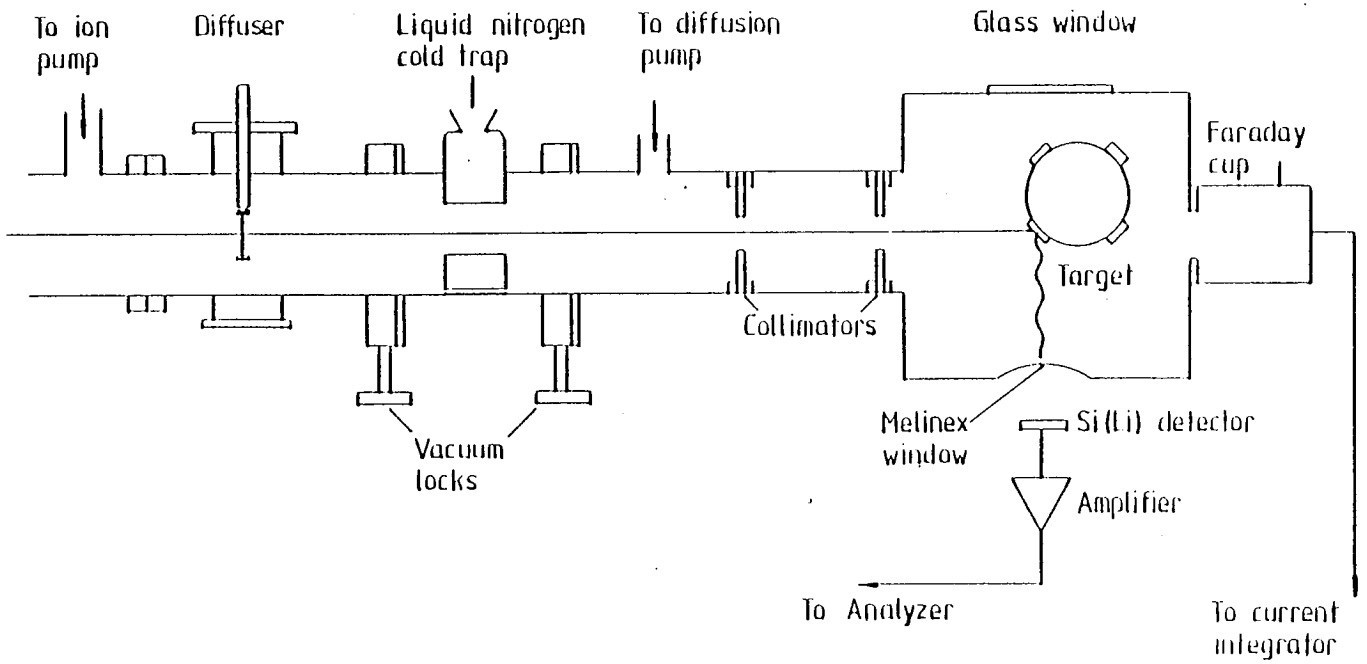

FIGURE 3.9 Previous PIXE Beam Line and Vacuum Chamber

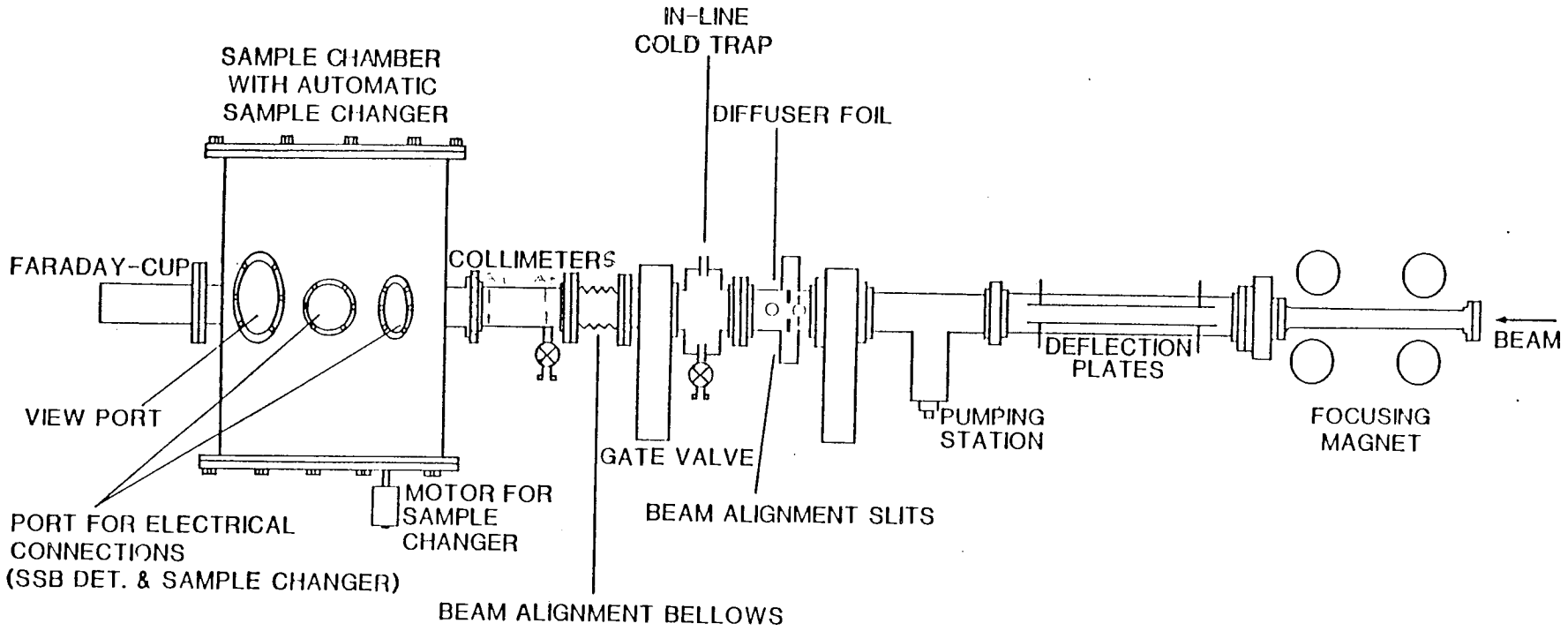

FIGURE 3.10 SCHEMATIC DIAGRAM OF THE BEAM LINE

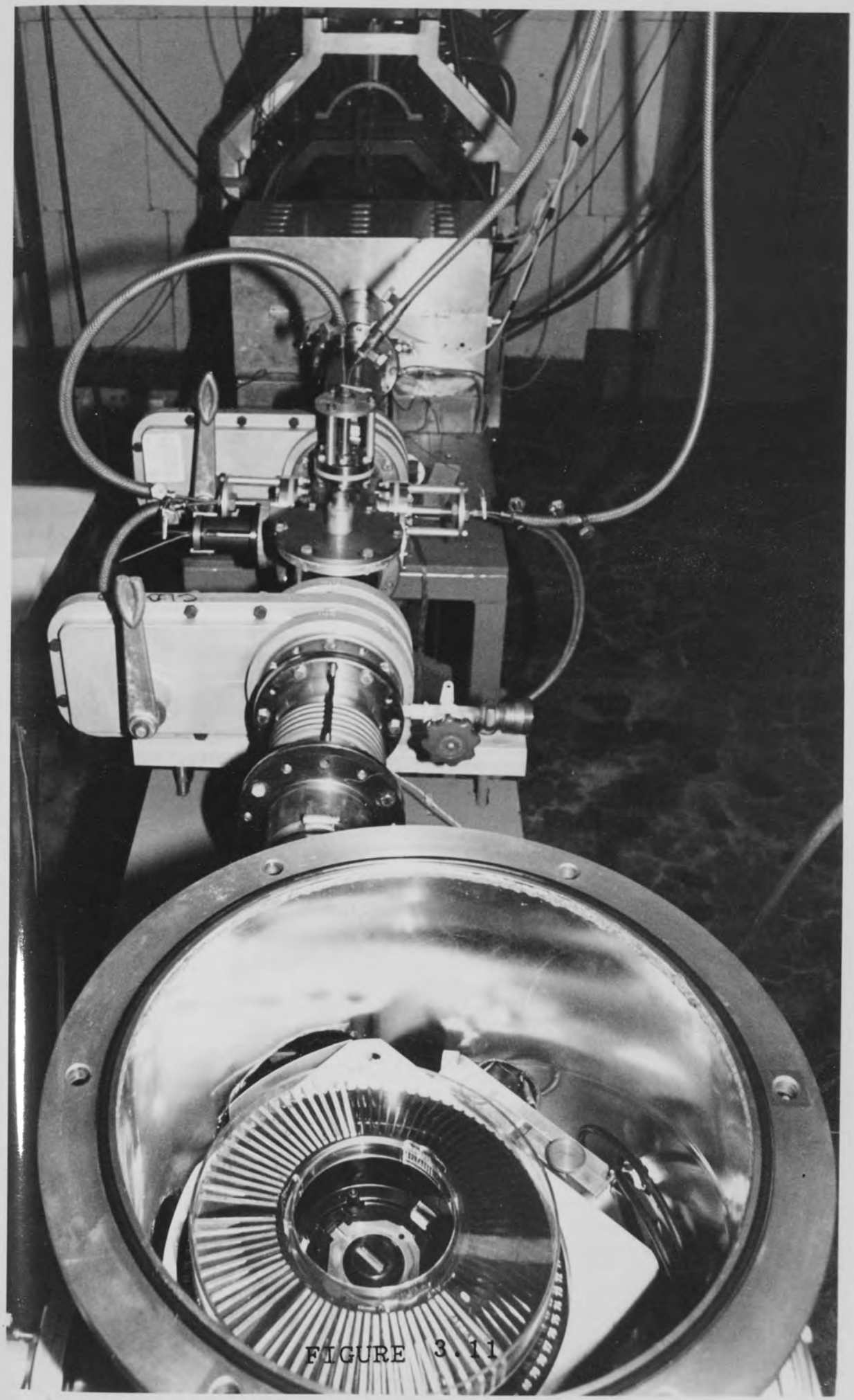

FIGURE 3.11

Photograph of the Beam Line, Looking Up Stream from the Vacuum Chamber

respectively are mounted 250mm apart inside the beam transportation line. Collimator A2 is at a distance of 150mm from the target. The beam area at the sample is defined by the collimator and can be easily varied to suit the sample by changing the collimator aperture. A simple method of estimating beam size is described by Khan and Crumpton, 1981. The final collimator provides effective skimming of particles scattered from the aperture edges of the first collimator. Both collimators are sharply bevelled to minimise beam scattering, as beam collimators can be an intense source of background radiation. The beam current on the collimator is continuously monitored during irradiations.

3.5.3. Beam Uniformity.

A uniform intensity distribution of the proton beam spot at the sample is essential in obtaining quantitative and reproducible measurements. A homogeneous beam compensates for any inhomogenity of the sample, provided the irradiation area is representative of the sample.

Production of a homogeneous beam can be achieved by the following methods:

(a) By passing the beam through a thin

diffuser foil and then collimating the resultant beam as described previously. The degree of uniformity achieved by this method depends not only on the characteristics but also on the its relative distance from the sample and beam and on the beam foculisation, Montengro et al, 1979. Several other publications have dealt in detail with this method, Bearse et al, 1974, Folkmann, 1975, Bauman et al, 1979, Akselsson and Johansson, 1979.

The diffuser foil used in this work was a 5 micron thick pure aluminium foil obtained from Good Fellow Metals, Cambridge, England. The diffuser foil was mounted on an eccentrical support to facilitate removal by rotating it away from the beam without breaking the vacuum.

(b) Production of a homogeneous beam can also be achieved by sweeping a well focused beam over the sample using electromagnetic deflectors as discussed by Johansson et al, 1972.

(c) By defocussing the beam in the accelerator and again using collimators to restrict the emmited beam to the central

region, Campbell et al, 1975.

3.5.4. Beam Current Monitoring.

For accurate PIXE analysis results, the need for precise beam current measurements is paramount if relative methods are not employed. The particle fluence is often determined by monitoring the charge placed on the sample during irradiation and is normally achieved by measuring the charge collected on an isolated target by connecting it to a current integrator.

The main problem with beam current integration techniques is due to the production of secondary and tertiary currents. The magnitude and characteristics of these currents have been investigated by Matteson et al, 1979. Secondary electrons introduce an error into the total charge deposited on the target since the negatively charged electron current is added to the positive ion current.

Also any secondary electrons generated from the ion beam collimators near the target may be carried along with the beam leading to inaccurate beam current measurements. These secondary electron currents are not only a function of target species, Dearnaley et al, 1973, but are also dependent on the angle at which the

sample is positioned with respect to the incident particle beam as discussed by Sternglass, 1957.

The beam current integration for self supporting thin targets can be monitored by the use of a Faraday cup, since most of the beam is transmitted through the target. In the case of insulated targets this is achieved by placing the sample inside the Faraday Cup as reported by Amsel et al, 1967. However depending on target material, thickness and the incident beam energy, even with good electron suppression or biased shields Matteson, 1979, electron stripping and multiple scattering effects, can take place producing inaccurate measure of current at the Faraday Cup.

The intial charge measurements on the Faraday Cup, using a Kiethley electrometer, for the K X-ray yields from standard calibration targets (Micro Matter Co) bombarded by 2.5 MeV protons were found to be unreproducible when measurements were repeated at different times. The inaccuracies produced were attributed to:

(i) charge leakage caused by secondary electrons escaping from the Faraday Cup into the chamber

(ii) direct leakage of current between the chamber and the Faraday Cup due to the very high input impedance of the Kiethley electrometer.

The measurements in the present studies were made by isolating the chamber and electrically connecting it to the Faraday Cup. This arrangement of combining the two into one Faraday Cup has been discussed in some length by Saied, 1981.

3.5.5. Determination of Target Charge.

The target current integration was achieved by means of a Kiethley electrometer (model 600B) which generates a voltage output for the charge collected. This voltage signal is proportional to the meter deflection. Full scale deflection is represented by 1V for all current ranges. The output voltage signal is fed into a voltage to frequency converter (VFC) which produces a pulse chain with frequency proportional to the input voltage, input of 1V producing a frequency of 10^5 Hz. This pulse chain is connected to a special decade divider unit, which scales the pulses making them suitable for counting on a scaler. Thus counting for a fixed number of these 'scaled' pulses is equivalent to counting for a fixed target charge. The scaler and divider were linked to an automatic stop

device, once a preset on the scaler had been reached the accumulation of the data stopped automatically.

The integrated target charge (I) was obtained from the following equation:

I(μC)=FSD on Keithley (μA)xN2 dividing Factor/10K x PSC ..3.1

Measurement of integrated target charge with the new chamber and Faraday cup combined together, although fairly satisfactory, was not entirely reproducible as seen from measurements tabulated in Table 3.1. Hence other relative methods for measuring target charge were pursued.

3.5.6. Elastic Backscattering from the Target.

An accurate alternative method which is independent of any current integration is to measure the flux of backscattered particles from the target itself. An absolute total charge (Q) on the target is calculated by using equation 3.2:

$$Q = Y / \Delta\Omega \left(\frac{d\sigma}{d\Omega}\right)_{eo} .N \qquad (3.2)$$

where Y is the number of backscattered

TABLE 3.1

Reproducibility Studies

Preset counts (PSC)	Time (sec)	Cu peak counts	Mu Peak centriod	BGD sum
10000	106.2	7080	211.2	142
10000	111.4	7375	211.2	210
10000	113.5	7365	211.3	142
10000	123.4	7529	211.2	258
10000	105.1	6908	211.2	127
10000	104.9	6984	211.2	131
10000	110.8	7198	211.2	123
10000	110.1	7113	211.2	127
10000	110.4	7127	211.2	172
10000	107.6	7067	211.2	132
Mean (x)	110.2	7174	211.2	156
σ_n		183.5		

protons from the target recorded in the SSB detector.

$\Delta\Omega$ is the solid angle in steradian that the detector subtends at the target.

$(d\sigma / d\Omega)_{eo}$ is the backscattering cross-section in cm^2 per steradian calculated at the mean energy of the ion beam as it passes through the foil and N is the foil thickness in atoms per cm^2.

For use as a relative comparator, only RBS counts are measured, provided all the samples analysed are of the same material or are deposited on the same backing material. In the latter case, all experimental runs on different samples were normalised to the backscattered counts from the backing material, i.e Nuclepore. This was achieved by using a computer to sum up the counts under the area of interest from the RBS energy spectrum. A typical spectrum, for example SiO on Nuclepore backing, is shown in Figure 3.12.

Backscattered ions were collected at an angle of 135° with respect to the incident beam direction, by a silicon surface barrier (SSB) detector with an active area of 75 mm^2 and

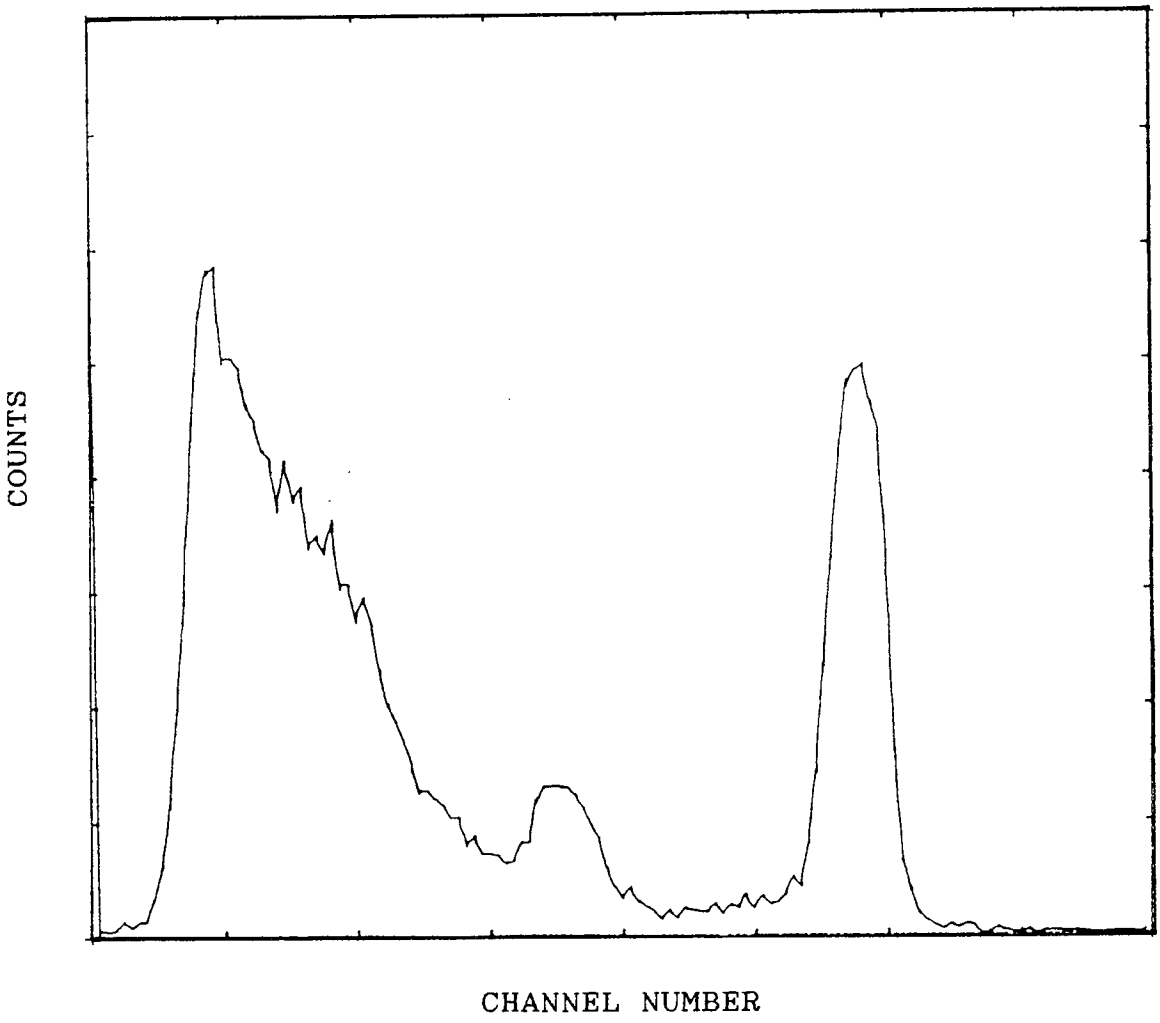

Figure 3.12

Typical RBS spectrum: Thin SiO on Nuclepore backing

thickness of 190 um. Two tantalum collimators, 5 mm apart with 2.5 mm apertures were attached to the detector face to ensure that a collimated backscatter beam strikes the centre of the active area. The (SSB) detector was connected via a short cable and vacuum feed through to an Ortec 125 preamplifier. The pulses were amplified using an Ortec 472A spectroscopy amplifier and processed by a data acquisition system HP 5406B which is a computer based multi-channel analyser (MCA). Performance and resolution of the electronics system was checked by a test pulse fed into the preamplifier. An energy spectrum of backscattered protons obtained for thick Si target, using the set up is shown in Figure 3.13.

3.5.7. The Foil Ion Beam Monitor.

A method of beam current measurement which is totally independent of the nature of the target is foil ion beam monitoring. This technique has been investigated by Mitchell et al, 1978b and 1980a.

A thin self supporting foil, thin enough to allow the beam to pass through without appreciable energy loss, is placed between the beam line and the target. Since the Rutherford backscattering

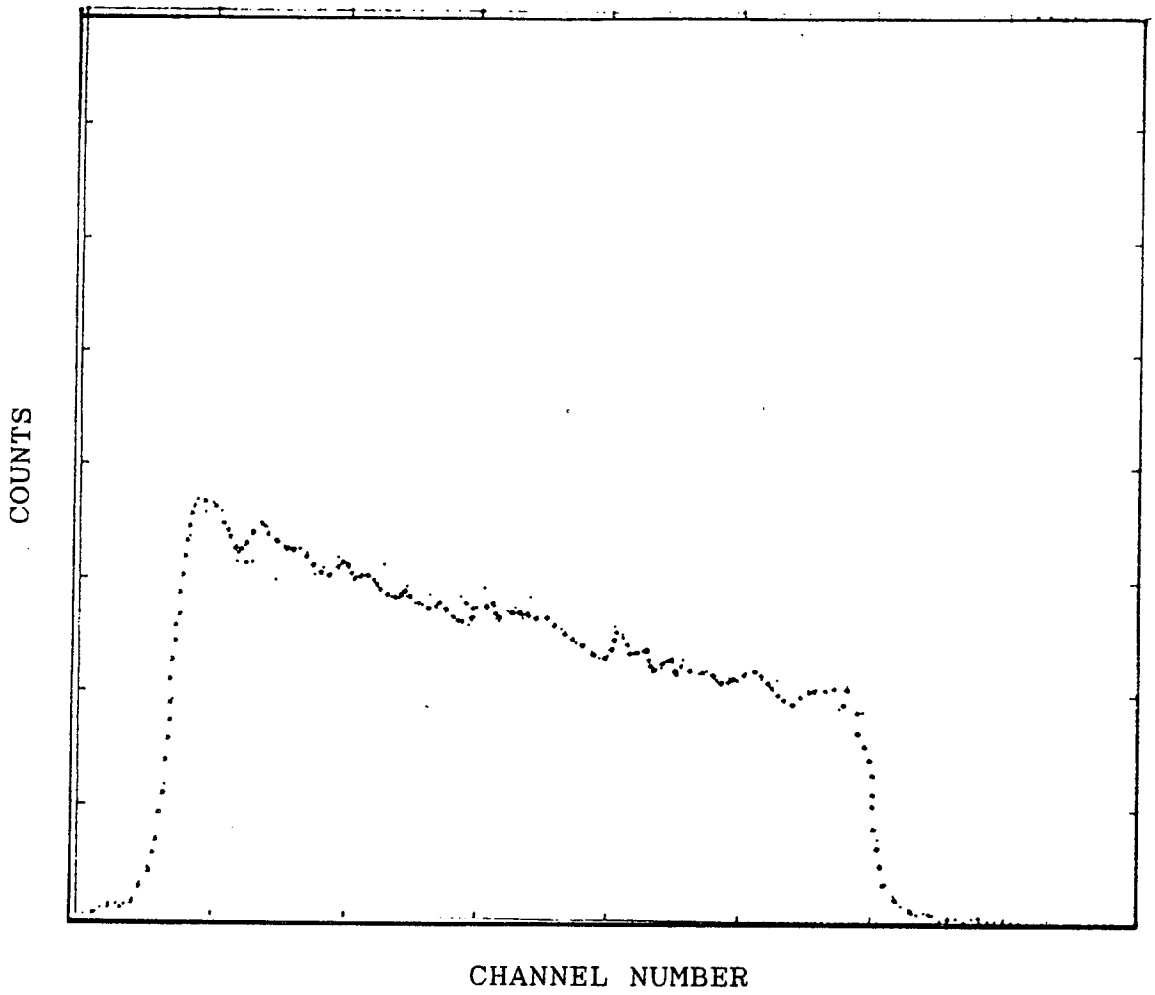

Figure 3.13

RBS Spectrum of Thick Si Target

cross-section is only dependent on the foil material and not on the nature of the target material, any fluctuations in the incident beam current is faithfully reflected in the RBS yield. Volkov et al, 1983, described a system of monitoring a low energy ion beam based on the use of the backscattering phenomenon and reported accuracy of charge measurements placed on the target to approximately 0.6%.

A schematic diagram of the set up is shown in Figure 3.14 , and the photograph, Figure 3.15, shows the detector and foil mounting details. A similar detector to the one described in the previous sub-section was used to measure the flux of backscattered ions. It was positioned at an angle of 180° with respect to the incident beam. The signal from the SSB detector was fed via a main amplifier into a rate meter or a scaler/timer unit. Reasonable counting statistics (200 c/s for a 2 MeV proton beam) were obtained by placing a suitable aperture in front of the SSB detector. Great care had to be taken in handling the foils during positioning and also during initial pump down and opening up to atmospheric pressure of the vacuum system.

Gold was chosen for its high backscattering

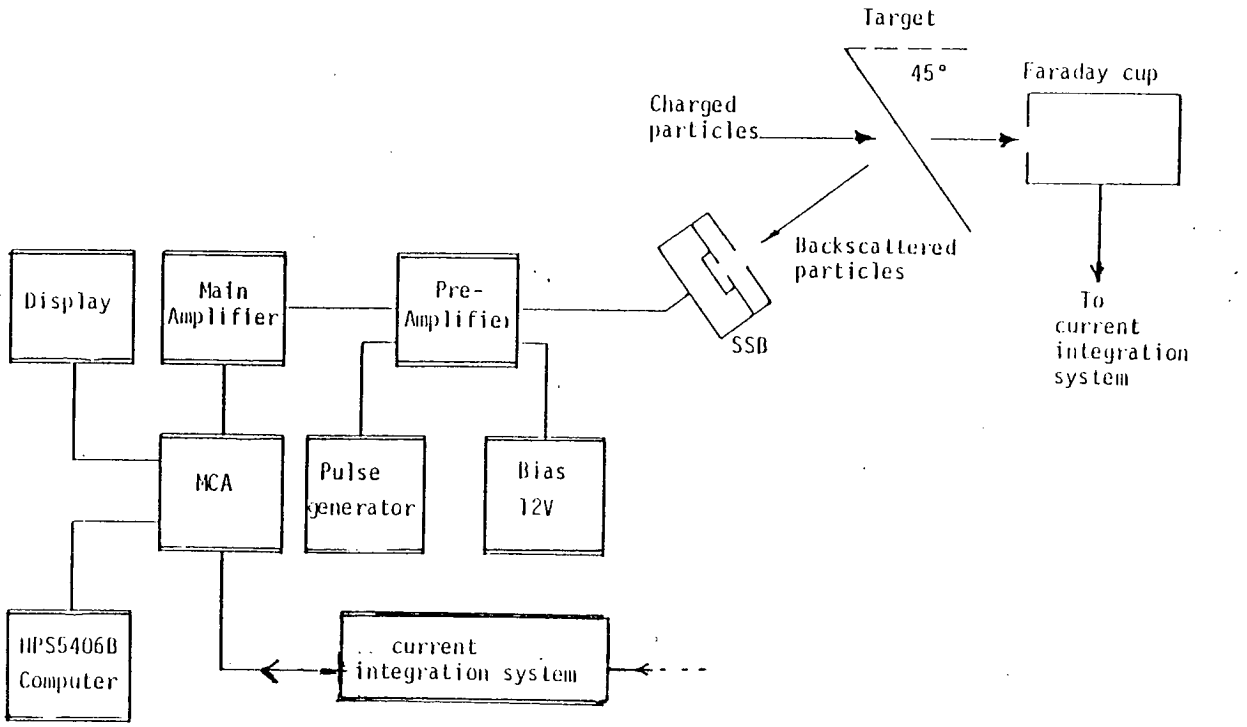

Figure 3.14 Schematic Diagram of RBS Set Up

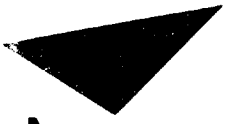

Aston University

Content has been removed for copyright reasons

cross-section and ease of preparation using evaporation techniques for uniform self supporting thin films. Several films in the thickness range of 50 μgcm^{-2} to 400 μgcm^{-2} were prepared by evaporating 99.95% pure gold onto detergent (TOT) treated 2.5 mm x 7.5 mm glass microscope slides. The foils were scribed into appropriate sizes while still on the slide and "floated" on the surface of clean water. These were picked up on specially constructed light gauge aluminium frames and stored in a dessicator until required. The foils were self supporting over an aperture of 14 mm diameter.

Most foils with a thickness less than 100 μgcm^{-2} were very easily ruptured during initial loading or during pump down probably due to the large size of 'foil' aperture. Foils with thicknesses greater than 200 μgcm^{-2} were found to withstand sample changing operations. However, in order to minimise energy loss due to the thickness of the foil, the thinnest self supporting foils, 80 μgcm^{-2} were used. The energy loss in an 80 μgcm^{-2} gold foil for protons of 2 MeV energy is 2 keV, Anderson et al, 1977.

Measurements for different methods, described above were carried out and the

intercomparison of the results for beam current measurements are given in Table 3.2. It is concluded from these results that the ion foil monitoring technique is the most accurate method for beam current measurement.

3.6 Beam Pulsing System

3.6.1 Introduction.

An on-demand beam pulsing system has been incorporated into the present ion induced X-ray emission analysis system, to over-come problems associated with high count rate effects. Beam pulsing has been successfully used by various workers to improve the spectral resolution of the PIXE system (Cahill 1975, Mingay et al 1978 and Malmqvist et al 1982). When analysing thick samples, e.g. alloy steel samples, bio-medical or other thick samples, very high characteristic X-ray yields are produced, resulting in spectral distortion due to pulse pile up. With thin sample analysis work described in chapter V, high count rates are not a problem.

TABLE 3.2

Comparison of beam current measurements using Current Integrator, Ion Foil Monitor and elastic backscattering from thin Cu target.

Au foil RBS pulses	BI pulses	Time sec	X-ray peak counts	B/scatter RBS counts
1000	7340	81.5	3904	2375
1000	7280	80.4	3894	2334
1000	7390	81.6	3899	2354
1000	7020	78.8	3884	2380
1000	7430	82.0	3890	2350
1000	7420	82.1	3886	2360
1000	7430	81.9	3913	2342
1000	7360	81.6	3902	2389
1000	7400	81.9	3881	2399
1000	7430	81.8	3897	2348
Total = 73500			38950	23629
σ_n = 119.25			9.48	20.59

BI = Beam Current Integrator

3.6.2 Pulse Pile Up.

A very short but finite time interval is required by the X-ray detector data processing electronics to process each incoming X-ray signal. At high count rates, above 1000 c/s, a second pulse can enter the system while the first pulse is being sorted, resulting in overloading of the signal processing electronics. This inability of the data processing system to keep pace with the detector output signals leads to pulse pile up and electronic dead-time correction problems, as well as spectral loss of signals in the continuum.

Three types of pile up, leading edge, trailing edge and sum peak are possible. These have been fully described with illustrations by Woldseth, 1973; Statham, 1977; and Khan & Crumpton, 1981. The pulse pile up and electronics dead time effects may be reduced by reducing the beam current to reduce the X-ray emission rate, or by inserting absorbers between the detector and target but this reduction in pulse pile up is at the expense of data acquisition time as longer measurement times are needed to obtain reasonable

counting statistics. This is a wasteful management of valuable machine time and contrary to the economical philosophy behind design work of this project.

Another solution is to use electronic pulse pile-up rejection circuits. The technique is based on an auxiliary inspection channel whose purpose is to sense and reject co-incident and other pulses which have lost their original amplitude and shape. Pulse pile-up rejector units are available commercially, (Kevex 4590 pulse pile-up rejector) can cope reasonably with moderate count rates i.e. 6000 c/s, but at higher count rates run into difficulties, distorting the spectrum.

A more satisfactory method as adopted by Jaklevic et al, 1972; Cahill, 1975; Koeing et al, 1977; Mingay et al, 1978; and Malmqvist et al, 1982; is to use a system which electrostatically deflects the beam as soon as an X-ray arrives at a detector. The beam is returned onto the sample only when the measurement of the signal pulse is completed. Such a system is self regulating in this respect and not only reduces the pulse pile-up but does away with the need for dead-time correction since the detector is 'live' only for the duration of beam on target. With a beam

pulsing system the analysis times are reduced considerably as compared to commercial pile-up rejectors. The time and hence cost savings is another distinct advantage.

3.6.3 Beam Pulsing : Requirement and Design.

Generally an on demand beam pulsing system consists of the following :

a) A beam deflection system.

b) Beam stop collimators.

c) Beam pulsing electronics.

The design of these features depend on the specific beam line configuration, types and energies of the ion beam and the application. A detailed design description of the system and associated electronics has been discussed by Al-Armaghany et al, 1987; only a general overview of the system and its installation into the present beam line will be discussed here.

3.6.3.1 Beam Deflection System.

A charged particle beam may be deflected or bent in two ways, one by electrostatic fields and secondly by magnetic fields. The former method was adopted in the present work since faster switching

times are possible with electrostatic systems than magnetic ones. It is also much more economical to run compared with the latter method, since resistive losses in the magnetic coil windings waste appreciable power.

Two deflecting plates were made from 1 cm thick polished stainless steel sheet 50 cm long and 4 cm wide. The side edges of the plates have been bent through 30° to provide extra strength and to reduce the edge effects. The plates were fixed 2.5 cm apart as shown in Figure 3.16 with the aid of clamps attached to the four vacuum high voltage lead-throughs, inside a standard 10 cm diameter beam transport tube. This deflecting system was installed between the focusing magnet and the triode ion pumping unit.

3.6.3.2 Beam Collimation and Beam Pulsing Electronics.

Accurate control of the ion beam position within the beam transport tube is an essential requirement for correct operation of the beam pulsing system. The beam line was modified to accommodate :

1. A set of four specially designed water cooled

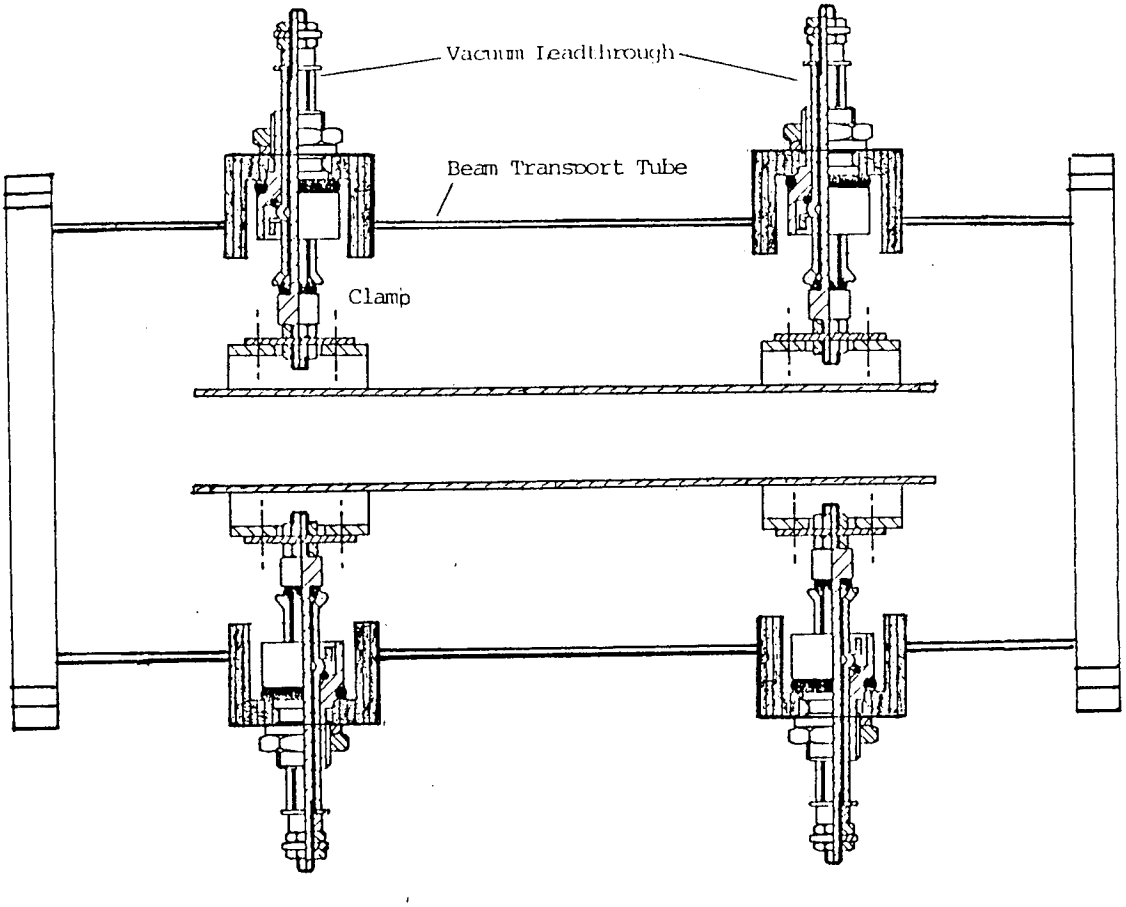

Figure 3.16
Design of clamping arrangement
of the deflecting plates

adjustable fingers forming an aperture, to define and monitor the beam before entering the beam pulsing system.

2. A second set of water cooled apertures as described above was installed just before the diffuser foil to act as a beam stop. This aperture was precisely aligned with the aid of fine laser beam. It allowed the beam to pass through but acted as a stop when it was deflected (figure 3.9).
3. The original 5 cm to 10 cm diameter adaptor had to be replaced by a specially designed copper adapter due to restriction of space in the Aston beam room. This was necessary as the standard diameter of the beam transport tube up to the focusing magnet is 5 cm and then onward a 10 cm standard stainless steel beam tube is used (figure 3.10).

The procedure adopted for electrostatic deflection of beam and all associated electronics, especially designed or otherwise has been fully described by Al-Armaghany, 1985; a block diagram showing the various electronic units used for the on-demand beam pulsing is given in Figure 3.17.

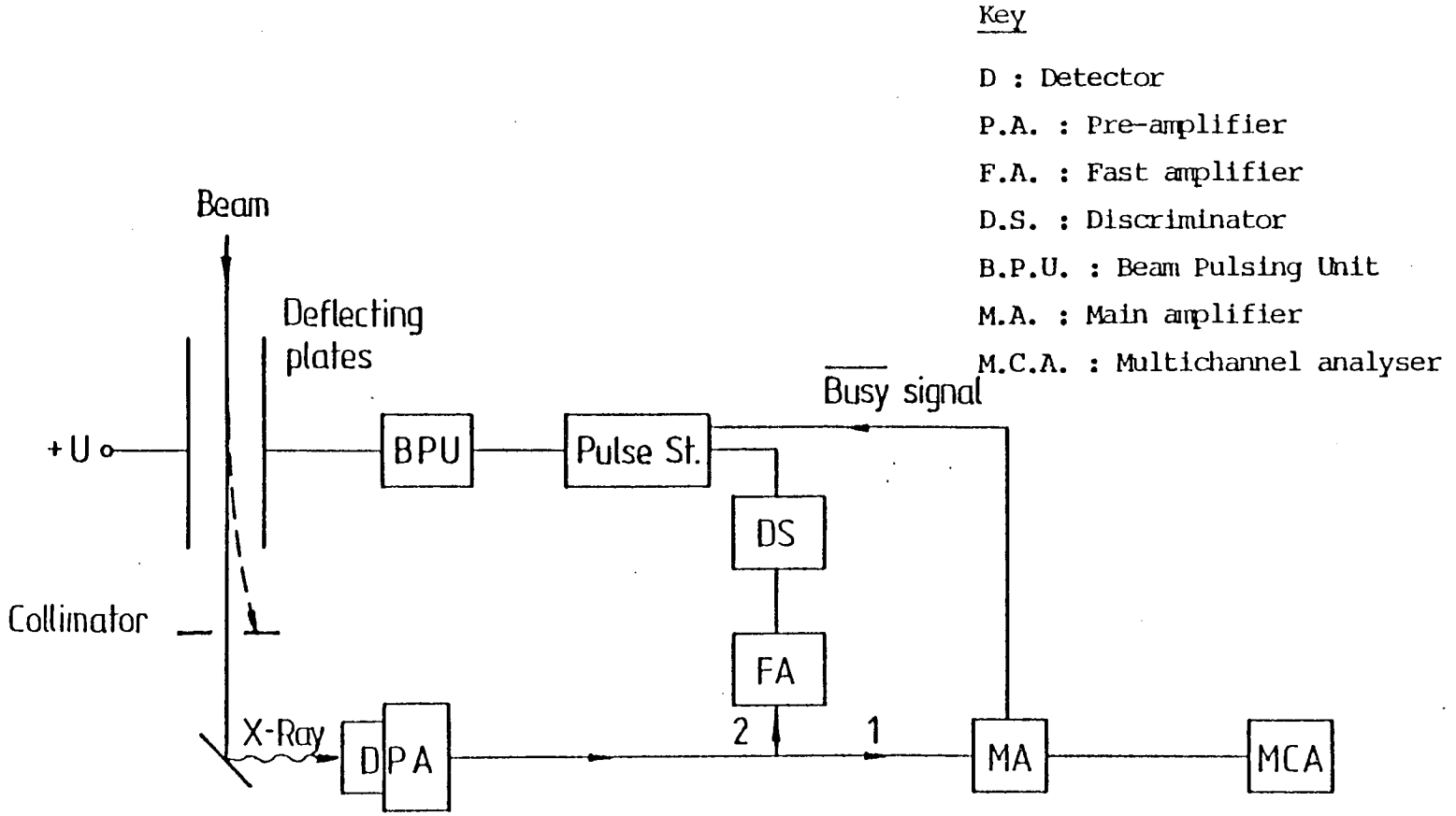

FIGURE 3.17

Block Diagram of the On-Demand

3.6.4 Electronic System for Beam Pulsing.

A switching circuit (BPU) using a TTL logic signal to trigger a high power thermionic valve (PL519) with delay time of less than 200 ns and switching off time of less than 500 ns was employed in the present work. Figure 3.18 shows the electronic circuit of the beam pulsing unit. A high speed optocoupler (HCPL-2601) integrated circuit is used for maximum DC and AC circuit isolation and its output is fed into two parallel VMOS devices, VN88AF. The drain of each VMOS-FET is connected to the cathode of two parallel thermionic valves. A positive 5 volt on the gate of the VMOS-FET, makes the valve conduct and discharge one of the deflecting plates to ground. Both plates are normally maintained at a high voltage of 2.5 to 3 keV.

The circuit is basically triggered by a signal generated by the pulse processor and discriminator in the pulse pile-up rejection unit. The use of a variable pulse stretcher circuit allows the deflection time of the beam to be controlled. One of the deflecting plates can be effectively ground in approximately 300 ns and while the amplifier is busy processing an event deflection is maintained. The beam returns to the target after ~ 100 μs. This longer time is due to the

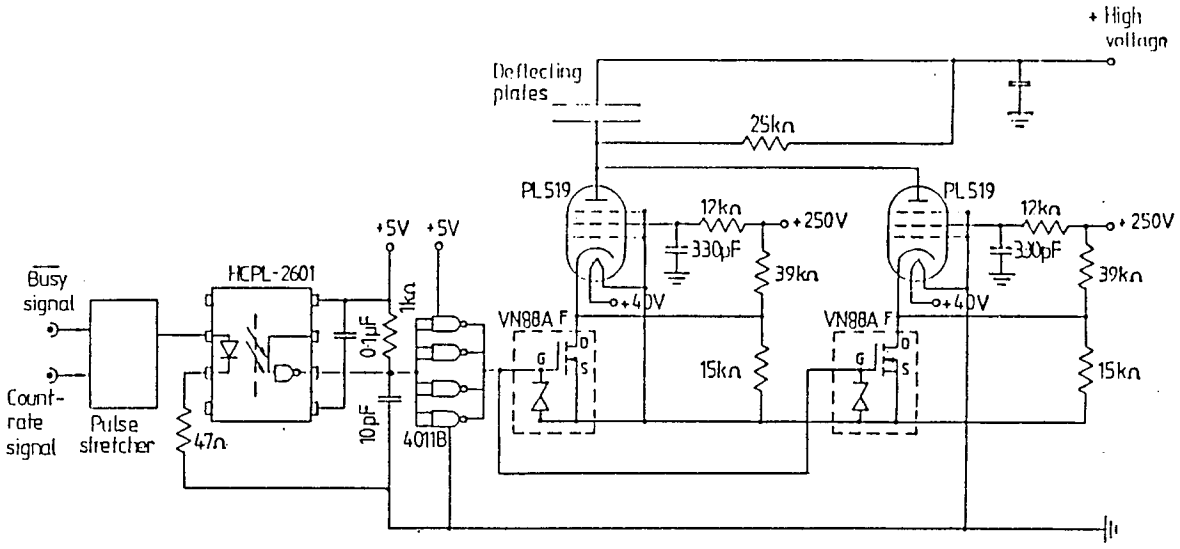

FIGURE 3.18

Circuit of the Beam Pulsing Electronics

time needed for the grounded plate to return to its initial voltage.

The performance of the beam pulsing system has been fully evaluated by Al-Armaghany, 1985. The system has improved count rate handling capability from 1000 c/s to 10000 c/s for the present X-ray detection system with the main amplifier time constant of 8 μsec.

3.7 X-RAY DETECTION SYSTEM.

X-Rays produced by charged particle bombardment of the target were detected with an X-ray detector system manufactured by Kevex Corporation, comprising of:

(i) Si(Li) detector Kevex-ray 3201 cryogenic sub-system.

(ii) Model 2002 Kevex-ray preamplifier with pulsed optical feedback system.

(iii) Kevex-ray pulse processor Model 4525P.

3.7.1. Detector.

The first stage of the preamplifier consisted of an Si(Li) detector and a field effect transistor mounted behind a 12.7 μm beryllium window which provides a vacuum seal as well as an optical shield. The detector is a lithium compensated disc shape silicon crystal with an active area of 30 mm and a thickness of 3 mm. The smaller diameter detectors yield better energy resolution at low energies, Jenkins, 1979.

Basic construction details of a Si(Li) detector are described below. On both parallel faces of the crystal a layer of gold is deposited to form an electrical contact. Beneath the gold layer on the front face lies a Si dead layer. This dead layer results in a detectors inefficiency to measure very low energy X-rays.

To prevent lithium diffusing through the crystal, the detector is cooled by liquid nitrogen (77 K). Cooling of the detector is also necessary to reduce the electrical noise produced by the thermally generated charge carriers in the crystal. The principles of the Si(Li) detectors are well known and shall be mentioned here very briefly.

photoelectric and Compton scattering processes. The photons absorbed in the active region of the detector loose their energy by excitation and ionization process creating electron-hole pairs. The amount of free charge thus generated is proportional to the amount of energy deposited in the detector by the X-ray photon. The average energy required to create an electron -hole pair in Si is 3.62 eV at room temperature. Generally the average energy required to create an electron-hole pair increases with increasing band gap of the material. The value of E versus energy bandgap Eg, for various solid-state crystal have been calculated by Klein, 1968. The free charges were collected by applying a bias potential of 1000 V across the crystal used for this work.

The characteristics of silicon and germanium semiconductor X-ray detectors of different designs (e.g. disc, tophat, grooved etc.) have been reviewed by Fink, 1979. Jaklevic, 1972; Woldseth, 1972, and others have also discussed solid state detector designs in detail.

3.7.2. Preamplifier.

The optical feedback pre-amplifier Model 2002 is of Landis, 1971 design. The feedback resistor in this design is replaced by an optical reset circuit.

Detailed circuit explanation of various types of pre-amplifiers used in X-ray spectroscopy is given by Woldseth, 1973 and Jenkins et al, 1981. Each charge pulse is integrated and converted to a voltage step proportional to the charge. The voltage is allowed to build up in the FET stage to a certain level. And is removed by pulsing a light emitting diode, which is optically coupled to the input FET, restoring the circuit back to its quiescent state, (Landis, 1971 and Woldseth, 1972). Pulsed optical systems offer both good resolution and low noise characteristics at moderate count rates (below 1000 cps) as discussed earlier in the Section 3.7.

3.7.3 Data Acquisition System.

The output pulses from the pre-amplifier were coupled to a Kevex pulse processor, Model 4525P. The pulse processor differentiated, shaped and amplified the signal to match the input requirements of a Multichannel Analyser (MCA).

An MCA basically consists of an analogue-to-digital converter (ADC), data handling and a memory store. The 200 MHz ADC provided conversion gain selections from standard 1024 channels to higher

the ADC provided visual display of the spectrum accumulated over 2048 channels.

The data acquisition system is shown schematically in Figure 3.19. It was interfaced to an Hewlett-Packard S5406A/B computer for fast storage and retrieval of data (Weaver, 1976). Each X-ray spectrum obtained is stored on the hard disc and then transferred to a magnetic tape for further analysis.

A number of computer programs, such as Peak routine, Neib and Krump are available for quantitative analysis on the Hewlett-Packard computer. The Peak routine program which was mostly used for the present work, calculated the sum of counts, centroid and the standard deviation of the peak. Two or more channels on each side of the peak were used in calculating the linear background counts. The procedure is fully explained by Saied (1981).

3.7.4 Detector Resolution.

The two important parameters which specify the performance characteristics of a Si(Li) detector are its resolution and efficiency. The basic description of a detector resolution is given as its ability to distinguish between two peaks that are close together

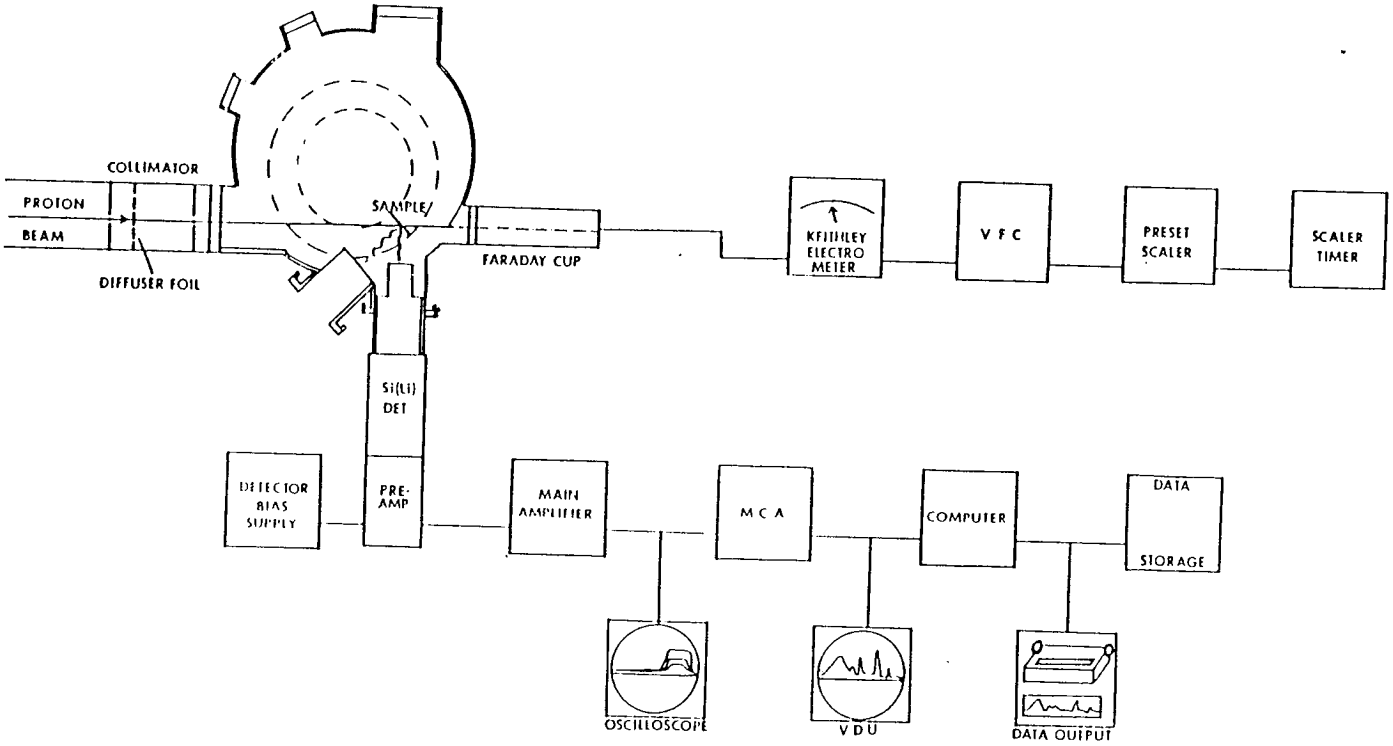

FIGURE 3.19

Data Acquisition System and the Experimental Set Up

in energy. The resolution of the system is conventionally defined as the full width of the energy peak at half maximum intensity (FWHM) expressed in energy units.

The overall resolution of a detector system depends partly on the electronic noise associated with the input amplifier stage, and partly by the detector leakage current and the uncertainty in the number of electron hole pairs produced by an X-ray due to its intrinsic random nature of ionisation. Hence effective resolution is a combination of both and is stated as a quadratic sum of the electronic noise and the intrinsic detector effect :

$$(FWHM)_{effective} = \left[(FWHM)^2_{elect.\ noise} + (FWHM)^2_{detector} \right]^{1/2}$$

The electronic noise component depends on the time constant τ for the amplifier and can be measured by applying an appropriate test signal to the preamplifier input. A time constant τ of 8 μs was used for present work. The electronic noise width was measured to be 119 eV.

The random component $(FWHM)_{detector}$ is given by

$$(FWHM)_{detector} = 2.35\ (EeF)^{1/2} \quad \ldots\ 3.4$$

Where the constant 2.35 relates one standard deviation of Gaussian distribution σ to the FWHM,

E = energy of detected photon,

e = the average energy required to produce a charge,

F = Fano Factor which corrects for the variation of the energy-loss process from a Poisson distribution, Knoll, 1979. If all of the incident photons energy were always converted into electron-hole pairs the Fano factor would be zero.

The above relationship shows that the detector resolution varies with X-ray energy and a convenient measure of the FWHM for any peak is given by Tiori et al, 1981, as:

$$FWHM_1 = 2.5(E_1 - E_2) + FWHM_2^2 \quad \ldots\ldots 3.5$$

Where $FWHM_1$ and E_1 are the peak width and energy of the peak of interest and $FWHM_2$ and E_2 are the known values for a standard peak of Mn K_α measured using same detector under similar conditions.

In general the continuum background is mainly produced from events within the detector. These are

a) incomplete charge collection due to carrier trapping

b) loss of charge in the side surfaces of the detector due to distortions in the electric field

c) escape of photo electrons from the detector

d) escape of photons after undergoing Compton scattering within the detector.

The Mn K line resolution was measured for the detector using an Fe^{55} and found to be 174+-6 eV. Figure 3.20 shows a spectra for the Mn K-X-ray lines. Although the system resolution is not particularly good, it is worthy of the measurement of elements of interest in the Amniotic Fluid samples discussed in Chapter V.

3.7.5 X-ray Energy Calibration.

An energy calibration of the Si(li) detector for easy identification of unknown elements in the sample was carried out using a commercially available variable X-ray energy source. It consists of a 10 mCi Am primary source giving 60 keV gamma-rays and six fluorescence targets, in the range $29<Z<65$. The X-ray emission from standard foils were also used to calibrate X-ray detection system. "PEAK" software package was used

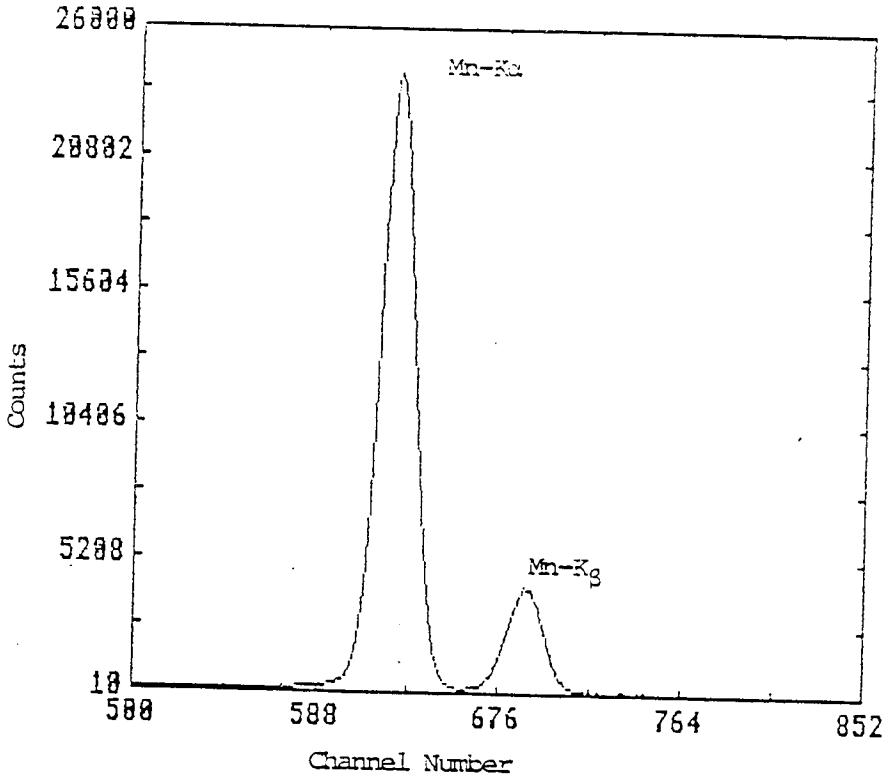

FIGURE 3.20

Mn K X-rays Detected with Si(Li) Detector Using Fe^{55}

to determine the peak centroids and standard deviations. The programme fits a single Gaussian distribution to an X-ray peak. Two or more channels each side of a complete peak are used in the estimations of linear background on which the X-ray peak is superimposed. A linear relationship between X-ray energies and peak centroids was obtained, as shown in Figure 3.21 for the calibration curve. This X-ray calibration was used for the identification of unknown elements.

3.8 Vacuum System.

The vacuum system is an important factor in the design and construction of a PIXE system. A system with a good vacuum is necessary to prevent energy loss and small angle scattering during transportation of the beam, from the accelerator to the target. PIXE analysis is mostly performed in an evacuated target chamber, although a number of investigators now make use of external beam to analyse samples in air. The advantage and disadvantages of an external beam approach is discussed in the sub-section 3.9.

The beam from the 3 MeV Dynamitron at the Radiation Centre is transported in a evacuated beam tube maintained at a pressure of 10^{-5} torr or better. An oil diffusion pump is employed at the

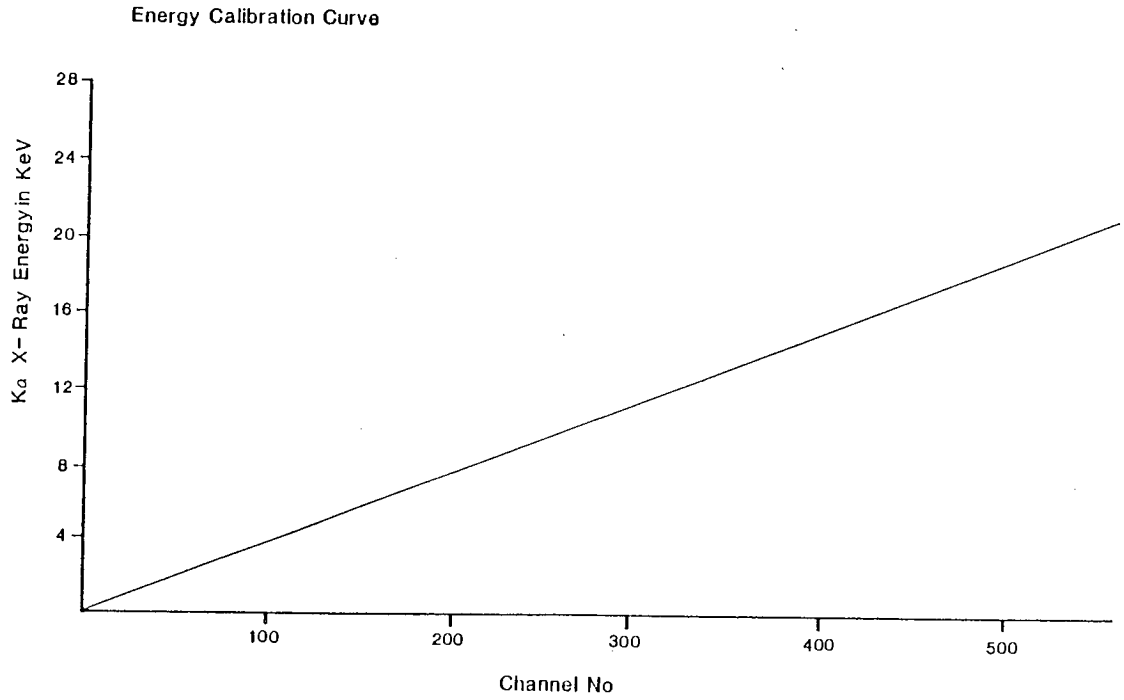

FIGURE 3.21

X-ray Energy Calibration Curve

base of the accelerator tank. Ion getter pumping is used at the target chamber end of the line to maintain the vacuum.

Stainless steel beam line and components and Viton "O" ring seals, were used to provide clean vacuum system. A cold trap was installed in the vicinity of the target chamber to preserve the clean conditions during irradiation of the sample.

Two manually operated vacuum gate valves were installed in the beam line and positioned on either side of the liquid nitrogen cold trap as shown in figure 3.10, and photograph Figure 3.22. This arrangement enabled the cold trap or scattering chamber or both to be isolated from accelerator vacuum. The working vacuum pressure in the chamber was attained in about 40 minutes. Flushing the chamber with dry nitrogen improved the pump down time by about 5-10 minutes.

3.9 External-Beam PIXE.

The usefulness of an external beam has been demonstrated by several workers, Jolly et al, 1974; Seaman and Shane, 1975; Deconnick, 1977; Khaliquzzanan et al, 1981; Raisanan, 1984;

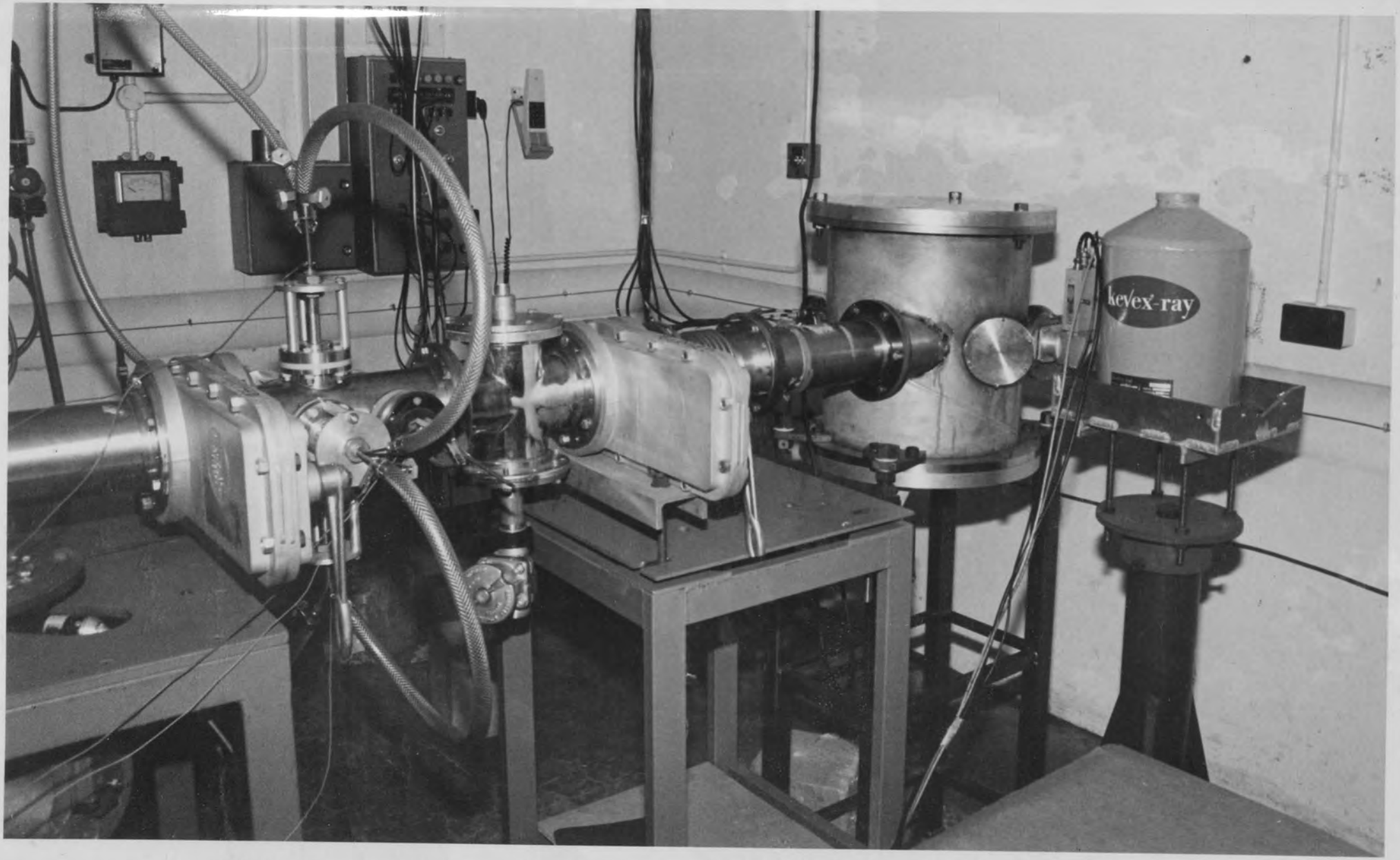

Figure 3.2.2 Beam Line: Showing Chamber and Vacuum

Eldred et al, 1984; and others. Williams, 1984 in his review article lists some thirty groups in the world currently using external-beam PIXE arrangement.

There is no essential difference from accelerator ion source to beam exit foil, between vacuum and external-beam systems. Any internal beam system can easily be modified to an external beam system. The detection and calibration method is the same for both systems.

The target chamber designed for the present work has a provision for beam exit set up to be fitted on the Faraday Cup port of the sample chamber, enabling the beam to be brought out into the air.

Helium atmospheric pressure devices have been used by many workers to avoid the presence of argon peaks due to air. Helium flow may also be used to cool the sample. Hietel et al, 1984, described a practical set up in helium at atmospheric pressure for the analysis of bio-medical samples.

Most commonly used material for the beam exit foil is Kapton (Dupont Co), this is a

polymide plastic of thickness in the range 7.5μm to 25μm. Other materials commonly used are Be and Al. While a thicker foil has the necessary strength to hold the vacuum unsupported over 10 to 15mm diameter exit hole, Bauman et al, 1979, thinner foils need some form of grid support to prevent them from rupturing over a similar diameter exit hole, Hyvonen et al, 1981.

The main advantage of external beam PIXE is that it offers convenience in terms of simplicity and subsequent economy of target holder and chamber. Objects of any shape and size with practically no sample preparations can be bombarded with the external beam. One unique example is the experiment by Baijot-Struobant et al, 1979, in which front tooth were analysed while still in the mouth of a living human patient.

Another advantage of external beam over internal beam PIXE is the freedom from problems due to the out-gassing of organic and some other samples owing to decomposition during irradiation. Also charge build-up on insulating targets particularly thick targets already discussed in the last chapter does not occur with external beam. However external beam does add to the problems of beam current measurements. Moreover

the exit foil is itself a source of disadvantage in several ways. The foil generates increased background of X-rays and gamma-rays when the beam hits the foil, Raisanen and Anthla, 1982. The exit foil reduces energy of the initial proton beam due to absorption. Beryllium foil 25μm thick induces an energy loss of 700 keV from the 1.8 Mev initial energy of protons, Summers et al, 1983. The foil has a limited lifetime with a high chance of rupture. Electro-pneumatic safety valves have been used, (Raisanen, 1984), to guard against the accelerator vacuum breakdowns. But this offsets the economical argument presented earlier in the favour of external beam PIXE system.

3.10 Rutherford Backscattering Spectrometry (RBS).

When used in conjunction with the PIXE technique RBS not only extends the range of PIXE analyses to elements lighter than sodium, Bohgard, 1984, but it also provides a powerful and well established method of depth profile analyses, film thickness measurements and determination of surface layers of bulk samples, Chu, 1978. Since these advantages make RBS an attractive complement to PIXE it was decided to incorporate the technique into the present system making it a much more versatile and valuable analytical tool.

For the simultaneous measurement of X-rays and scattered protons or alpha particles a partially depleted surface barrier detector (Ortec TA014-25-300) collimated to 2mm² was fixed at a backward direction in a solid angle ($d\Omega$) of 1.8±0.1 msr. A second surface barrier detector of similar specifications was placed under the beam and tilted upwards with the diode pointing at the ion monitoring foil for the detection of scattered charged particles.

Figure 3.14 and (photograph) figure 3.15 shows the set up of the two surface barrier detectors and an adjustable stand for the gold foil fixed 100mm in front of the target, inside the scattering chamber. The orientation of RBS1 detector was 135° relative to the incoming beam and that of RBS2 detector (placed under the beam) was 180°. Both the detectors were mounted on specially machined P.T.F.E cradles to isolate them from the target holder mechanism and target chamber to avoid any electrical interference via earthing loops.

Electrical connections to the detector were made with double screened cable inside the target chamber. Through BNC vacuum feed-throughs both

detectors were coupled by very short cables to individual preamplifiers (Ortec 142A). The signals were then fed into Ortec spectroscopy amplifiers (Model 472A) in the computer room. The amplified and shaped pulses resulting from RBS1 detector (used for film thickness measurements) were analysed by HP5416B ADC and linked for spectrum display and storage purposes to an HP2100 computer. Pulser test signals were used for rapid detector resolution and electronics verification before the beginning of the run each day.

The signals from the second SSB detector RSB2, were fed straight from the amplifier into a rate meter and scaler/timer unit. This pulse count was related to the integrated beam charge as discussed in the next chapter. A set (RBS) pulse count was used for normalising between sequential irradiation for reproducibility studies and for quantitative analysis.

3.10.1 Areal density measurements.

The uncertainty in the areal densities of the foils, used for measuring the systems F(xz) response function, were quoted by the manufacturers, Micro Matter Co as ±5%. The

measured value of F(xz) response functions (see section 4.3.2.1) for Ti foil were found to be always low by as much as 20%. It was therefore decided to measure the areal density of certain foils. To measure this quantity RBS technique was employed.

The areal density is given by :

$$(\rho t) = \frac{A_2 \, Y_B}{N_0 \sqrt{2} \left(N_p \Omega \sigma + Y_B \frac{\varepsilon(E)}{E} \right)}$$

Where (pt) denotes the target areal density, p is the mass density of the target with atomic mass A_2, Y_B is the experimentally measured back-scattered yield, Ω is the SSB solid angle, Np is the number of incident particles with energy E, σ is the Rutherford scattering cross section, $\varepsilon(E)$ is the stopping power of the particles at energy E in the target and N_0 is the Avogadro's number.

The computer programme given in appendix A2 was used to calculate the areal densities. All the foils measured were within the manufacturers specification, except for Ti foil which was found to be 12% lower than the quoted value of 71 $\mu g cm^{-2}$.

CHAPTER IV

4.0 SYSTEM EVALUATION

4.1 Introduction.

The total system for PIXE analyses consists of the various parts described in the previous chapter. Once the complete system had been installed and commissioned, the next step as with any other analytical technique is to assess its performance. The function of analysis, using the present system is to identify the various elements in an unknown sample and to determine the amount of each element present. Qualitative analysis of the unknown elements in the sample is relatively simple and is carried out by using an energy-dispersive X-ray detection system, discussed in Section 3.8.6.

Accurate quantitative analysis is also possible when a comparator standard sample, similar in nature to the unknown is available. However, in many instances where suitable standard samples are not available, PIXE's remarkable capability as an absolute method can be relied upon, (Johansson et al, 1976), but it is not easily accomplished.

The performance of the system is evaluated in

terms of its precision, accuracy and sensitivity. The precision of the system is a measure of its reproducibility. It establishes how well the system gives reproducible results for many replicate targets from the same specimen under identical experimental conditions, over a long period of time. It is dependent on random errors which evolve from the fundamental properties of the instruments employed in the measurements.

The accuracy of an experiment relates to how well the systematic errors are overcome and is of major importance if reliable quantitative analysis is to be obtained. The amount by which a measured value differs from the true value is the error of the result (Zemany, 1978). The main factors which affect the accuracy of a PIXE analysis system are the uncertainties due to sample preparation, detector geometry, charge integration, beam energy calibration, beam profile, peak and background evaluation. Hence great care and attention has to be paid to the initial system set up.

The determination of precision and accuracy is primarily achieved via a rigorous system calibration procedure.

Before proceeding with a system calibration, one of the first concerns is to assess the performance of sample chamber and beam collimation in terms of photon

background production due to scattered protons and fluorescence due to chamber components. In order to obtain the best sensitivity this background contribution has to be minimised.

4.2 Photon Background.

The central part of the diffused beam is transmitted through collimator apertures as described in sub-section 3.6.2. With this arrangement most of the beam intensity is stopped in the collimator system. The interaction of incident and scattered protons with collimator material and sample chamber components can produce a large amount of X and gamma radiation. The experimental set up, especially of the sample chamber, can thus give rise to photon background in the absence of a target or a sample in position. It is here, referred to as a "blank" background.

The source of such a background can be investigated by obtaining a "blank" background spectra. The major X-rays observed in a "blank" spectrum helps to identify the component material responsible for the contribution to the background.

The "blank" background can be reduced or eliminated by carefully covering the components with aqua-dag or P.T.F.E spray or covering the parts as seen by the detector with P.T.F.E tape.

With the present system, the "blank" background spectra at Ep = 2.5 MeV and 1.5 MeV showed no characteristic X-ray peaks and is flat over 3 to 20 keV for both detector positions of 90° and 135° with respect to the beam direction. Next an aluminium sample holder, (25 x 25 mm) and sample retaining ring with an aperture of 14mm was inserted and "blank" background spectrum obtained. Again no characteristic X-ray peaks were seen.

The beam monitoring foil, described in sub-section 3.5.7, was then inserted and the experiment repeated. The foil used in the initial stages was a platinum foil of 600um thickness,which was more robust than the gold foils normally employed for the purpose. The object was to scatter the beam through as wide an angle as possible and investigate the sample chamber background. Figure 4.1, is the X-ray spectrum obtained with detector positioned at 90° and Figure 4.2, at 135° for 2.0 MeV proton energy accumulated for 0.1 uC charge. It clearly shows a number of characteristic X-ray peaks for Mn, Fe and Ni. There is a slight difference in the "background" observed at 90° and 135° positions. The Fe peak at the backward angle is slightly more pronounced than at the normal 90° position. Sample changer mechanism parts shown in photograph figure 3.15, were covered with aqua-dag and where possible by P.T.F.E tape to mask parts seen by

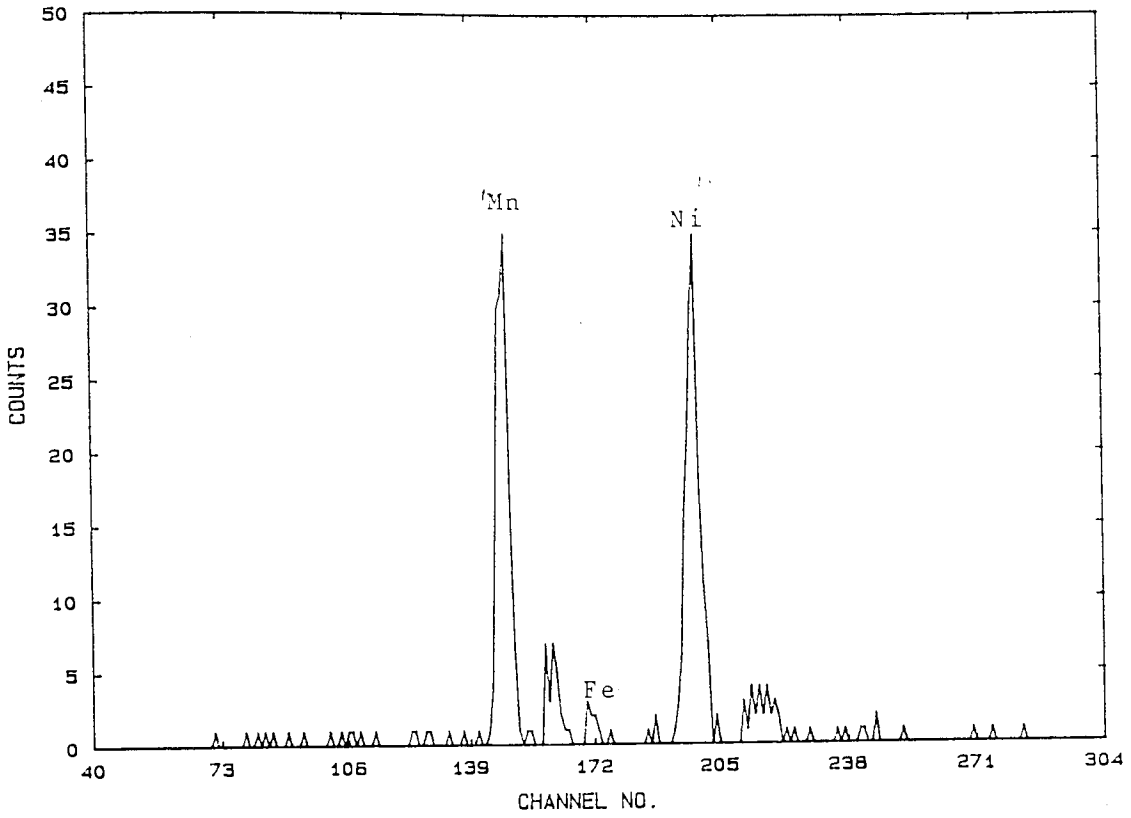

4.1 X-ray spectrum of "blank" background from the chamber with detector positioned at 90° (Ep=2.0 MeV, Q=0.1 uC)

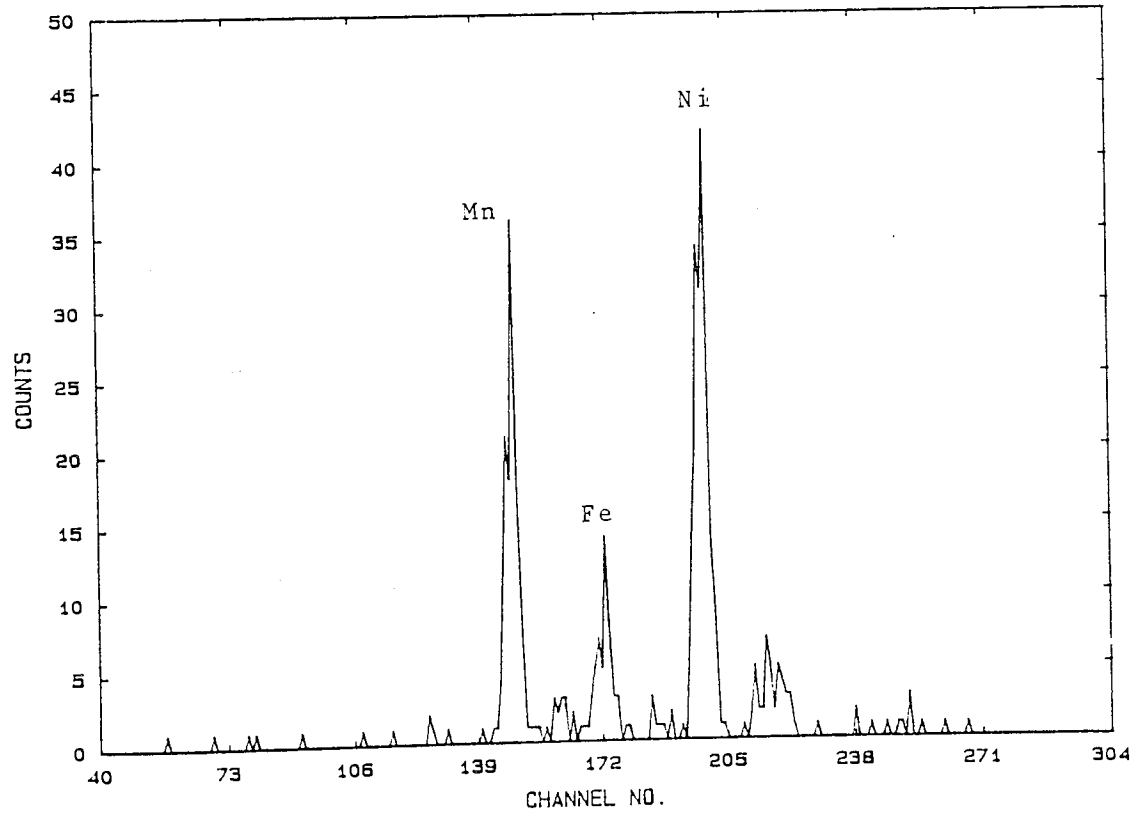

4.2 X-ray spectrum of "blank" background from the chamber with detector positioned at 135° (Ep=2.0 MeV, Q=0.1 uC)

the detector. The experiment was repeated and practically no 'chamber background' was observed.

Measurements were repeated with platinum (600μm) foil having been replaced with a thinner gold foil (200μm). The spectrum obtained showed practically no characteristic X-ray peaks in the "blank" background.

Once the system's background is eliminated or minimised, any photon "background" observed with the sample in position must be due to the sample itself. The final measurements were made using a thin Cu (59 μg/cm) target, at both 90^{o} and 135^{o} detector positions. Figures 4.3 and 4.4, shows the spectra obtained. The background was normalised in both cases to 800 Cu K_{α} peak counts in channel 211. Figure 4.3 represents the spectrum at 135^{o} and Figure 4.4 is the spectrum at 90^{o} position. Both spectra are very similar and show no characteristic X-ray peaks.

However a "blank" photon background could also arise from nuclear reactions of backscattered protons with filter or window material in front of the detector. This was not observed with the present system.

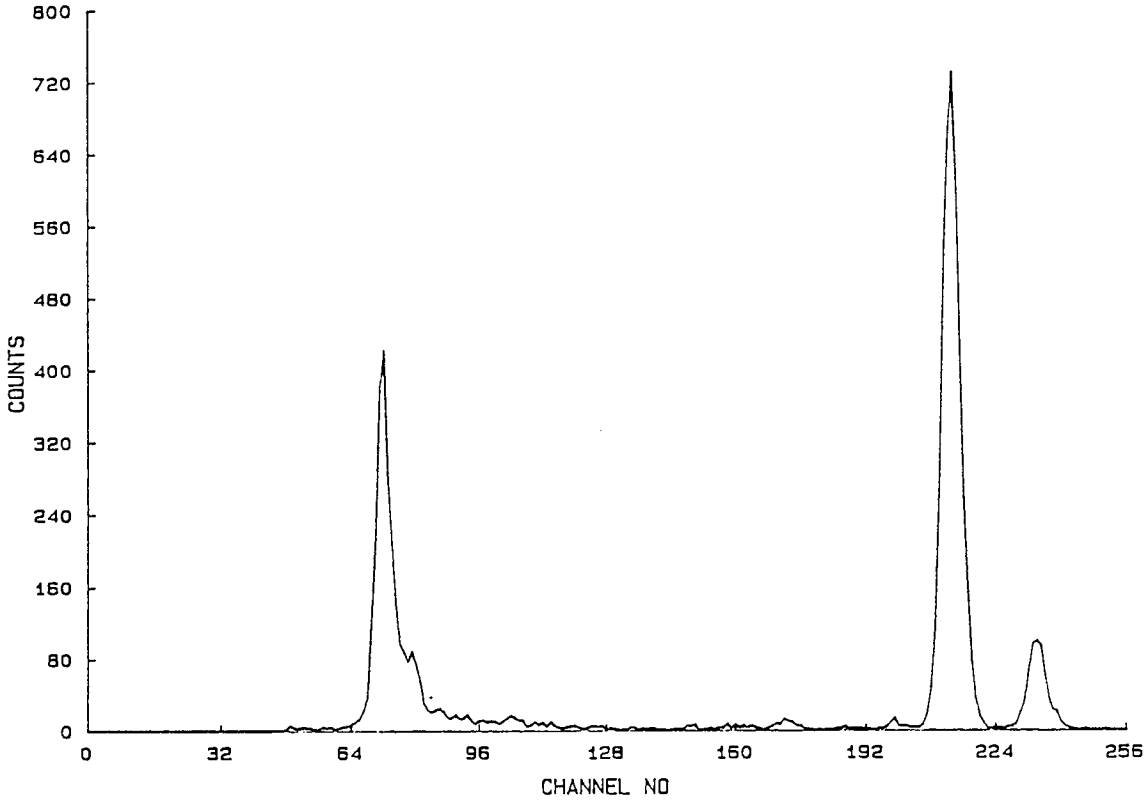

FIGURE 4.3

X-ray spectrum at 135° for thin
Cu foil on Nuclepore

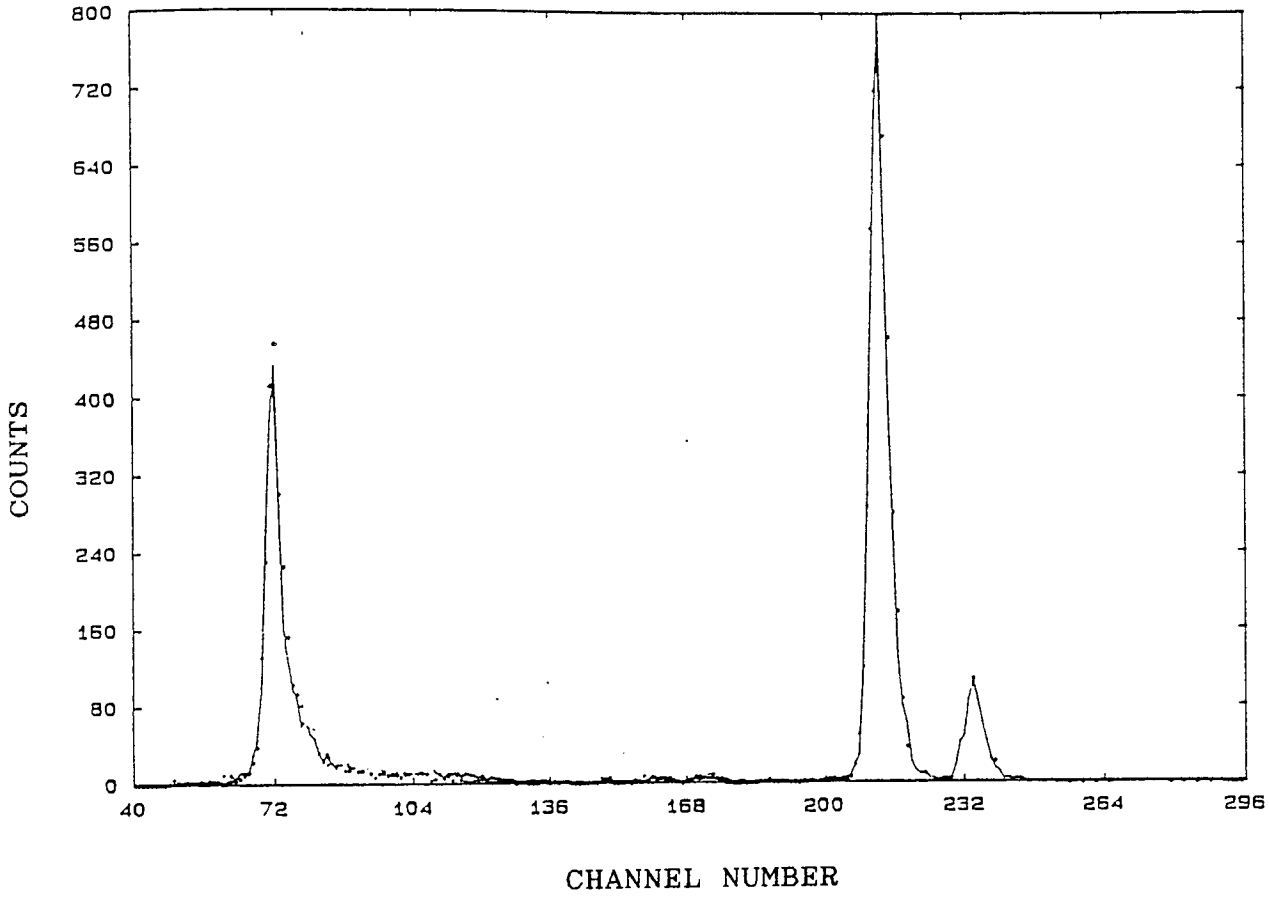

FIGURE 4.4

X-ray spectrum at 90° for thin Cu foil on Nuclepore

4.3 System Calibration.

Calibration of a PIXE system requires that the experimentally observed quantity i.e. X-ray yield Yz, observed per unit charge Q, collected on the sample, be precisely related to the physical quantity $(\rho t)z$ areal density or (Mz) mass of the element Z (μg) in the irradiated region of the sample, for all elements of interest. The relationship of X-ray yield (Yz), for a thin target assuming isotropic distribution of characteristic X-radiation and taking into account the various absorption coefficients is given by Cahill, 1975 and Khan and Crumpton, 1981, by the following expression:

$$Yz = (N/A).Q.\sigma xz(Eo).(\rho t)z.(d\Omega/4\pi).\varepsilon.CA.CW.CB....4.1$$

where,

A is the atomic weight of the element

N is the Avagadros Number

Q is the total proton charge incident on the sample (μC)

$\sigma xz(Eo)$ is the total X-ray production cross-section for K shell for element z at incident proton energy Eo.

$(\rho t)z$ is the areal density

$d\Omega$ is the detector solid angle

ε is the detector efficiency

CA, CW and CB are absorption corrections for air path, Melinex chamber window and detector beryllium window.

Since the quantities $(N/A).(d\Omega/4\pi).\varepsilon.CA.CB.\sigma xz(Eo).\omega$ are constant for a particular element and X-ray transition, fixed proton energy and detector geometry, the expression 4.1 may be written as:

$$Yz = F(xz).Q.(\rho t)z \quad \ldots\ldots \quad 4.2$$

where,

F(xz) is the system response function and is given by:

$$F(xz) = (N/A).\sigma xz(Eo).(d\Omega/4\pi).\varepsilon.CA.CW.CB \quad \ldots 4.3$$

From equation 4.2

$$F(xz) = (Yz/Q).(\rho t)z \quad \ldots\ldots \quad 4.4$$

The value of areal density $(\rho t)z$ or Mz the mass of element z can be calculated for thin sample if F(xz) value is known by:

$$(\rho t)z = (Yz/Q).(1/F(xz)) \quad \ldots 4.5$$

The above expressions show that all quantities are either known or can be experimentally determined hence making PIXE an absolute method. However this expression is only valid for the conditions that the area of sample irradiated be larger than the beam spot. Where the sample area is smaller than the beam area the value of the charge accumulated on the sample has to be calculated from the ratio of sample and beam area and from the total charge integrated on a Faraday Cup, i.e

$$Qs = Q \times (As / A_B) \quad ..... \quad 4.6$$

where,

As = area of the sample,

A_B = area of the beam.

Now equation 4.5 may be expressed as:

$$\rho t = (Yz/Q) \times (As/A_B) \times (1/F(xz)) \quad .... \quad 4.7$$

The possibility of quantitative analysis without having to use standard samples or internal standards is an important advantage over many other analytical technique. It is however, initially necessary to establish a reliable calibration of the system generally in terms of its F(xz) response function.

Once the agreement between the experimental and the theoretical F(xz) values has been established,

can tabulate the theoretical F(xz) values for all Z. Such a tabulation can then be used to determine the areal density of an unknown element using equation 4.5. This procedure of establishing a good agreement between the theoretical and experimental F(xz) values reveals the presence of any systematic error, due to experimental arrangement, and is the main consideration for achieving a calibrated PIXE system.

Several methods are available to carry out the system calibration:

1) Theoretical Evaluation of F(xz) values.
2) Experimental evaluation of F(xz) values,
   a) using elemental thin standards
   b) using standard reference materials.

An alternative approach is to calibrate the system on a relative basis using external standards as discussed later in this chapter.

4.3.1 Theoretical Evaluation of F(xz) Response Functions.

The F(xz) values for preliminary calibrations were calculated semi-empirically, since most of the values in the F(xz) response function equation 4.3,

$$F(xz) = (N/A).\sigma xz(Eo).(d\Omega/4\pi).\varepsilon.CA.CW.CB,$$

are known or can be experimentally determined.

A computer programme was written to facilitate computations of the F(xz) values. The ionization cross-sections were calculated from the polynomial given by Khan et al, 1977, already discussed in sub-section 2.4.6.2. The polynomial is valid within $20<Z<50$. For elements below $Z<20$, the $K\alpha$ X-ray production cross-sections by Johansson et al, 1976 were used.

The solid angle $d\Omega$, subtended by the detector was kept fixed for the duration of experiment, and determined by the geometry of the experimental set up. A lead collimator of 3 ± 0.5 mm thickness, with a precise aperture of 4 ± 0.5 mm was placed in front of the detector, to overcome the problem of not knowing the size of the detector accurately, owing to the presence of annular dead-layer. This arrangement allowed an uncertainty of less than 0.5%. The target aperture distance was 940 ± 2 mm for previous chamber arrangement. For the present arrangement the target aperture distance is fixed at 645 ± 1 mm at 90^0 and 970 ± 1mm at 135^0 with respect to the incident beam, figure 3.3.

A proportion of the emitted X-rays from the sample are absorbed by the following absorbers:

(i) the chamber Melinex ($C_{10}H_8O_4$) window

(ii) the air path between the Melinex and the detector

(iii) the combination of absorbers in the detector, i.e beryllium window which provides vacuum and optical shield; the gold layer on the front face of the crystal and a silicon "dead layer".

The silicon crystal is coated with a gold layer of approximate thickness of 200 Å on both front and back sides to provide electrical contact. It also has a comparatively thin silicon dead layer. The thicknesses of these layers are not specified accurately by the manufacturer. The absorption of X-ray energies employed in this work can be ignored with 0.1μm silicon dead layer but are at the most 2% in the 200 Å gold layer, (Sokhi, 1984).

The fraction of X-rays transmitted through the various absorbers described above, may be expressed as:

$$\left[\left(1 - e^{-\mu_{Si}(\rho t)_{Si}}\right) x_i . e^{-\Sigma\left[\mu_{air}(\rho t)_{air} + \mu_{Be}(\rho t)_{Be} + \mu_m(\rho t)_m\right]}\right] \quad \cdots 4.7$$

where

U_{air}, U_m and U_{Be} are the mass absorption coefficients of air, Melinex and beryllium respectively

ρt are the thicknesses that photons must transverse.

Combination of Bragg additivity rule and

weighted averages of the individual elemental constituents for Melinex and air gave:

$$U_m = 0.625\ Uc + 0.04197\ U_H + 0.3329\ U_o$$

$$U_{air} = 0.78\ U_N + 0.21\ Uo + 0.01\ U_{air}.$$

The value of U_{Be} and U_{Si} were taken from Storm and Israel, 1970.

The results of the theoretical F(xz) values are tabulated for some of the elements for 2.5 MeV protons in Table 4.1. The overall uncertainity in F(xz) calculation varies from 6% to 14.8% depending on the element. This uncertainity is due to

(i) uncertainity of the X-ray production cross-section data estimated by the authors between 6% to 10%.

(ii) The uncertainity in the measured solid angle $d\Omega$ estimated to be 1.8%.

The total uncertainity in the absorption correction $e^{-\xi\mu_i x_i}$ varied from about 4% for Cu rising to about 7.8% for K. For elements higher than Cu these uncertainties are less than 1% and can be neglected.

Satisfactory agreement was obtained between the calculated F(xz) and the experimentally measured

TABLE 4.1

System response functions F(xz).

Ep = 2.5 MeV

F(xz) counts/$\mu C \mu g cm^{-2}$

Elements	Experimental	Calculated	Ratio exp/the
Si	3 ± 1	2.8 ± 1.4	1.07
P	50 ± 5	44 ± 7	1.13
S	228 ± 14	218 ± 16	1.04
Cl	613 ± 41	542 ± 60	1.13
K	995 ± 55	1168 ± 127	0.85
Ti	1066 ± 58	1198 ± 135	0.88
Mn	828 ± 44	841 ± 66	0.98
Co	548 ± 30	569 ± 44	0.96
Cu	351 ± 18	364 ± 24	0.94
Ga	183 ± 8	229 ± 18	0.80
Rb	49 ± 3	52 ± 4	0.94
Y	32 ± 2	31 ± 3	1.03
Mo	16 ± 1	15 ± 1	1.06

values. These also are given in Table 4.1 for comparison.

4.3.2 Experimental Evaluation of F(xz) Value.

4.3.2.1 Using Elemental Thin Standards.

The approach of calibrating a PIXE system with an external set of thin standard foils of elements or compounds of known areal density is widely used. These foils can be with or without backing, depending on the preparation method and the thickness. Suitable thin standards in the range of 10 to 100 $\mu g/cm^2$ are readily available from a variety of sources.

A target is described as thin if energy loss of the proton beam and the X-ray absorption is negligible. Campbell, 1977 has adopted a definition of thin target as one when the effective ionization cross-section σ_E is 5% less than σ_{E0} and this criteria is used here for all thin sample definitions.

Standard foils from Micro-Matter Co RT 1 Box 72-B, Eastsound, WA, USA 98245, of 14 elements or compounds, in the range $14<Z<42$ were selected for calibration of the system. The standards consisted of a 20 to 71 $\mu g/cm^2$ vacuum evaporated single element or compound layer on a thin Nuclepore filter. Nuclepore, a

polycarbonate has an approximate areal density of 1mg/cm^2. According to the manufacturer the specified thickness are accurate to within $\pm$5%.

Data obtained from the irradiation of these standards with protons of energies 1.00, 1.20, 1.50, 2.00, 2.50 and 3.00 MeV is used to generate a family of calibration curves. The F(xz) values were calculated from equation 4.4. The typical values used for 2.5 MeV proton energy for elements Si, S, P, Cl, K, Ti, Mn, Co, Cu, Ga, Ge, Rb, Y, and Mo are given in Table 4.2, for the previous system and in Table 4.3 for the present system at 90°. The number of K X-rays per unit charge (μC) and unit mass of element were plotted against atomic number Z for different proton energies. A best fit smooth curve is determined and used as the standard calibration curve of proton energy of interest. A family of response functionsF(xz) plotted against atomic number Z are shown in Figure 4.5 for the previous system and in Figure 4.6 for the present system.

A complete calibration of the system with the X-ray Si(Li) detector positioned at 135° with respect to the incident beam was also undertaken for proton energies of 1.50, 2.00 and 2.50 MeV and is given in Table 4.4. Figure 4.7. shows the response function values plotted against atomic number Z.

TABLE 4.2

Experimental F(xz) response functions
at 2.5 MeV proton energy (previous system).

Z Element	Yz counts	Q (μC)	ρt.√2 Areal desity	F(xz) Counts/ μC/μgcm^{-2}
Si	455	3.5	44.2	2.94 ± 0.3
S	1230	1.5	19.1	42.9 ± 3.4
P	2287	0.5	28.3	161 ± 14
Cl	1446	0.1	23.5	615 ± 32
K	2921	0.1	25.9	1125 ± 45
Ti	3090	0.05	58.0	1065 ± 68
Mn	3959	0.05	100.4	789 ± 29
Co	1927	0.1	35.4	544 ± 27
Cu	1983	0.1	56.6	351 ± 20
Ga	1132	0.3	20.6	183 ± 11
Ge	1732	0.15	76.4	151 ± 9.3
Rb	1172	1.0	23.7	49.5 ± 2.4
Y	1635	1.5	33.8	32.2 ± 2.1
Mo	1278	1.5	52.8	16.1 ± 1.1

TABLE 4.3

F(xz) response functions (present system)
Detector position 90 ^{0}

Element	Ep = 1.5	Ep = 2.0	Ep = 2.5
Si	60.8 ± 3.61	71.7 ±3.82	77.4 ± 3.92
P	407 ± 24.6	478 ±24.4	518 ± 27.3
S	1035 ± 60.5	1383 ±69.7	1402 ± 71.8
Cl	1883 ± 82.3	2511 ±128	2635 ± 140
K	2582 ± 124	3670 ±188	4253 ± 218
Ti	1068 ± 54.7	2090 ±109	3002 ± 154
V	1252 ± 65.3	2008 ±102	2943 ± 152
Mn	750 ± 39.4	1372 ±69.8	2101 ± 107
Fe	582 ± 29.9	--	1605 ± 82.4
Co	433 ± 21.2	894 ± 45.8	1289 ± 65.8
Cu	284 ± 14.2	547 ± 23.6	849 ± 44.9
Ga	147 ± 7.82	320 ± 16.9	--
Ge	113 ± 5.98	250 ± 12.7	395 ± 19.8
Y	16.8 ± 0.89	33.1 ± 1.78	59.3 ± 2.52
Mo	7.52 ± 0.16	15.5 ± 0.78	27.8 ± 1.42

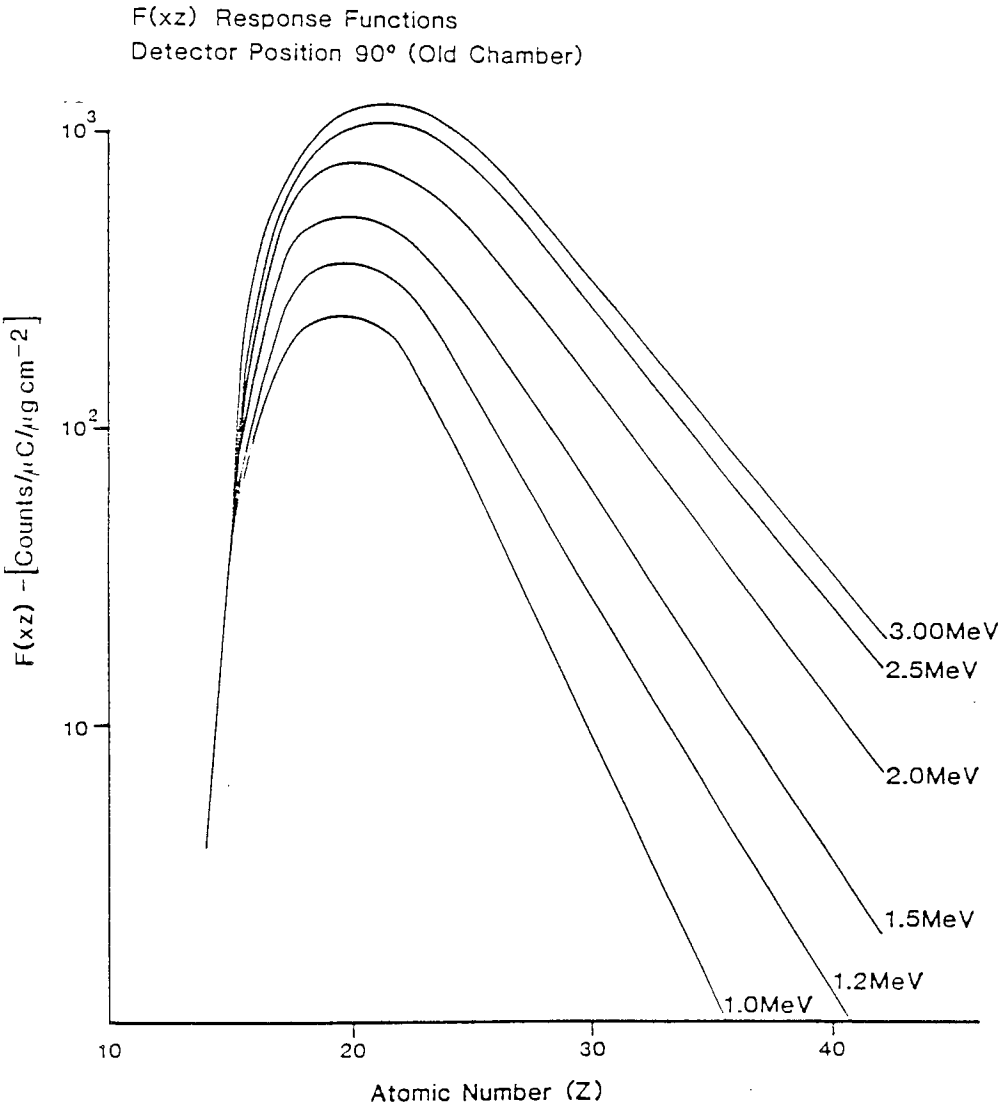

FIGURE 4.5

System response functions (Fxz) for previous system

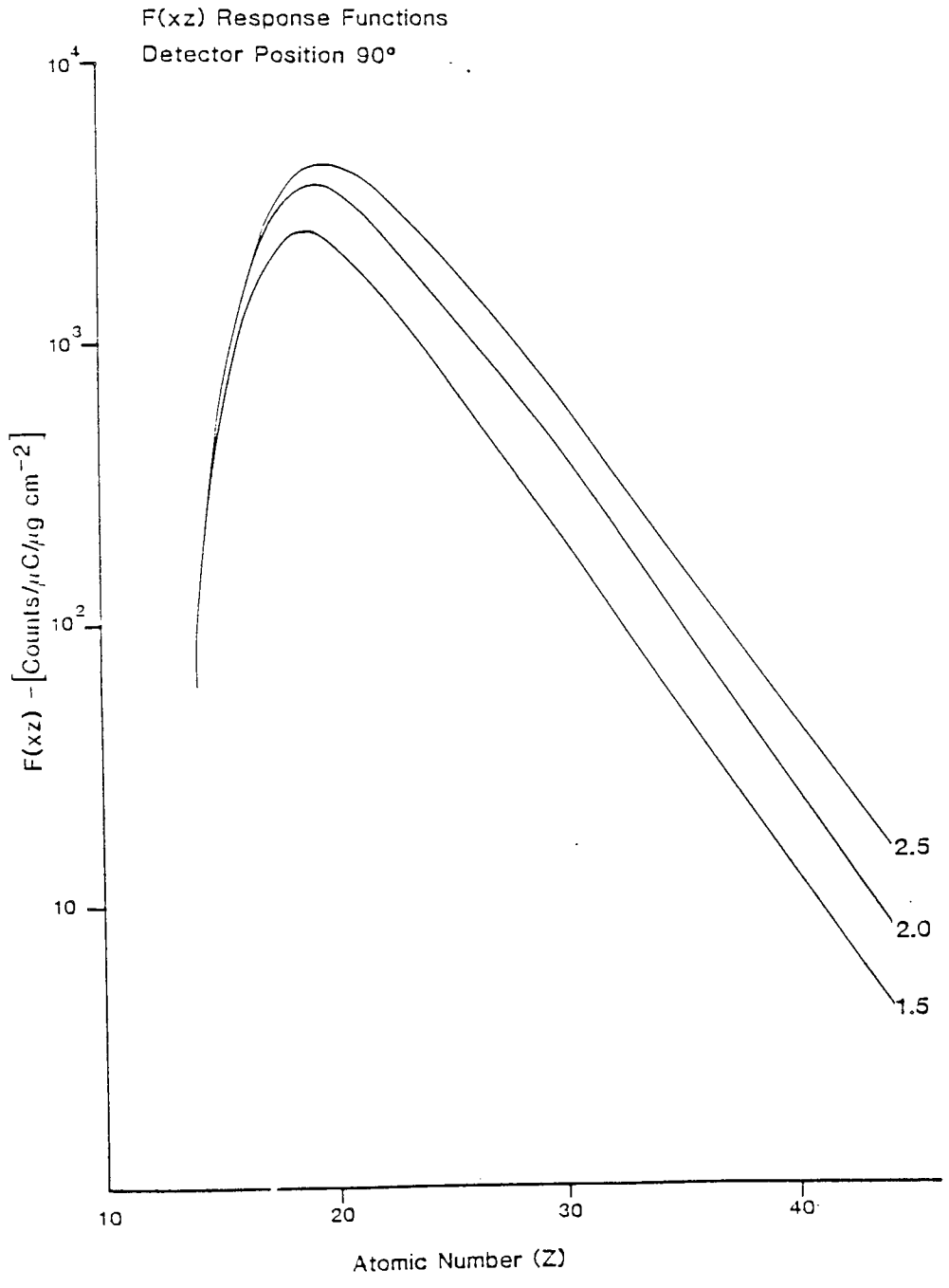

FIGURE 4.6

System response functions (Fxz) for present system (at 90°)

TABLE 4.4

F(xz) response functions (present system)
Detector position 135°

Element	Ep = 1.5	Ep = 2.0	Ep = 2.5
Si	22.7 ± 1.1	16.9 ± 0.96	11.5 ± 0.68
P	200 ± 11.2	148 ± 8.70	100 ± 6.01
S	703 ± 37.9	339 ± 20.3	320 ± 19.2
Cl	1470 ± 88.3	931 ± 55.8	534 ± 32.1
K	2247 ± 135	1352 ± 81.1	854 ± 51.8
Ti	1465 ± 77.6	--	--
V	1504 ± 86.6	--	--
Mn	980 ± 59.3	535 ± 32.1	250 ± 15.0
Fe	814 ± 48.6	--	--
Co	662 ± 40.0	350 ± 21.0	--
Cu	404 ± 24.2	201 ± 12.1	91.0 ± 5.51
Ga	--	124 ± 7.45	53.8 ± 3.18
Ge	185 ± 9.94	--	--
Y	31.7 ± 1.86	14.2 ± 0.85	5.80 ± 0.35
Mo	14.5 ± 0.84	6.50 ± 0.39	2.55 ± 0.15

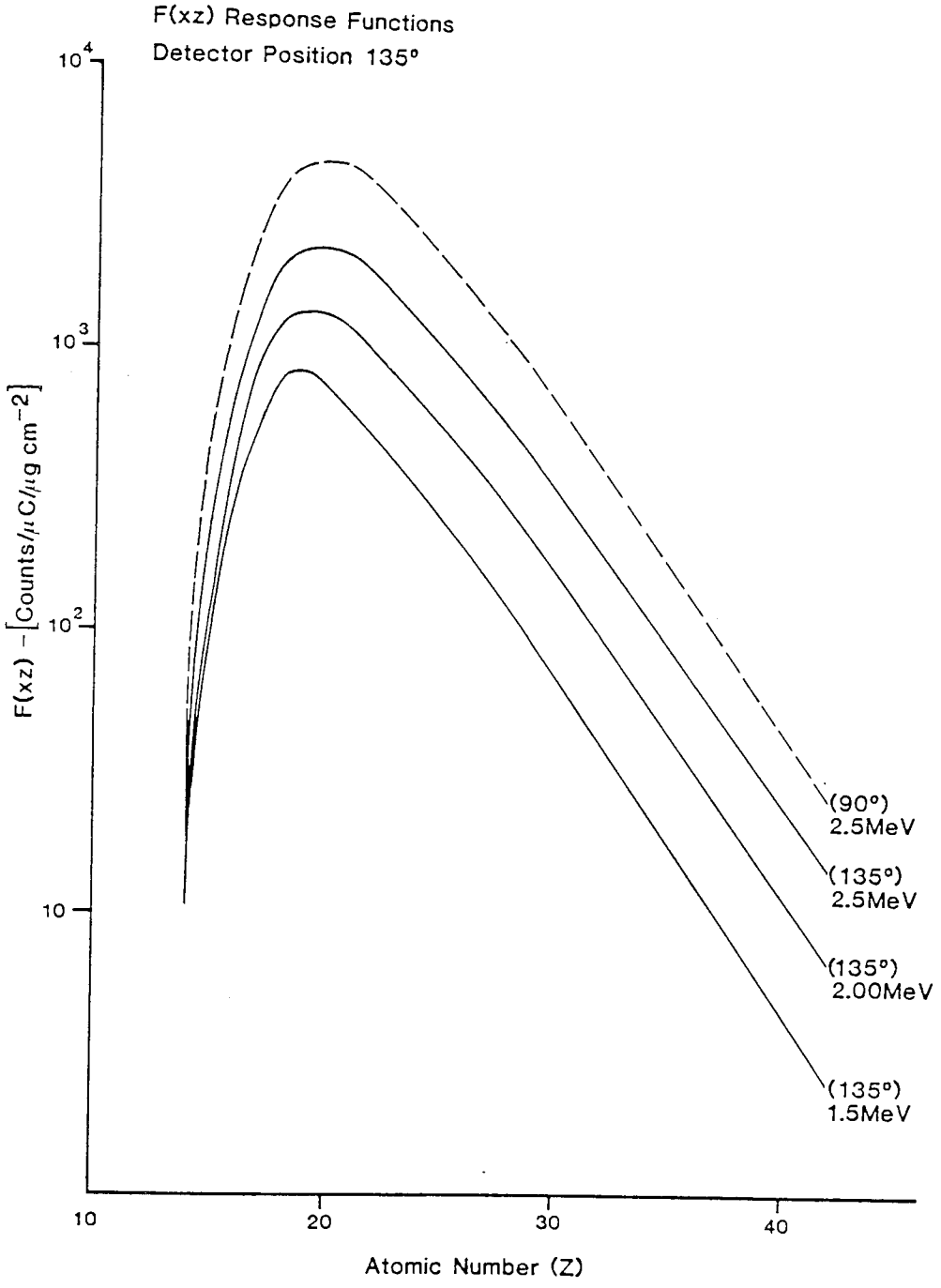

FIGURE 4.7

Response functions (Fxz) at 135°

As the target was positioned at 45° to the incident beam, modified values of areal densities ($\rho t.\sqrt{2}$) were used for the calculations of F(xz) response function.

The X-ray yield as discussed previously is predominantly determined by the X-ray production cross-sections σ_{x}^{Prod}, which in turn, is strongly dependent on the energy (Eo) of the incident proton beam and on the atomic number Z of the target atoms.

The F(xz) response curves (figures 4.5, 4.6 and 4.7) clearly indicate higher X-ray yield (Yz) measured per unit of proton bombarded and per unit mass of element for all targets of atomic number $14 \leq Z \leq 42$, with increased incident proton beam energy.

However the response curves are seen to peak in the region of $18 < Z < 24$ and drop on both the low and the high Z sides. For the low Z elements, since the X-ray ionisation cross-section (σ_{x}^{ion}) are higher compared to high Z elements one expects the measured X-ray yield (Yz) and hence the F(xz) value of the response functions, to go up rather than drop down as seen in practice. The drop at the low energy (low Z) region is due to the combined effects of:

(i) increased absorption losses of soft X-rays in absorbing windows and air passage

discussed earlier

(ii) decreasing values for the fluorescence yield (Krause, 1979)

(iii) the falling detector efficiency of Si(Li) detector used (Sokhi, 1984).

The high Z (high energy) fall-off in the F(xz) value of the response curves is predominantly due to the rapidly decreasing X-ray production cross-section $\sigma_{x}^{Prod} \propto 1/Z^{12}$, equation 2.6, and falling detector efficiency.

The uncertainties which contribute to the final uncertainties in the system response function F(xz), determined using this method are mainly due to :

(i) counting statistics

(ii) areal density ($\mu g/cm^2$)

(iii) beam energy

(iv) beam integration.

The statistical uncertainty in a peak of an X-ray spectrum is given by $(Nt+Nb)^{1/2}$ where Nt is the total number of counts in the peak and Nb is the background under that peak. Since statistically well defined single peaks were involved in this experiment, the precision of spectrum evaluation varies between 1% and 3% for largest and smallest peak. The precision

becomes worse for small peaks sitting on a high background.

The accuracy of the areal densities of the thin standard foils (Micro Matter) is quoted by the manufacturer as +/-5%. Areal density measurements, using RBS technique, were made to check the uncertainties. The experimental F(xz) values for Ti foil were found up to 12% below the values obtained from F(xz) response curves. These results of the thickness measurements are discussed later.

The beam obtained from the accelerator is not entirely mono-energetic, there is a ripple of about 3 keV FWHM when using protons. Any fluctuations in the the proton beam energy contributes to the uncertainty in elemental X-ray yield. The uncertainty in the beam energy is estimated to be less than 10 keV at 2.5 MeV resulting in a X-ray yield error of 1.6% for the samples.

The uncertainty in the beam integration to measure the total accumulated charge can arise from instrumental error and leakage current problems. The uncertainty due to the instrumental error is of the order of 1% at full scale deflection. The leakage current errors are difficult to assess directly. Two separate methods, both relying on RBS (Rutherford backscattering) technique:

(i)elastic backscattering from the target as described in sub-section 3.5.6.

(ii)the foil ion beam monitor as discussed in sub-section 3.5.7.

were used to compare total integrator pulses and X-ray yield measured over a 1000 RBS counts from Au ion beam monitor. The standard deviation for beam integrator pulses was found to be 119.25, where as the standard deviation for the X-ray yield was only 9.48. The standard deviation for elastic backscattering from the target was 20.59.

The total uncertainties due to contributory error in the quantities, Yx, ρt and Q for the experimental F(xz) values are combined together and estimated as $\pm$9% for the smallest peak.

4.3.2.2 Using Standard Reference Material.

Standard References Materials developed by the National Bureau of Standards (NBS), Washington, provide another method of calibrating a PIXE system. The concentration in the Standard reference materials, for all major and trace elements are certified by NBS.

The usefulness of the Standard reference

materials for calibration purposes lies in its known accuracy of constituents, determined by different laboratories. Hence it provides an excellent means for inter-laboratory comparison.

The preparation and evaluation of two common standard reference materials, SRM-1571, Orchard Leave, and SRM-1577, Bovine Liver have been discussed by La Feur, 1974.

Analysis of a homogeneous Bovine Liver (SRM-1571) sample was used for providing a check on the present system. It was made up into a sample by digesting 250mg of bovine liver in 6.0ml of nitric acid and depositing 3μl of the digested solution onto Kimfol backing. The sample was bombarded with 2.5 MeV protons, for a total charge of 25μC collected on the sample. Table 4.5 gives the results for the present system and their comparison with other workers measurements, Saied 1981; Pallon and Malmquist, 1981; Maenhaut et al, 1980.

The agreement between the present measured values and values reported by other workers is reasonable. The results were solely used as a check for the overall accuracy of the new system rather than as a means for system calibration.

Element	NBS	Maenhaut (1980)	Pallon (1981)	Saied (1981)	Present work
K	9700 ± 600	5000 ± 700	8594 ± 352	7700 ± 1400	10050 ± 596
Ca	123	90 ± 13	178 ± 21	-	120 ± 17
Mn	10.3 ± 1.0	8 ± 1	10.24 ± 0.3	9.63 ± 0.83	10.3 ± 1.3
Fe	270 ± 20	248 ± 16	242 ± 9	262 ± 18	290 ± 38
Cu	193 ± 10	179 ± 16	170 ± 4	182 ± 13	193 ± 11
Zn	130 ± 10	116 ± 18	120 ± 9.2	132 ± 10	136 ± 10
Se	1.1 ± 0.1	1.0 ± 0.2	0.9	1.05 ± 0.16	0.94 ± 0.88
Rb	18.3 ± 1.0	9.9 ± 1.6	17.5 ± 1.0	18.3 ± 2.0	18.7 ± 1.0

TABLE 4.5 ELEMENTAL LENELS IN BOVINE LIVER (SRM - 1571)

4.3.3 Use of Internal Standards.

The addition of an internal standard to the sample provides an alternative technique of effecting relative calibration. A known amount of the standard is mixed with the unknown sample and the "spiked" sample is then irradiated. Relating the X-ray yields from the known amount of standard with those from the sample forms a basis of relative calibration.

A number of workers have reported the use of this method in the analysis of a wide range of samples, Valkovic et al, 1974; Ishii et al, 1975; Campbell, 1975; Barrette et al, 1976; Torrisi 1982; Badica, 1984; Sousavi-Yeganeh, 1984.

Biomedical samples were analysed using ytterium as an internal standard. Figure 4.8, shows the resulting spectrum from one of the samples spiked with 1000 ppm (μg/ml) of ytterium. The areal density (ρt)s for the standard and (ρt)z for an element of interest is given by equation 4.4. If Ys is the X-ray yield detected for standard and Yz for element of interest then:

$$(\rho t)s = Ys/(Q.F(s)) \quad \ldots\ldots \quad 4.7$$

and

$$(\rho t)z = Yz/(Q.F(z)) \quad \ldots\ldots \quad 4.8$$

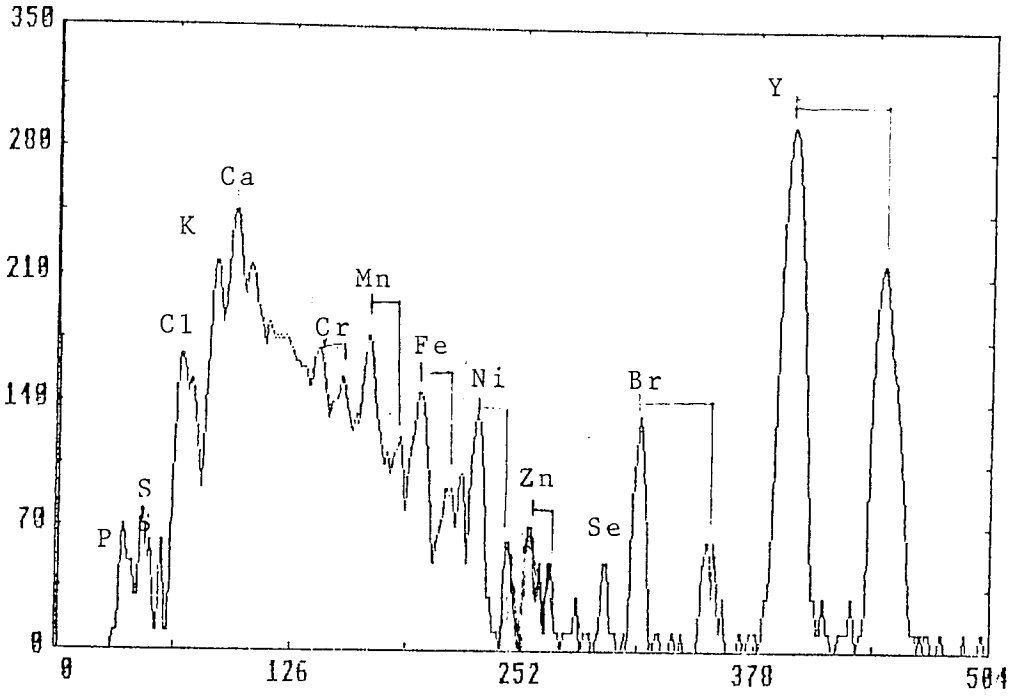

FIGURE 4.8

Typical spectrum of amniotic fluid
spiked with yttrium (1000 ppm)

where, s and z refer to the standard and the element of interest respectively.

Hence

$$(\rho t)z = (\rho t)s.(Ys/Yz).(F(s)/F(z))$$

Since the standard and the unknown sample element constitute the same sample, the mass of the element M(z) can be determined

$$M(z) = M(s).(Yz/Ys).(F(s)/F(z))..4.9.$$

where the ratio F(s)/F(z) is obtained from the relative calibration curve.

This technique has an advantage over "absolute" calibration method in terms of better accuracy, as the uncertainties in relative measurement are certainly smaller than those in "absolute" values, such as ionization cross section and absolute efficiency of system's detector, especially at low energies. Moreover any systematic errors are likely to affect the standard and the sample elements by the same amount, hence it virtually cancels out any variations in parameters such as beam energy and charge integration.

However, this method is not suitable for certain types of samples, i.e microtome slices of tissue materials and for very small quantity of powder

samples, due to the difficulties in achieving a homogeneously 'doped' sample. Samples in the form of solution are obviously most suited to internal standardization.

4.4 Sensitivity.

4.4.1 Introduction.

There are several ways of defining the sensitivity of the system as pointed out by Curie (1968). The most basic definition of sensitivity for an analytical system is its minimum detectable limits (MDL), or in other words the lowest concentration of trace element that it can detect. At low concentration the 'peak height' resembles the 'background' and the problem is that of distinguishing a true peak from spectral background or noise. The signal-to-noise ratio effectively determines the smallest quantity of an element of interest that can be detected and hence defines the sensitivity of the system.

4.4.2 Definition.

The standard definition of statistical significance according to the International Union of Pure and Applied Physics, (IUPAP), is that the number of counts in the peak must be three times greater than the uncertainty in the background counts within an interval equal to the width of the peak. This definition is given as :

$$Nx = 3(Nb)^{1/2} \quad \text{---} \quad 4.10$$

where Nx is the number of counts in the peak and Nb is the number of counts due to background under the peak.

In the present work this criterion is used in evaluating the minimum detectable limits. Maenhaut et al, 1980; Aprilesi et al, 1984; Khaliquzzaman et al, 1984 also used the above criterion for their work. Other workers have used different criteria, such as :

$$Nx = 2(Nb)^{1/2} \quad \text{---} \quad 4.10\,a$$

used by Flocchini et al, 1972; Ahlberg et at, 1976; Mommsen, 1978.

Folkmann et al, 1974, used a more popular definition requiring a peak to background ratio of 1 or greater than 1 for positive identification within a

window width equal to the peak width. Their results, Figure 4.9, for theoretical minimum detectable limits for all trace elements from 10<Z>70, for proton beam energies of 1, 2, 4, 7 and 10 MeV were calculated using this criteria.

With the convention $N_x = N_b$, because the peak to background ratio remains constant, it suggests that by optimising parameters such as beam energy, integrated sample charge, sample backing etc., no improvement in minimum detectable limit should take place. This is contrary to experience, optimising the above mentioned parameters does improve the sensitivity of the system considerably. Hence using this criteria may lead to erroneous conclusions.

4.4.3 Sensitivity and Backing Material.

Central to any analytical technique is the problem of sample preparation. When thin samples are prepared for excitation by charged particles the material to be analysed is normally deposited on some suitable backing. The properties of the backing material, as discussed below, and its thickness affect the sensitivity of PIXE analysis. The choice of backing material was based on the following characteristics

(a) absence of energetic characteristic X-rays

Aston University

Illustration has been removed for copyright restrictions

FIGURE 4.9

Calculated minimum detectable concentration as a function of atomic number Z, for 1-10 MeV proton energy (from Folkmann,1974a)

(b) freedom from impurities

(c) high mechanical strength

(d) good electrical and thermal conduction

The backing material must consist of low-Z elements so that the backing itself does not contribute any characteristic X-rays to the spectrum. For the same reason it should be free of impurities. The backing should ideally be of minimum thickness since bremsstrahlung produced is proportional to the sample thickness.

Some of the backings that have been used successfully by various workers include carbon foils, Mylar (Du Pont Co.), Kimfol (Kimberly-Clark Co.), Nuclepore (Nuclepore Co.), Formvar (Mansanto Co.), Millipore (Mllipore Filter Co.), Kapton (Du Pont Co.) A wide range of different backing material including carbon, aluminium and commercially available plastic material have been studied by several workers, e.g. Johansson, 1976; Thomas et al, 1974; Mangelson, 1974; Sharon, 1977; Walter and Willis, 1977; Valkovic, 1980; Folkmann et al, 1974; Russel et al, 1981 and Campbell, 1981.

Carbon foils have two main advantages over polymer foils.

(i) They are not attacked by acids, and thus

prove useful where samples are prepared in concentrated acids using the digestion method.

(ii) They can withstand very high beam currents and are thus excellent for the analysis of very small amounts of sample material.

The main disadvantage with these foils is their fragility. They are very easily ruptured hence are not suitable for extensive handling or for work involving a great number of samples. Bussel et al, 1981, investigated a range of different foils and found carbon foils to be most useful for PIXE analysis.

Figure 4.10 shows a typical background spectrum obtained by irradiating a carbon foil obtained from Micro Matter Co., with 3.00 MeV protons. Intense characteristic peaks are present, indicating either impurities in the foil or most probably contamination of the foil from water during the mounting process. Hence these foils were not used as backing for specimen analysis in the present work.

Other backing materials investigated were Nuclepore and Kimfol. The selection of these foils were based on the work of Sharon, 1977; Campbell, 1977 and Walter and Willis, 1977, who showed Nuclepore as the best overall backing material for PIXE analysis. Russel et al, 1981, found Kimfol as most attractive of

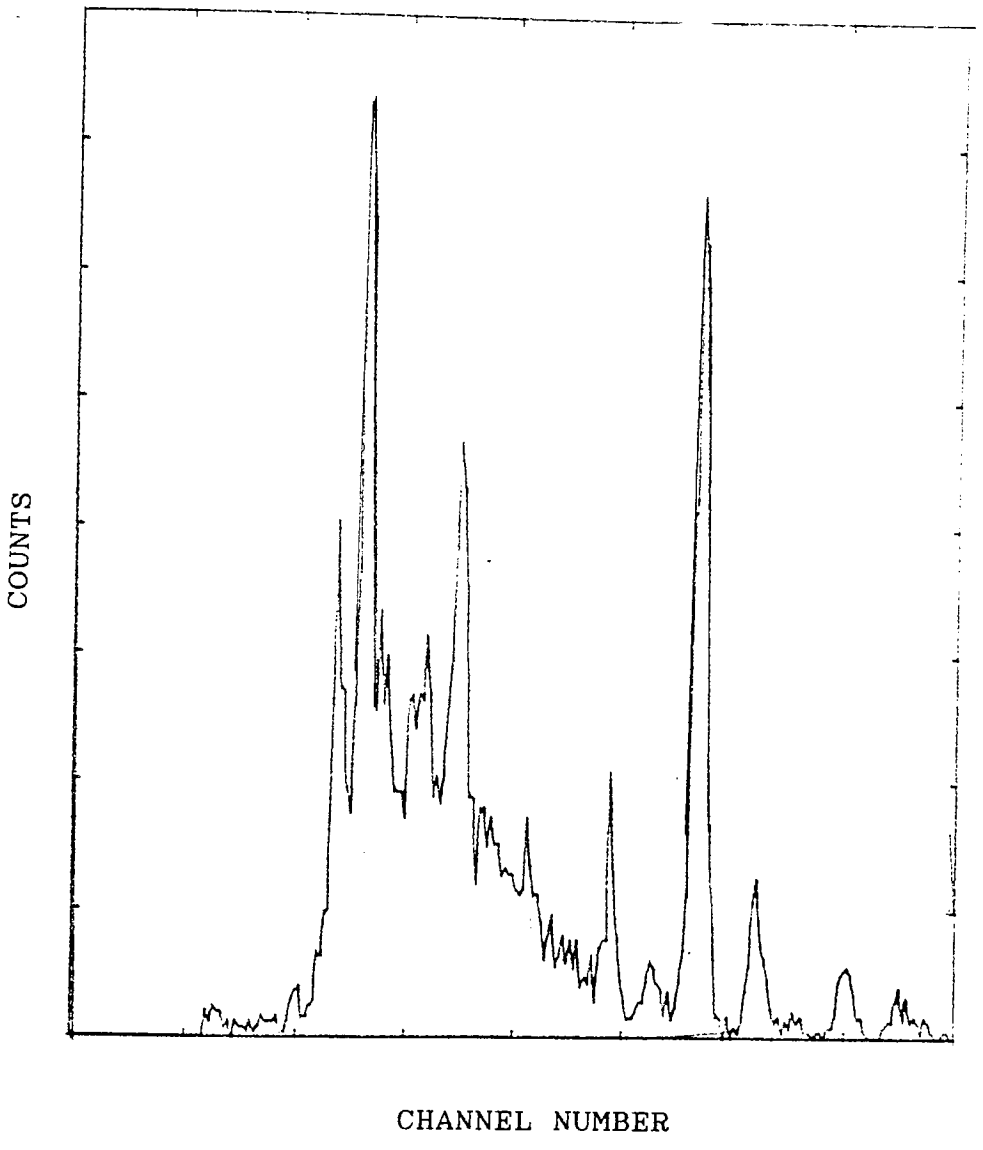

FIGURE 4.10

The background spectrum of a carbon foil shows impurities in the foil

major commercial plastics as backing material. Hence Nuclepore and Kimfol were used as backing material in this work.

4.4.4 Background and Beam Energy.

Both Kimfol and Nuclepore backings were irradiated with protons of energies 1.5, 2.0 and 2.5MeV. The background spectrums were obtained for 30 μC to 50 μC charge. The total charge accumulated was noted and background counts in the region of interest calculated per μC.

Experimental results for different incident proton energies and the effect on the measured background is shown in Figure 4.11, for Nuclepore backing. Spectra were obtained using the previous PIXE system at proton energies of 1.0, 1.5, 2.0, 2.5 and 3.0 MeV, Comparison of spectra shows a clear shift in Tm, i.e shift towards low energies with lower proton beam energy (Ep) since Tm is proportional to Ep.

Figure 4.12 show comparison of background measurements for substrate Kimfol (5 μm) and Nuclepore (10 μm), made under similar experimental conditions and for the same charge. The average integrated background counts were found to be 180 and 240 for Kimfol and Nuclepore respectively in the region 2keV to 6keV for

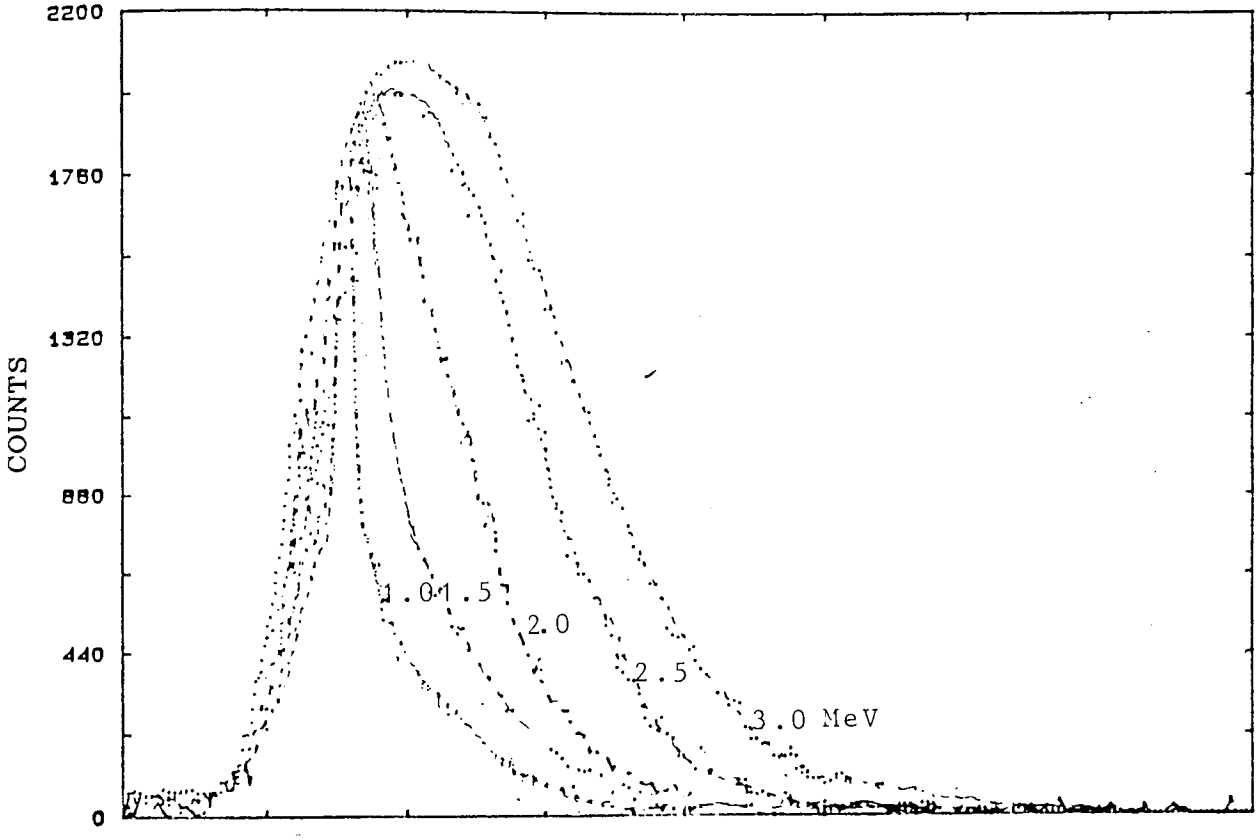

FIGURE 4.11

The background spectra obtained by irradiating Nuclepore backing at proton energies of 1.0, 1.5, 2.0, 2.5 and 3.0 MeV

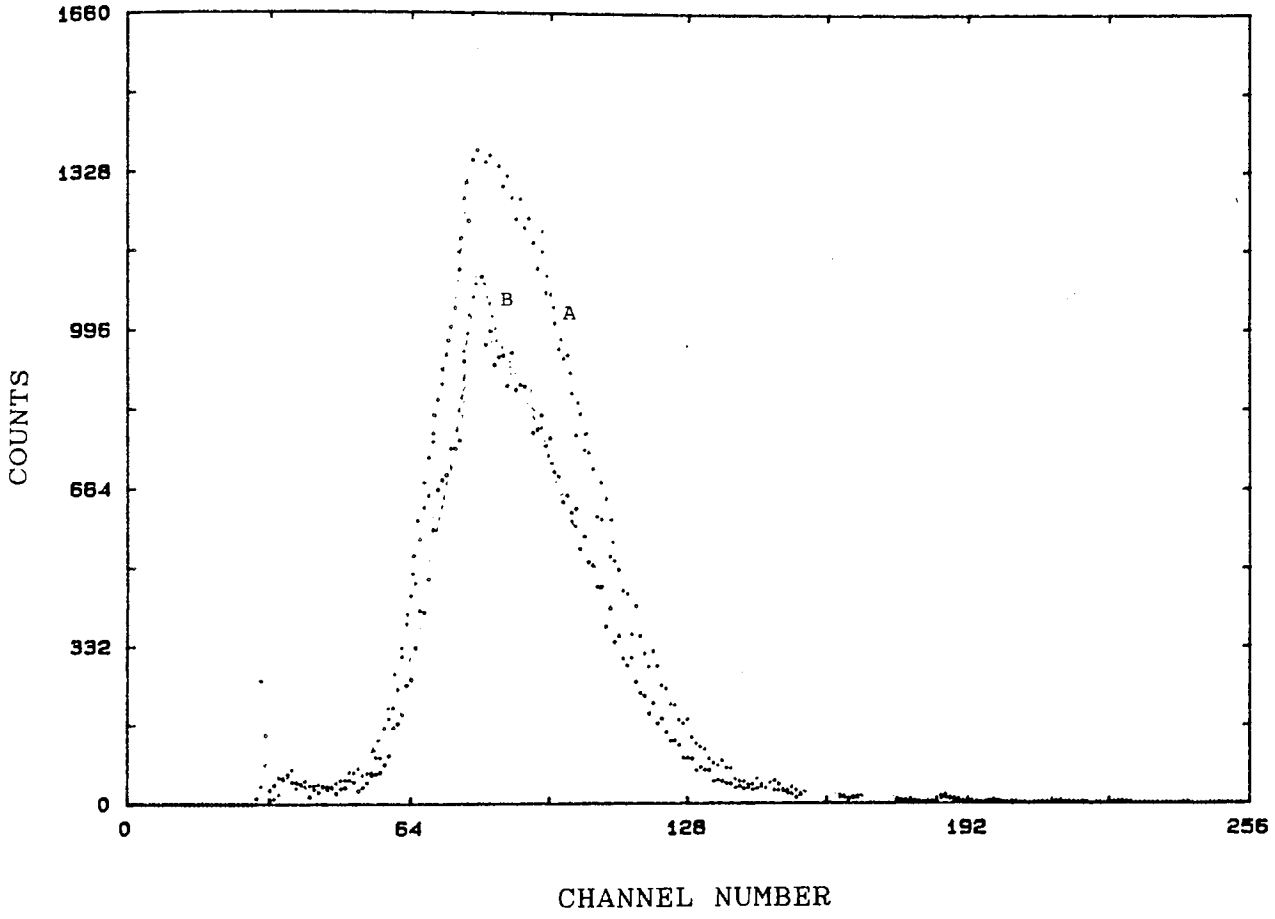

FIGURE 4.12

Comparison of background spectra measured for Nuclepore and Kimfol at 2.00 MeV proton energy for 1μC charge

over 10 foils irradiated at proton energy of 2.00 MeV for 1μC charge. This demonstrates clearly that the thinner substrate (Kimfol) produces less background compared to the thicker (Nuclepore) backing.

4.5 Measurement of Angular Distribution of bremmstrahlung.

With most PIXE systems excited X-rays from the sample are measured with a detector positioned at 90° with respect to the incident beam. Ishii et al, 1977; Kaji et al; 1977 and Folkmann et al, 1984, have studied both theoretically and experimentally the angular distribution of secondary electron bremsstrahlung. Their results suggest that PIXE measurements should be made at the largest backward angle as possible, because a substantial reduction of the continuum radiation is encountered. In addition the number of elastically scattered protons which may reach the detector is also at a minimum. Hence the sensitivity is much improved at backward angles compared with 90° which has been usually adopted. Campbell et al, 1981, however demonstrated that for their PIXE system the decrease in bremmstrahlung afforded by the backward angle of 135° relative to 90° was offset by the loss of efficiency.

The detector solid angle ($d\Omega$) at 90° was found to be

3.02×10^{-3} stradians and in the backward direction of 135^0 the solid angle $d\Omega$ was measured to be 1.34×10^{-3} stradians. Hence, if all other parameters are unchanged solid angle alone would reduce the detector efficiency in the backward direction by 44%. The total number of counts in a 20 channel width were measured at Ep= 2.5 MeV for 1.0 μC at 90^0 and 135^0 found to be 18,614 and 10,984 counts respectively. Hence, a reduction in the backward direction amounted to approximately 41% compared to the background at 90^0 .

Kimfol and Nuclepore backing material as well as thin Cu (50 μg/cm2) and SiO (67 μg/cm2) standards on Nuclepore backing were irradiated at both 90^0 and backward angle of 135^0. The standards were used in this study to normalise the characteristic Kα peak of the element (Cu or Si) to a set value for comparison of X-ray spectra measured at different angles. Results were obtained for proton bombardment at energies of 1.5, 2.0 and 2.5 MeV.

An example of results obtained is shown in Figure 4.13, for Si at Ep = 2.00MeV and Figure 4.14, for Kimfol at Ep = 2.5 MeV. A clear reduction in the bremmstrahlung at 135^0 position is observed in both cases and is in good agreement with results of Kaji et al, 1977, Chu et al, 1977 and Folkmann et al, 1984. Results of Chu et al are reproduced in Figure 4.15.

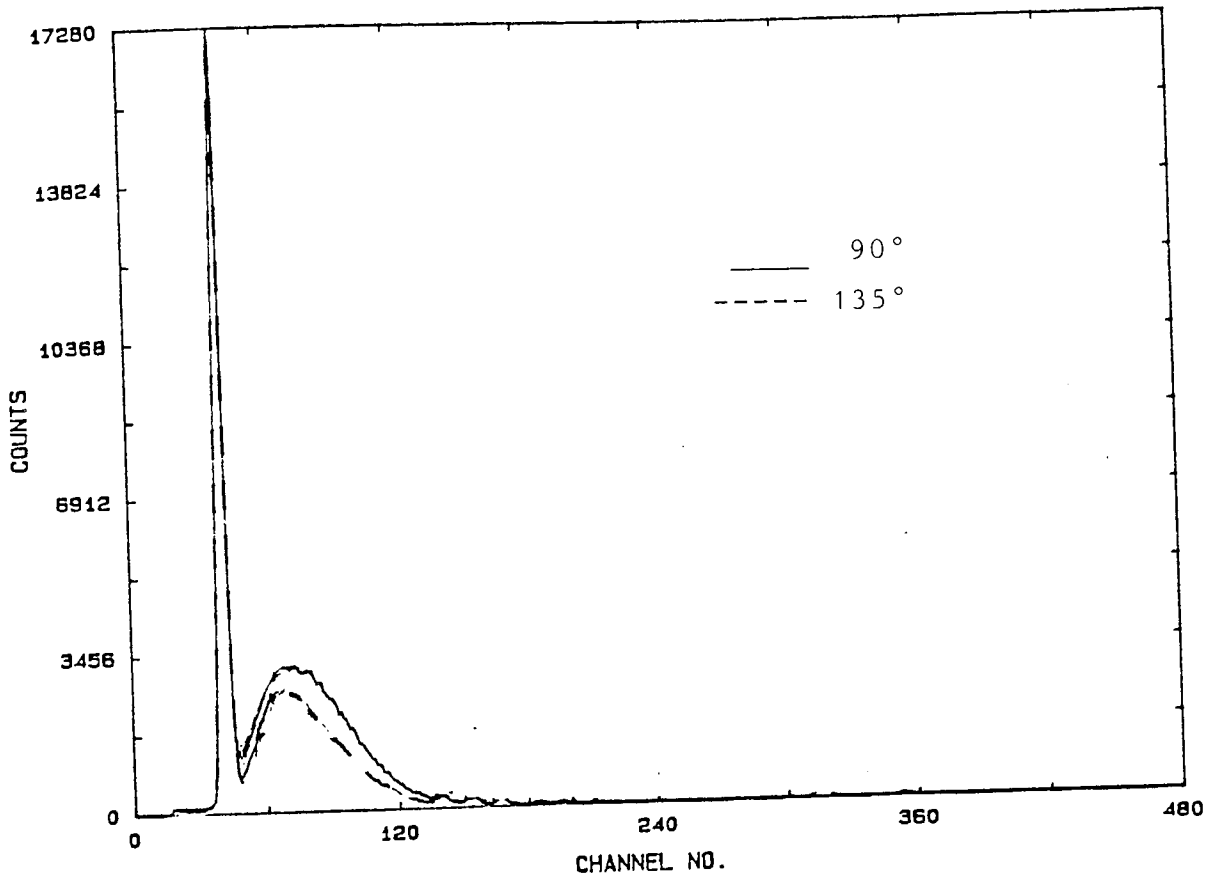

FIGURE 4.13

Comparison of the bremsstrahlung continuum at 90° and 135° for thin Si standard foil on Nuclepore (normalised to same Si K X-ray peak counts) at 2·00MeV proton energy.

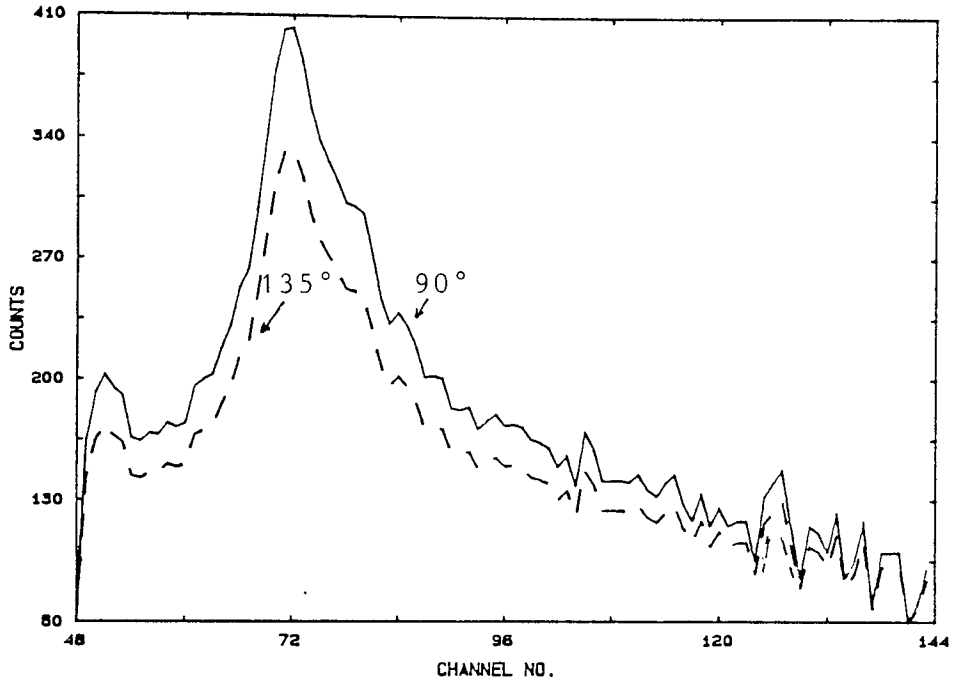

FIGURE 4.14

Comparison of the background spectra obtained at 90° and 135° for Kimfol at 2.00 MeV proton energy for 10 μC charge

FIGURE 4.15

Angular dependence of the bremsstrahlung for Mylar at 90° and 135° for 3.5 MeV
(From Chu et al, 1977)

To summarise briefly the experimental observation in the last three sub-sections which affect the sensitivity of the system, we have seen:

(i) Optimisation of sensitivity for particular Z region can be effected through choice of proton energy (Ep).

(ii) Thinner backing foils produce less background than thicker backing material.

(iii) Reduction in bremsstrahlung is encounteredfor measurements made in the backward angle of 135° compared to the normally adopted angle of 90° with respect to the incident beam.

The major factor that limits the efficiency of the detector in backward direction is the detector-target distance. The detector could not be moved any closer to the target to improve the solid angle due to the restriction of chamber design. However with recent detectors such as Kevex Extra, described by Johnson 1982, where axial movement of the detector probe is made possible through use of stainless steel motion bellows, the chamber design should present no problems. With these detectors the probe position is controlled by a hand-crank and it is very easy to 'wind' the detector to any required detector-target distance.

4.6 Experimentally Determined Minimum Detectable Limits (MDL's).

The detection limit is widely used as a criterion to evaluate and compare the capability of different analytical techniques. Since a major attraction of PIXE is its high sensitivity i.e detectable limits, over a boad elemental range. It becomes necessary for evaluation purposes, to determine experimentally the minimum detectable limits achievable for a wide range of proton energies as a function of atomic number Z.

The MDL's for the present system were evaluated with particular reference to light and intermediate weight elements for proton energies of 1.00 to 3.00 MeV. From the experimentally measured system response function F(xz) described in section 4.3.2 (equation 4.4) and from the "peak to background" criteria discussed in sub-section 4.4.2 , the detectable limits are given by

$$(\rho t)MDL = (3.\sqrt{NB})/(Q.F(xz)).....4.11$$

In order to determine the MDL's, using the above expression it is imperative that the background against which the characteristic X-rays are detected, be accurately defined at all the incident proton energies

employed. Hence background spectra from blanks of Nuclepore and Kimfol backings were obtained for proton energies Ep = 1 to 3 MeV in steps of 0.5 Mev. The backings were bombarded with protons and the X-ray spectra recorded every 0.5 μC. The proton charge accumulation was carried over untill well defined spectra were obtained.

It should be remembered that this background in practice will change, although by a very small amount by the disposition of the sample, which will bring its own background. For calculation of MDL in the present work we have assumed this to be negligible. Typical background spectrum at Ep = 2.00 MeV for Kimfol backing at 90° detector position is shown in Figure 4.16. The background counts were taken over 2 FWHM interval equal to the peak of element of interest and scaled for 1 μC of charge for all elements measured. This scaling to a set value of charge (Q) for all elements is essential, since MDL of a system is directly related to the value of charge, equation 4.11.

4.7 Results and Discssion

Figure 4.17 show the MDL curves for proton energies Ep of 1 to 3 MeV for Kimfol substrate for the previous system.

Figure 4.18 show the MDL curves for proton

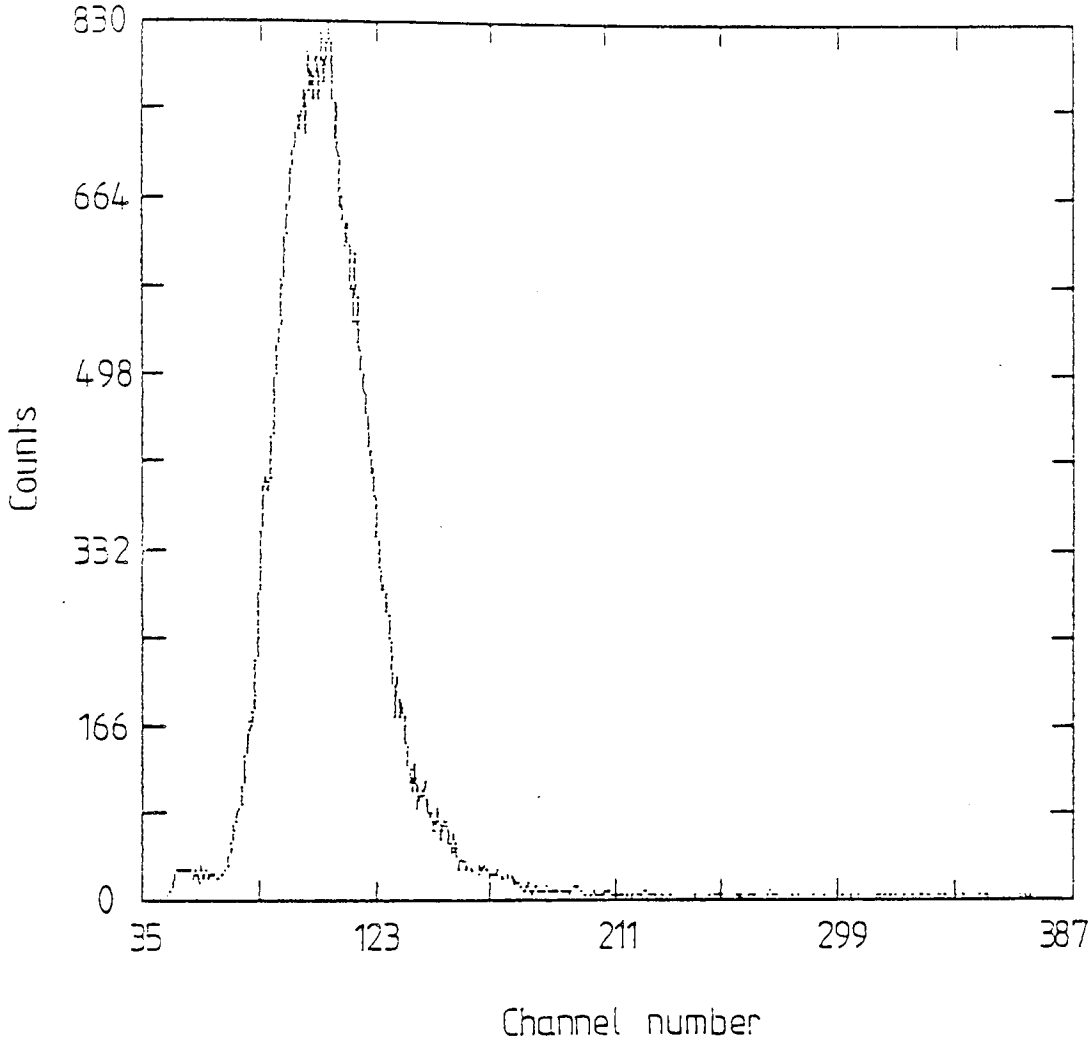

FIGURE 4.16

Typical spectrum of Kimfol blank obtained at 2.00 MeV proton energy.

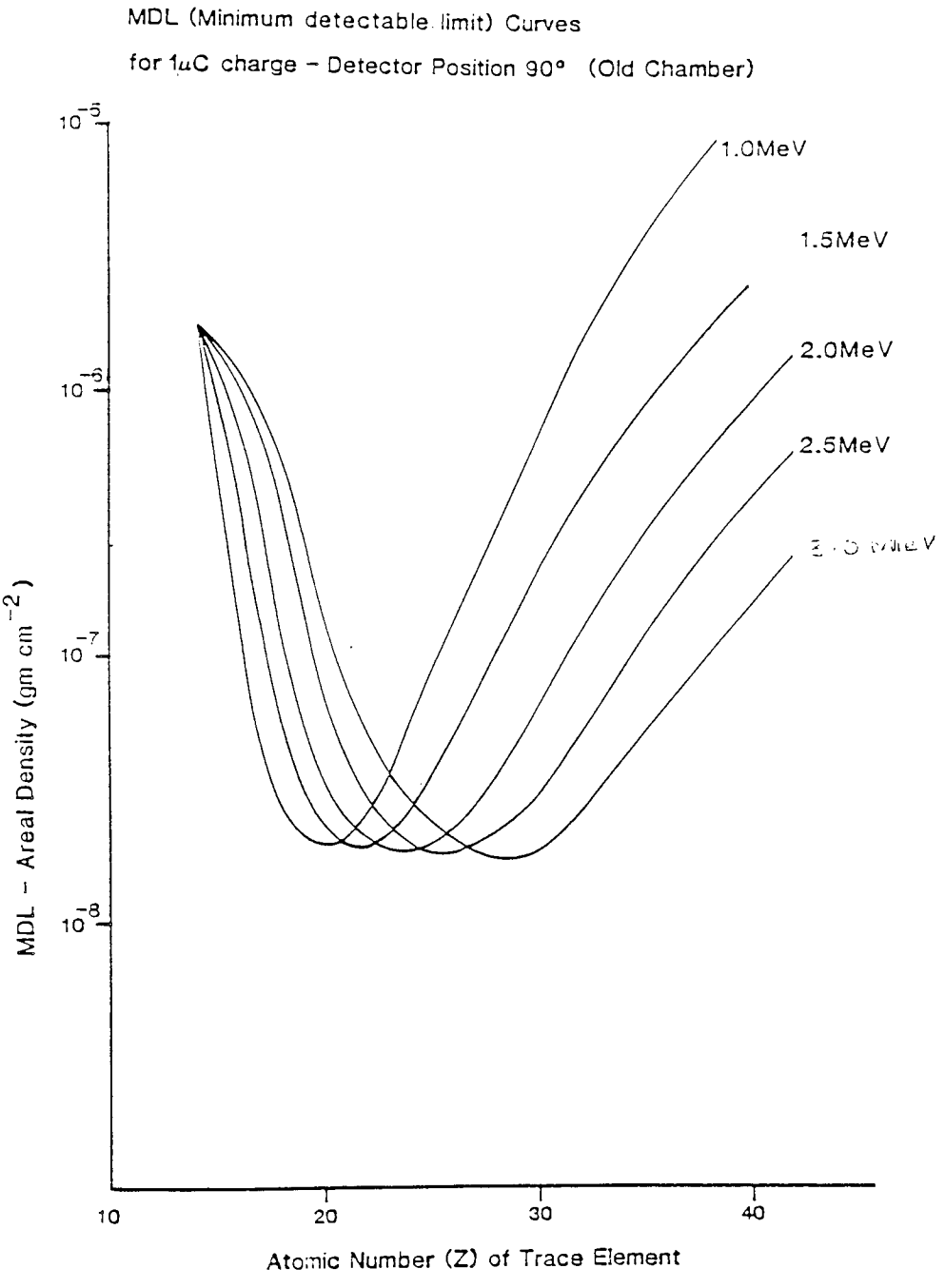
MDL (Minimum detectable limit) Curves
for 1μC charge – Detector Position 90° (Old Chamber)
1.0MeV
1.5MeV
2.0MeV
2.5MeV
MDL – Areal Density (gm cm⁻²)
10⁻⁵
10⁻⁶
10⁻⁷
10⁻⁸
10
20
30
40
Atomic Number (Z) of Trace Element

FIGURE 4.17

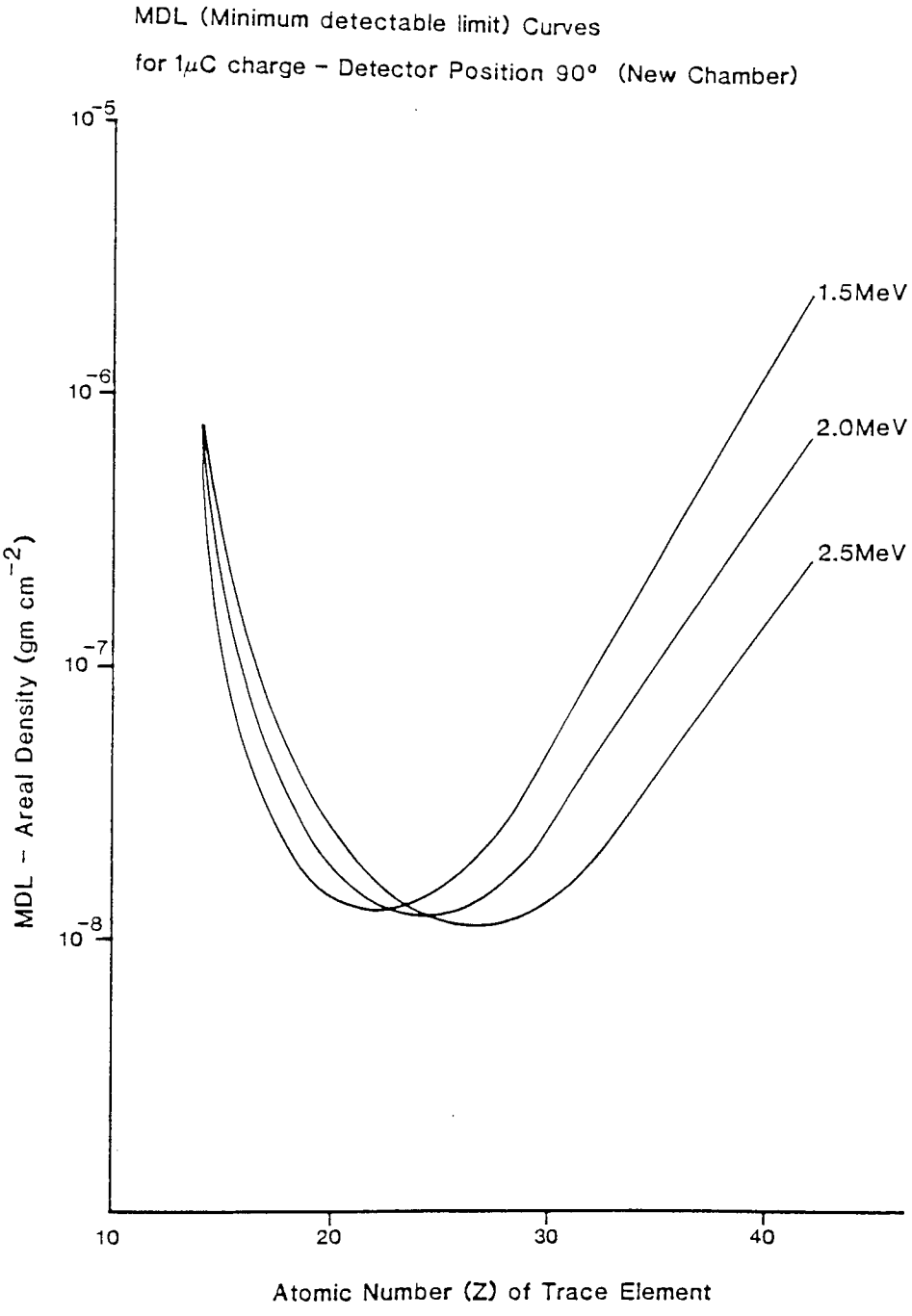
MDL (Minimum detectable limit) Curves
for 1μC charge - Detector Position 90° (New Chamber)
10^-5
10^-6
10^-7
10^-8
MDL - Areal Density (gm cm^-2)
1.5MeV
2.0MeV
2.5MeV
10
20
30
40
Atomic Number (Z) of Trace Element

FIGURE 4.18

energies of Ep 1.5, 2.0 and 2.5 MeV for Kimfol at 90° detector position with respect to incident proton beam. While Figure 4.19 show MDL curves at 135° at Ep of 1.5, 2.0 and 2.5 MeV.

Several noteworthy features are to be observed in the sensitivity curves shown in figure 4.17, 4.18 and 4.19.

(1) All curves show a smoothly varying dependence on the atomic number Z, reaching a minimum (corresponding to optimum sensitivity) for Z between approximately 26 and 34, and increasing to maximum values (poorest sensitivity) at low-Z and high-Z extremes. The relative poor sensitivity for light weight elements is mostly due to the same reasons which affect the response functions F(xz) as discussed in section 4.3.2.1, namely

(a) declining detector efficiencies below X-ray energies of 5 keV

(b) decreasing values for the fluorescence yields

(c) increased absorption losses of low-energy X-rays in absorbing windows and air passages

(d) the relatively large background intensity due to secondary electron bremmstrahlung which attains maximum intensity in the low-Z region.

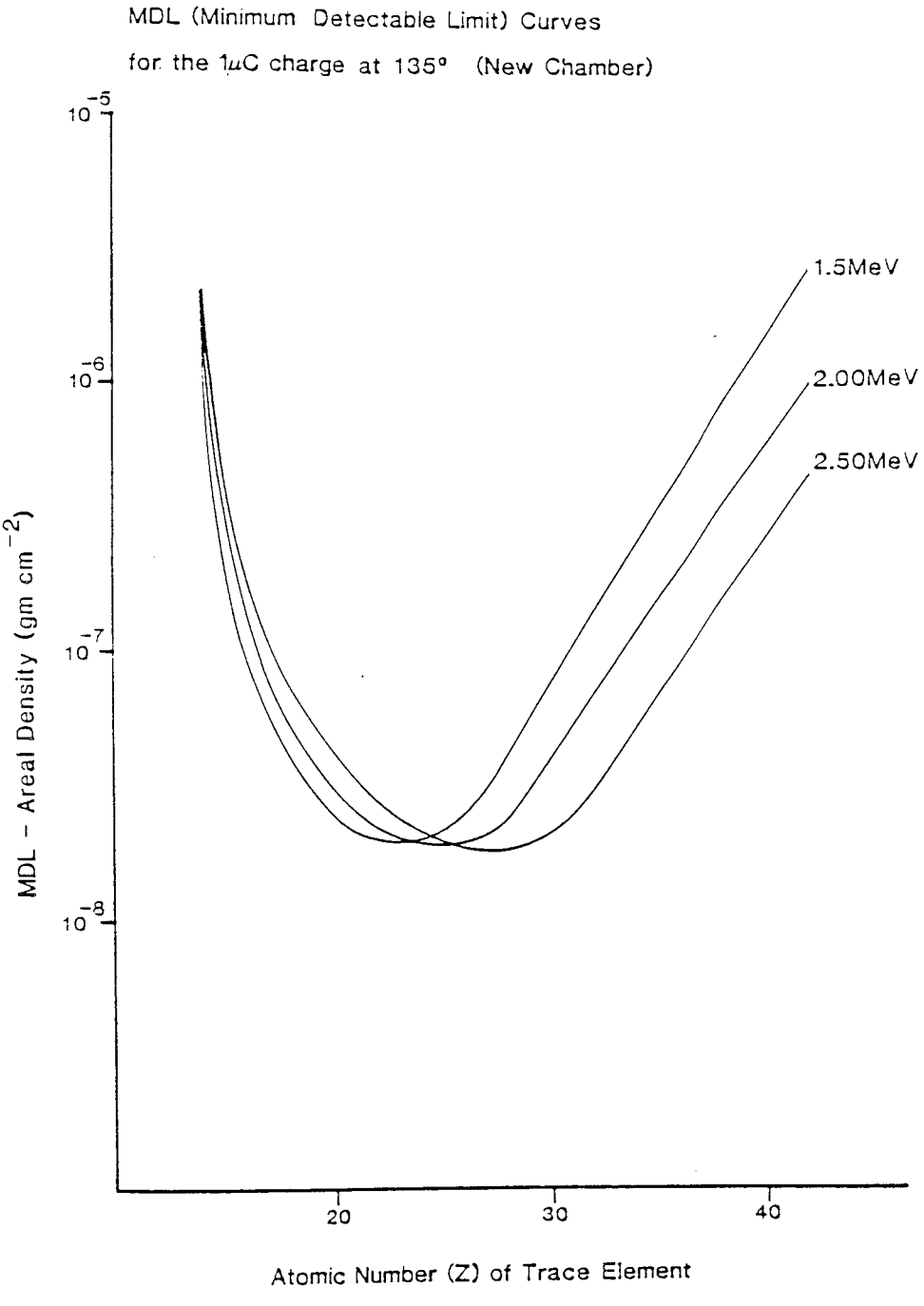
MDL (Minimum Detectable Limit) Curves
for the 1μC charge at 135° (New Chamber)
MDL - Areal Density (gm cm^{-2})
10^{-5}
10^{-6}
10^{-7}
10^{-8}
1.5MeV
2.00MeV
2.50MeV
20
30
40
Atomic Number (Z) of Trace Element

FIGURE 4.19

The fall off in sensitivity at high-Z is mainly due to rapidly decreasing X-ray cross-section, while the background remains relatively constant. The decreasing detector efficiency for X-ray energies > 20 keV is another contributory factor in this instance.

(2) As Ep decreases (figure 4.17), the minimum in the sensitivity curves shift to lower value of Z. Advantage can be taken of this behaviour in order to optimise sensitivity of the system for a particular elemental region of interest.

(3) The reduction in bremmstrahlung in the backward direction of 135° mainly due to angular distribution of secondary electron bremmstrahlung was estimated at 40% from the blank Nuclepore and Kimfol backings for proton charge (Q) of 1 μC at Ep of 1.5 to 2.5 MeV.

4.8 Factors Affecting the MDL & Practical Considerations.

The affect of various experimental parameters on the minimum detection limit of the system can be assessed from expression (4.11)

$$(pt)_{MDL} = 3.\sqrt{NB}/\ Q.F(xz)$$

here $(\rho t)_{MDL}$ is proportional to $NB/\ Q.F(xz)$

and since $NB \propto (\rho t)_B\ Q.F(xz)_B$ and ΔE

where $(\rho t)_B$ = areal density of both the backing material and matrix.

ΔE = FWHM resolution of X-ray detector.

Substituting the physical quantities for F(xz) from (equation 4.1), it can be shown, (Cahill 1974, Johansson, 1976 and Folkmann, 1975) that $(pt)_{MDL}$ scales as:

$$MDL\ \alpha\ [(\rho t)_B\ \frac{\sigma_B}{\sigma_{xe^2}}\ \frac{\Delta E}{Q\varepsilon d\Omega}]^{1/2}$$

where

σ_B , σ_{xe} = background and characteristic X-ray production cross-section respectively,

$d\Omega$ = solid angle of the detector,

ε = detector efficiency for the element of interest

Q = integrated proton charge on the sample.

All the parameters in this expression influence the sensitivity. In practice, the improvements in detection limit are limited by practical considerations:

(i) Reduction in $(\rho t)_B$ improves the sensitivity, since

the production of background radiation is dependent upon matrix and backing material mass thicknesses. However due to manner in which thin samples are prepared and presented for analysis in a practical PIXE analysis, the limit is imposed by factors dictating the backing materials requirements (discussed in sub-section 4.4.3).

(ii) Sensitivity can be improved by counting the sample for a longer period (for higher charge Q), but the problems of target damage due to to excessive beam heating and cost factor places restriction on analysis time.

(iii) Production cross-sections for background and characteristic X-rays are dependent upon incident proton energy. Hence optimisation of the energy for a limited region of elements of interest is possible as shown in the MDL curves.

(iv) Some gain in sensitivity is possible by improving the detector-target geometry. Moving the detector closer to the target is limited by counting rate limitation and by sample chamber design.

(v) Sensitivity of thin targets can be improved by increasing the target thickness within the constraints of "thin" target definition, which requires that the slowing down of the proton and the

absorption of the X-ray photon can be neglected.

For the optimisation of sensitivity target thickness is not regarded as a free parameter.

From practical considerations it can be seen, that of all the parameters, only beam current has any real chance of being optimised for improved detection limits with respect to any particular element.

CHAPTER V

5.0 APPLICATION.

5.1 Introduction.

During the past 20 years substantial advances in physical methods of analysis, such as X-ray Fluorescence, Atomic Absorption, Neutron Activation and the development of new methods such as PIXE has led to renewed interest in trace element analysis in many fields of research. At the present time nutritional, environmental and biomedical materials are among some of the more important areas of applications.

The criteria which determine the most suitable analytical technique for trace elemental analysis include sensitivity, accuracy and precision, sampling requirements, preparation of standards, interferences and cost factors. Sensitivity is of prime importance in the above applications as none of the other criteria merit consideration if adequate sensitivity can not be achieved.

PIXE is unique among analytical techniques in that it exhibits sensitivity that has the right order of magnitude, 1 ppm to 0.1 ppm, for the simultaneous detection of a wide range of elements $14 \leqslant Z \leqslant 42$. It has

been applied to a wide variety of specimens in such areas as pollution monitoring, elemental analysis of biomedical, geological, archeological and forensic samples. The fundamental aims of analysis in most studies have been the identification and quantification of the trace element constituents exploiting the multi-elemental nature of the technique.

5.1.1 Environmental Applications

In the environmental applications, PIXE analysis allows simple and fast determination of elements present in water or air. The water sample to be analysed is usually evaporated onto a thin carbon foil or plastic backing which is allowed to dry and then irradiated. Parts-per-million levels of many elements can be detected in this manner, Hansson et al, 1984; Campbell et al, 1985, and others. PIXE analysis of water at the parts-per-trillion level has been reported by Johansson et al, 1984, using a preconcentration technique. The trace elements are extracted from water by a complexing agent and dissolved in nitric acid. The acid solution droplet is placed on a very thin carbon foil and evaporated.

The harmful effects of air-borne pollutants on man and environment are well known. Studies of airborne contamination using PIXE have been reported through out the literature (Grieken et al, 1976; Maenhaut et al,

1981; Akselsson, 1984; Eldred et al, 1984). In USA, PIXE research laboratories based at Davies, California and Tallahasee, Florida are almost totally dedicated to air pollution studies.

5.1.2 Biomedical Applications

Another important area of PIXE application, which has received a great deal of attention is in biological and medical studies. Interest in these areas is not only due to the multielemental nature of the method coupled with small sample size requirements but also because of the non-destructive nature of the technique.

Trace elemental imbalances which reflect physiological changes or disorders in the body are increasingly being recognised in medicine as important diagnostic aids,(Cotzias and Foradori, 1969; Underwood, 1977; Brown et al,1980; Valkovic, 1980; Cesareo, 1982; Bratter and Schramel 1983. Hence the elemental analysis of biomedical tissues and fluids has become a very rapidly expanding field. A typical biological application is the study into how individual metals are bound to various proteins in the enzymes. The amount of sample achieved for analysis after separation and purification of proteins is usually very small. Hence the use of conventional analytical methods prove inadequate and difficult.

Trace elemental analysis of cells, micro-organisms, tissues and fluids in animals and human beings have been reported widely in the literature using PIXE analysis technique. Recent reviews of biomedical applications i.e. from last PIXE conference alone shows the scale of interest in this work.

5.1.3 Other Applications

Other varied and interesting recent applications of PIXE has been the analysis of Pottery samples by Lessard and Houdayer, 1984. The study of ancient soldering of gold, by Demortier et al, 1984. Analysis of the Gutenberg Bible by Kusko et al, 1984, and the determination of trace elements in Lunar rocks by Blank et al, 1984.

5.2 Trace Elements.

From the beginning of civilization, man in his search for food must have found it desirable to recognise harmful as well as beneficial effects due to the ingestion of materials into his body. With the advent of science the research has passed through the age of essential and harmful major constituents of food into the age of trace elements essential for healthy

organisms in animals and humans.

5.2.1 Elements in Living Organism

The bulk of living matter is made up of eleven elements H, C, N, O, Na, Mg, P, S, Cl, K and Ca. These elements have been known to be essential for life for a long time because their presence is easy to detect, some, however, occur in such small quantities that their concentrations were not determined until recent developments in analytical techniques. They were often mentioned as occurring in "traces", Underwood 1977.

For an element to be "essential" for life it must satisfy some criteria. According to Cotzies et al 1969, and Underwood 1977, these are as follows:

(i) element is present in healthy tissues of all living organisms
(ii) its concentration is fairly constant in different species
(iii) Its withdrawl from the body induces the same structural abnormalities or specific disease in all species
(iv) its addition either prevents or reverses their abnormalities
(v) it has a direct influence on the organism and is involved in metabolism.

Figure 5.1 from Valkovic 1980, summarises our present knowledge about essential elements. Elements in the black boxes, H, C, N, O, Na, Mg, P, S, Cl, K, and Ca are major essential elements where as the elements in dashed boxes, F, Si, V, Cr, Mn, Fe, Co, Ni, Cu, Zn, As, Se, Mo, Sn and I are essential trace elements for life. Besides the 15 trace elements shown as essential each organism contains traces of elements which have a neutral function (e.g. cadmium, lead, mercury) or have an unknown function (e.g. bromine, rubidium, strontium etc).

The concentration of the trace elements in organism is often critical, in view of the narrow range between beneficial and toxic levels. Essential trace elements such as Co, Cu, Mo and Se can prove to be toxic when ingested in excess whereas a toxic element like As may be essential at low levels. It is now well established that many clinical and pathological disorders arise in the organism due to specific trace element deficiencies or excesses. For example copper and zinc in Menke's disease (trichopoliodystrophy) and Danbolt's disease (acrodermatitis enteropathica), Sunderman, 1980. Dyson et al, 1978, found iron deficiency in liver tissue in the case of alcoholic cirrhosis.

While symptoms of acute metal toxicity due to environmental and occupational exposure to metals are

Aston University

Illustration has been removed for copyright restrictions

FIGURE 5.1

Elements that form the bulk of living matter and essential trace elements for warm-blooded animals (From Valkovic, 1980)

generally well documented, effects of long term exposure to low level concentrations of metals remain a concern.

Cancer is a special category of effects which may be induced by long term exposure to relative low level concentrations of metal. Less severe results, involving changes in the function of various organs and tissues, to a degree which does not give rise to known clinical disorders, may occur more commonly as a result of both occupational and environmental exposure.

Living organisms acquire metals via various routes since metals are present in air, water and soil. As an example sources of exposure for cadmium, which is studied closely in respect to cancer, hypertension and renal diseases are given by Friberg et al, 1971, as being occupational, diet and cigarettes. Most elements enter the human body mainly through the intestinal tract and by the lungs and then transported by blood via liver to other organs.

5.2.2 Role of Trace Elements in Living Organism.

The varied physio-chemical and biological role of all trace elements is not fully understood. Trace elements seem to be involved in many phases of metabolism. The majority of trace elements form key

components of enzyme systems, or of proteins with vital functions. If the metal is removed, the protein usually losses its capacity to function as an enzyme. Hence the chemical interest in the identification of the role of trace elements in disorders of human metabolism is rapidly expanding.

The role of some essential trace elements are summarised below as it gives an insight into the present analytical work:

Fluorine (F):

Soluble fluorides are completely absorbed from the gastrointestinal tract and distributed rapidly throughout the body. An extremely high proportion of the total body burden of fluorine is present in bones and teeth. Its beneficial effects on dental health has long been recognised, Dean 1942. Excessive intake of fluoride leads to fluorisis, which impairs the ability of organism to metabolise fat in animals.

Silicon (Si):

Silicon is absorbed by the alimentary tract from food. Silicon is essential for growth and skeletal development, Schwarz 1972. Requirements compatible with satisfactory

growth are largely unknown Underwood 1977. Toxicity of silicon may lead to malignancy due to chromosome mutation.

Vanadium (V):

Absorption of vanadium is from human gut and appears generally to be poor. It is distributed throughout the organism in very low concentration 0.02 to 0.03 ppm, except for lungs 0.6 ppm, Tipton et al 1963. Vanadium deficiency leads to impaired growth and disturbed lipid metabolism in chicks and rats, Nielsen et al 1973. Vanadium is a relatively toxic element as demonstrated by Hill, 1975. He observed depressed growth and increased mortality in chicks, fed 20 ppm Vanadium.

Manganese (Mn):

Manganese is absorbed throughout the length of the small intestine. In human blood it is found almost totally associated with B-globulin. Mn levels in the red cells is notably higher in rheumatoid arthritis patients. Secretion of excess amount of Mn in urine indicates Mn toxicity, Bowen 1980. Chronic poisoning is an industrial problem among manganese miners.

Iron (Fe):

Iron is more efficiently absorbed from foods of animal than plant origin (Underwood 1977). It is a vital constituent of living organisms, and its function in blood is well known. The human body contains approx 70 ppm of iron. Iron occurs in blood as haemoglobin in the erythrocytes and as transferrin in the plasma. Deficiency of Fe in human adult results in listlessness, fatigue, anaemia and in children anorexia, depressed growth and decreased resistance to infection.

Cobalt (Co):

Cobalt is unique among trace elements, it is biologically active only when absorbed as a component of vitamin B12. Nearly half of the total Co content of adult human is stored in muscles.

Copper (Cu):

Copper is absorbed by the mucosa of the small intestine, where it is passed into the blood, and transported to the liver. Copper is present in almost all cells Valkovic, 1980. The healthy adult body contains approximately 80mg of copper. High serum copper levels are observed in pregnancy, infections, acute leukaemia, Hodgkins disease

and hyperthyroidism, while copper deficiency is observed in Wilson's disease, cystic fibrosis and Menke's disease.

Iodine (I):

The thyroid gland in healthy human adult contains the highest concentration of trace element iodine. Its metabolism and role in synthesis of thyroid hormones is well known. Iodine deficiency can lead to retarded growth during early life both in humans and animals.

Zinc (Zn):

Absorption of zinc occurs in the small intestine and involves mucosal transport by a zinc binding protein, Kowarski et al 1974. Several diseases such as Danbolt's disease, by-progonadal dwarfism, dermatitis of certain areas of the body, chronic and acute infection, malignant tumours, several liver diseases and some others, are linked to Zn deficiency. The richest dietary source of Zn are oysters, other sea-foods and nuts.

Selenium (Se):

This trace element is present in human tissue and body fluids in various concentrations. Selenium in most biological material is found largely in the protein

fraction. Foods low in protein contain a very low level of selenium. Deficiency of Se may lead to protein-calorie malnutrition and because selenium is necessary for growth, children are more prone to develop it than adults.

Molybdenum (Mo):

Molybdenum is easily and quickly absorbed from the diet. It occurs in all tissues and fluids of the body in low concentration, however human dental enamel can contain relatively high levels of molybdenum. Low levels of dietary Mo has been shown to affect Cu metabolism in man, Doesthale 1974. This metabolic interference of copper by Mo plus sulphur has been extensively studied in animals.

The biological and medicinal effects of particular elements where possible should be considered in relation to other elements. Interelement correlation can often indicate effects on metabolism which are not apparent when considering a trace element in isolation as indicated in the case of trace element molybdenum.

Future trends in trace element analysis would not only require the total amount of element of interest present in a specimen but also its different chemical

composition, where these exist, Sarx and Bachmann 1983. A well known example is the essential higher toxicological effect of AsO_3 in comparison to AsO_5 for the same amount of arsenic.

5.3 Amniotic Fluid - The need for elemental analysis.

The introduction of amniocentesis, a safe technique for acquiring amniotic fluid sample, has made amniotic fluid fairly generally available for optical and biochemical examinations. The analysis of amniotic fluid has played a very important role in assessment of foetal growth and in the prenatal diagnosis of genetic disorders.

The question as to whether the trace element levels in amniotic fluid might be a helpful indicator in the diagnosis and differentiation of disease state from healthy one, remains open at present, although some promising hints with regard to Cu and Zn are found in the literature, Chez, 1978; Prasad 1978.

The elemental analysis of amniotic fluid also provides valuable information regarding fetal nutrition in terms of trace elements. While trace element nutritional requirements based on human breast milk analysis and animal studies have been more or less established, Hambridge 1983, reference data on foetal

nutritional needs is extraordinarily scarce.

The fetus spends approximately 9 months submerged in this fluid which provides nourishment and protection before birth. Fetal swallowing and absorption by the fetal gastrointestinal tract is a major route of amniotic fluid turn over. The rate of swallowing is about 1/3 of its volume each hour, Hall et al, 1984.

It is therefore anticipated that trace elemental composition of amniotic fluid which is so intimately connected with the fetus should provide accurate information for prenatal diagnosis.

5.3.1 Sampling - Amniocentesis.

Blood and urine are the two most commonly used body fluids in clinics, for the diagnosis of disease in individual patients. This is mainly due to the ease with which these fluids can be obtained for analysis.

In recent years increased recognition of the importance of trace elements and human disease, and other biochemical diagnosis of disease has led to the examination of other body fluids and tissues.

The need for samples that are obtained from the

area related to the intimate environment of the problem under investigation is increasingly being recognised by workers in the biomedical field as essential in improving the reliability of diagnostic studies.

For certain fluids this entails a complicated sampling technique such as is necessary for cerebrospinal fluid or amniotic fluid.

A simple and easy method of obtaining amniotic fluid specimens for the obstetrician would be transvaginal amniotomy. However amniotomy usually induces labour, and due to the high risks involved the technique is not suitable as a routine procedure for diagnostic or research applications. Hence the specimen is usually obtained by transabdominal amniocentesis, Alpern, 1977.

Amniocentesis is done under sterile conditions using a long narrow guage spinal needle to penetrate the amniotic cavity through the maternal abdominal wall. Care is taken to determine the location of the fetus and placenta so that accidental injury to these parts may be avoided.

The use of ultrasonic scanning considerably reduces this risk. Figure 5.2, from Seeds and Barnes, 1968, shows known and postulated sites of amniotic fluid formation and removal in pregnancy.

Aston University

Illustration has been removed for copyright restrictions

FIGURE 5.2

Known and postulated sites of amniotic fluid formation and removal in pregnancy (from Seeds and Barnes, 1968)

Amniocentesis may be performed after 20 weeks of gestation to the termination of pregnancy, Holton 1983, while some workers have suggested that amniocentesis can be performed as early as week 12 of gestation.

At 12 weeks of gestation, the amniotic cavity normally contains 50ml of fluid. The quantity of fluid increases at a rate of 25ml per week until 15 weeks and then increases at double the rate until week 28. The amniotic fluid quantity appears to reach a maximum of about 1 litre at 38 weeks of gestation and then decreases to less than 400ml at week 42. Figure 5.3 shows the mean volumes at various periods of gestation taken from Elliot and Inman, 1961.

When a clinician can not obtain fluid by amniocentesis, it may be because the volume of amniotic fluid is small. A significantly low volume of the fluid indicates a placental defect and may result in retarded foetal growth. When the fetus dies in utero, the colour of the amniotic fluid changes to green and then to black.

5.3.2 Sampling Problems.

In biomedical related studies one of the main problems is that of collecting samples. Sampling in a

Aston University

Illustration has been removed for copyright restrictions

FIGURE 5.3

Mean amniotic fluid volumes at various periods of gestation (From Elliot and Inman, 1961)

hospital or outpatient clinics is undertaken by very differently qualified people. Which particular group of staff is required depends on a number of factors such as the kind of sampling technique to be used, the kind of sample required, time factor and other particular problems associated with a particular examination or analytical technique to be used.

While qualified support staff such as nurses and medical technicians can take blood samples from the veins, they are barred on legal grounds from obtaining other body fluids which require puncturing. Such sampling as in the case of amniotic fluids described in the previous sub-section 5.3.1, can only be done by specialised doctors. The need for a specialised person to collect samples not only reduces the number of samples that can be collected round the clock, but makes sampling less cost effective. Moreover sampling, transportation, and storage of the sample has to be carried out by staff who are well informed about their role in the sampling action. Frequent changes and variation of staff add to the problems of maintaining standardisation of sampling in clinics.

At times it can prove to be extremely difficult to combine medical needs with the demands of trace element analysis where contamination free samples are vital for any worthwhile studies.

In short all equipment used, that gets into contact with sample at any stage should be free from all forms of contamination. A relevant example is the case cited by Kynast, 1983. Amniotic fluid for trace elemental analysis was obtained using available syringe needles. It was found that the needles themselves contained too many trace elements and therefore led to contamination of the withdrawn sample. The problem was solved by using special nickel needles.

For trace elemental analysis of biomedical specimens, where element levels involved are very low, it is imperative that all staff handling samples realise the problems and the sources of sample contamination. It is also important that the staff are made aware of the fact that sterility and lack of contaminating substance is not the same thing. Purity of all materials including distilled water, solvents and detergents and equipment used is necessary. Along with this, protection against contamination, once the sample has been obtained is essential.

Contamination of the sample can occur at different stages, such as during sampling, transportation, storage, sample preparation and during measurements. Hence appropriate precautions against contamination must be taken for the analysis to be accurate.

5.4 Sample Preparation.

The wide range of PIXE applications for biomedical materials requires a correspondingly wide range of sample preparation techniques, Galuszka, 1984. The nature and expected concentration of elements present in a sample dictates the suitability of a particular sample preparation method.

5.4.1 Liquid Samples.

Thin specimens obtained by drying droplets of liquid analytes such as urine, blood, serum and other body fluids, on thin polymer backings is one of the most commonly used sample preparation technique in PIXE analysis. Johansson 1970, Walter et al 1974, Valkovic 1974, Torrisi 1982, Campbell et al 1985. The prepared target is irradiated in the normal manner. This is a simple technique which requires no, or very, little special preparation. However, "liquid droplet" method do not always produce uniform samples, either in the distribution of elements in the target or in its thickness or both, due to non-uniform drying. In addition blood and liquid samples with fibrous suspensions prepared in this manner tend to deform the thin backing materials when they dry, Khan and Crumpton, 1981.

Roboye, 1980, demonstrated through photomicrographs that an addition of a liposome solution (synthetic phospholipid bilayer vesicles) as a homogenizer renders residual deposits uniform. It prevents crystallization and non-uniformity which can occur in certain biological samples upon drying. In the case of analysis of samples subject to crystal formation a correction factor, as described by Ahlberg, 1977, should be applied to correct for enhancement and absorption effects.

5.4.2 Solid Biological Samples.

The preparation of solid biological tissues and organs for trace elemental analysis by PIXE is often more difficult. It can involve sectioning with a Microtome, fragmentation, powdering, drying and ashing.

5.4.2.1 Sectioning with a Microtome.

Thin sections of organ material or tissue are normally sliced and irradiated as self supporting targets, Kemp et al, 1975, or mounted on a thin backing, Campbell, 1975. The primary material is either frozen or embedded in a hardening agent before slicing with the aid of a cryostat microtome. The main problem with the use of hardening agent preparations is the

likelihood of contamination of the sample. Evidence shows that the very small samples obtained in this manner are often unrepresentative of the bulk of the material in certain tissues, Campbell, 1977.

5.4.2.2 Fragmentation and Powdering.

Fragmentation and powdering of tissues is usually accomplished through the use of a "microdismemberator" comprising a teflon vessel in which the sample is vibrated rapidly, together with a teflon covered metal ball, at liquid nitrogen temperature, Iyenger 1976, Van Rinsvelt et al 1984. Powder obtained by this technique is either pressed into a self-supporting pellet or attached to a backing material using polystyrene glue before irradiation. For the powder specimen to be homogeneous it is essential that particle size be uniform. Otherwise segregation of particles in a sample containing a wide range of particle sizes may result in a non-uniform distribution of elements.

5.4.2.3 Drying and Ashing.

Drying and ashing are commonly used as a means of pre-concentration of samples containing very low levels of trace elements less than 0.1 ppm, and to

achieve homogeneous samples from non-homogeneous samples. The main methods of drying are oven drying and freeze drying; air drying is not normally recommended in trace element work due to the increased likelihood of sample contamination due to air borne particles.

Freeze drying or lyophilization is a process in which a biological material is pre-frozen and then subjected to a low vacuum pressure for a relatively long time to sublimize the ice while the sample is still in the frozen state. A solid residue achieved is then thoroughly powdered to obtain a homogeneous sample. Campbell, 1977, reported that vacuum freeze drying technique concentrated the mass of the sample by a factor of 5.

Ashing may be defined as the removal of low atomic number elements such as hydrogen, carbon, nitrogen and oxygen from tissues by oxidation. Since these elements are the major constituents of biological material oxidation results in a form of sample residue concentrated in non-volatile metals. Ashing methods commonly used include wet ashing and low or high temperature ashing.

Wet ashing involves digestion of biological material using suitable acids or other oxidising agents at low or high temperatures. Gorsuch, 1970, gives a review of the different methods reported for wet

ashing. He also reports a very good recovery rate >95% for wet ashing. However, Nielson et al, 1976, claims that wet ashing may not reduce the matrix material to the same extent as low or high temperature ashing since the sample is not oxidised completely.

Both wet and dry ashing have their advantages and disadvantages. Overall, wet digestion at present seems to offer a greater number of advantages over dry ashing in the preparation of biological samples for trace elemental analysis. It is increasingly being used in PIXE due in part to the availability of ultra pure digestion agents.

5.5 A pre-concentration method for PIXE analysis of amniotic fluids.

For many elements the level of occurrence in amniotic fluid samples are low e.g. Fe, Cu, Zn ,Se levels can be as low as 0.1 ppm, or lower. Consequently analysis requires a rather long irradiation time, approximately 60 minutes or 25μC of integrated sample charge to obtain good sensitivity for some elements of interest. Long irradiations however increase the cost of the sample analysis and the possibility of taget damage.

To improve both sensitivity and cost for the

amniotic fluid analysis, a non-selective pre-concentration technique was used in the present work. A low pressure evaporation method was adopted. This simple but effective method has not been reported for PIXE analysis of fluids to our knowledge.

The apparatus and the set up was as shown in Figure 5.4. The low pressure chamber consisted of an 8" diameter Pyrex glass vessel. A rubber vacuum seal was fitted to form a vacuum tight chamber with a glass cover plate. The glass cover plate had three 1" diameter holes made along its centre line to accommodate rubber bungs which enabled vacuum tight connection for 1/2" glass vacuum line, an air inlet valve and a 0-50^{o}C thermometer which also acted as stirrer. The other end of the vacuum line was connected to a 5" diameter glass 'bottle' acting as a pressure regulator. This in turn was connected to a vacuum pump (Filter Pump, type PXY-260-R).

The main function of the regulator was to act as a water 'trap', in case of water mains failure. In-line stop valves were fitted to the vacuum line between the main chamber and the regulator, and between the regulator and the vacuum pump. A tap attached to the 'regulator' was used both as an air inlet valve and as a drainage tap in case of 'back-water' suction from water mains.

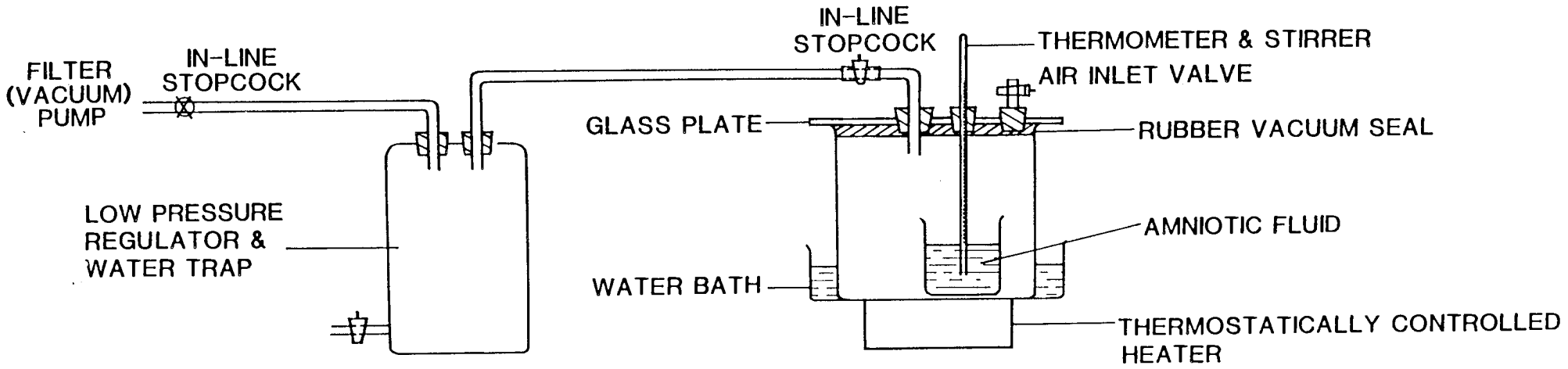

FIGURE 5 . 4 NON SELECTIVE PRE-CONCENTRATION METHOD FOR AMNIOTIC FLUID

A 25ml quantity of the stock sample was transferred to a clean 50cc beaker and placed inside the low pressure vessel. The temperature of the heater placed under the vessel was carefully controlled. The temperature of the sample inside was not allowed to rise higher than 40°C to prevent 'generation' of proteins found in amniotic fluids.

A sample concentration of approximately a factor 5 was obtained by this method in about 8 hours. The sensitivity obtained was good for most elements in a 15 to 20 minutes irradiation time.

Figures 5.5 and 5.6 shows spectra of a pre-concentrated sample and a sample in its natural state respectively. Both were irradiated for approximately same the K-α peak counts for yttrium internal standard.

5.6 Amniotic Fluid Samples and Preparation.

Ten amniotic fluid samples from normal pregnancies were supplied by Fazakeley Hospital, Liverpool for investigation in the present work.

The samples were divided into two categories

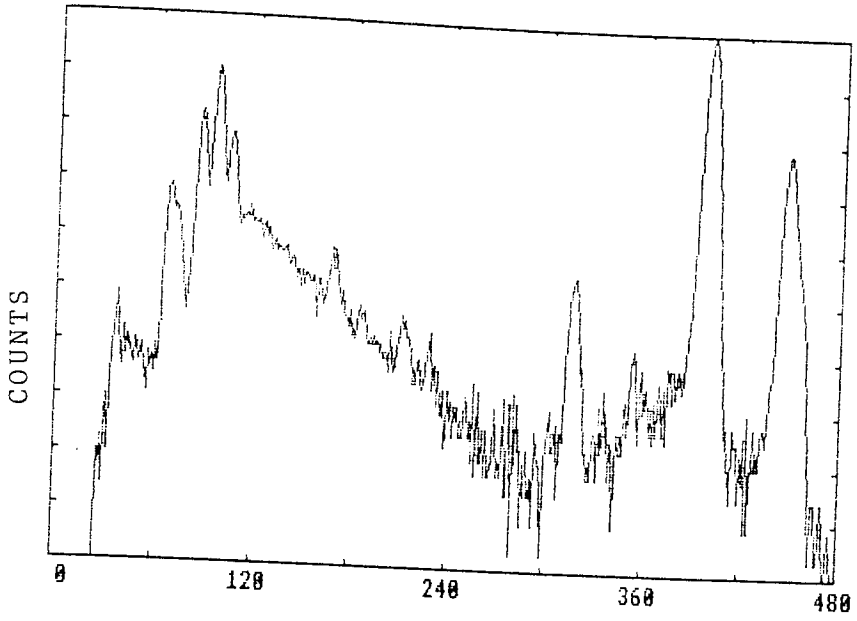

FIGURE 5.5

Typical PIXE spectrum of "raw" amniotic fluid at 2.5 MeV proton energy for 10 μC charge.

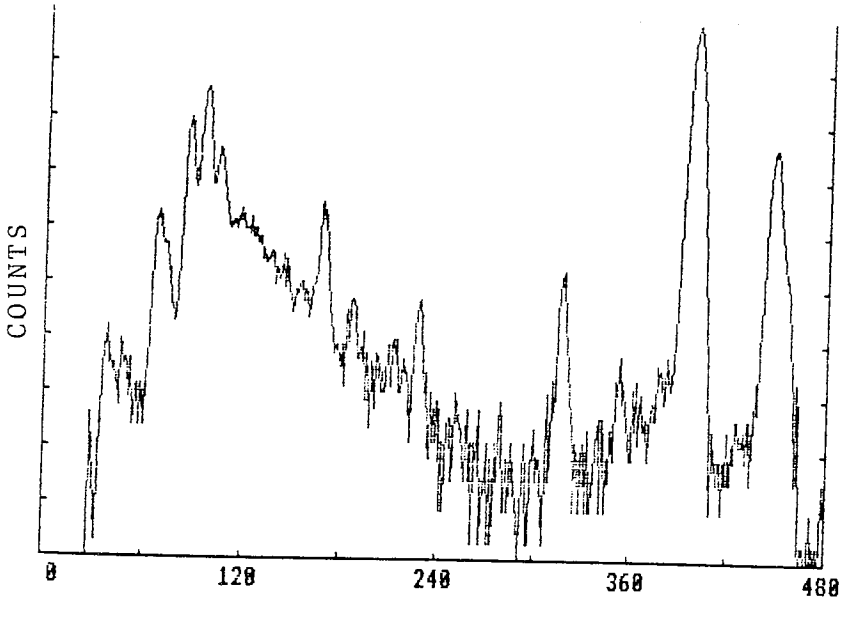

FIGURE 5.6

Typical PIXE spectrum of concentrated (x5) amniotic fluid at 2.5 MeV proton energy for 10 μC charge.

namely "fresh" samples and "pools" samples. The five "fresh" samples were the ones collected quite recently i.e. matter of days before analysis while the other five "pools" samples were the ones which had been collected some time ago.

Both categories of samples comprised 20 to 30 µl of the fluids contained in sterile plastic bottles. The samples had been frozen immediately after collection and stored under -20° C until analysis. Most samples were clear except for two samples (Code AF6 and AF9) which had a slight milky appearances.

Thin targets of the samples were prepared on 5 µm Kimfol polycarbonate backing in the following manner. 1 ml of a preconcentrated sample fluid prepared as described in Section 5.5 above, was taken and transferred to a test tube. The sample fluids were shaken well before transferring the required quantity into a test tube.

All pipettes, test tubes and bottles were thoroughly cleaned before hand to avoid contamination of the condensed fluids.

A known quantity of yttrium (see Section 5.6) was then added to the working sample and carefully labelled indicating fluid sample code, the concentration of internal standard used, and date of

preparation. The remaining concentrated solution was then returned to the refrigerator.

After the sample and the standard solution were well mixed, an adjustable sampler 2-10 µl, Oxford Micro-pipetting system, (Oxford Laboratories International Corporation, Ireland), was used to dispense 4 µl aliquots of doped amniotic fluid specimen onto a backing foil. This backing foil had previously been mounted on the specially designed pure aluminium frame, discussed in section 3.4.1. Each sample was labelled with a code for later identification.

Sampling precision rules suggested by the manufacturer were adhered to and are summarised;

(i) sampler plunger was depressed and released smoothly to ensure the same speed of intake and delivery

(ii) the plunger knob was always depressed to a proper stop before insertion of the tip into the solution as depression of the plunger knob after insertion may cause the formation of an air bubble in the tip and result in a filling error

(iii) The sampler was held vertically and the tip

was inserted approximately the same depth into the sample fluid each time

(iv) a new tip was used for each target

(v) Extra care was taken to prevent the tip from touching the test tube sides or the backing foil.

The prepared samples were carefully loaded into a clean desiccator, with a special shelving system, which allowed easy drying, storage and transportation of the samples.

Visual inspection of the first set of dried samples showed that a few targets had a powdery appearance. Although adherence of the dried material appeared satisfactory it was decided to use a polystyrene "glue" for the fixation of the dried sample to the Kimfol backing to avoid any risk of flaking off during irradiation.

For comparison purposes two sets of 4 similar targets were prepared and dried. No fixation or glue was used in the first set. For the second set fixation was achieved with the glue prepared in the following manner.

125 mg of polystyrene, (obtained from

Polysciences Inc, Warrington U.S.A, through Windsor Laboratories Ltd, Bedford Avenue, Slough, Berks), was dissolved in 3.8ml of "Analar" high purity benzene to form a very low Z "glue". The selected dried targets were fixed to the Kimfol backing with a 2 ul of the prepared glue.

It can be seen from the spectrum of glue residue on Kimfol, Figure 5.7, that no major characteristic X-ray peaks are observed. Figure 5.8 shows PIXE spectra obtained from sample AFF2 with and without polystyrene glue fixation respectively. Both spectra are identical except for slightly higher bremmstrahlung background in the case of the sample with glue. Otherwise confirming that adherence of the dried sample was good enough and capable of withstanding 10 nA beam current at 2.5 MeV proton beam energy for the required 15 to 20 minutes irradiation time with no obvious sign of target damage. Hence no fixation of the targets was really necessary.

5.7 Internal Standard in amniotic fluid sample.

Yttrium in the form of yttrium nitrate, $Y(NO_3)_3.3H_2O$, was used as an internal labelling element for amniotic fluid samples. Yttrium was chosen because of its marked absence in biological

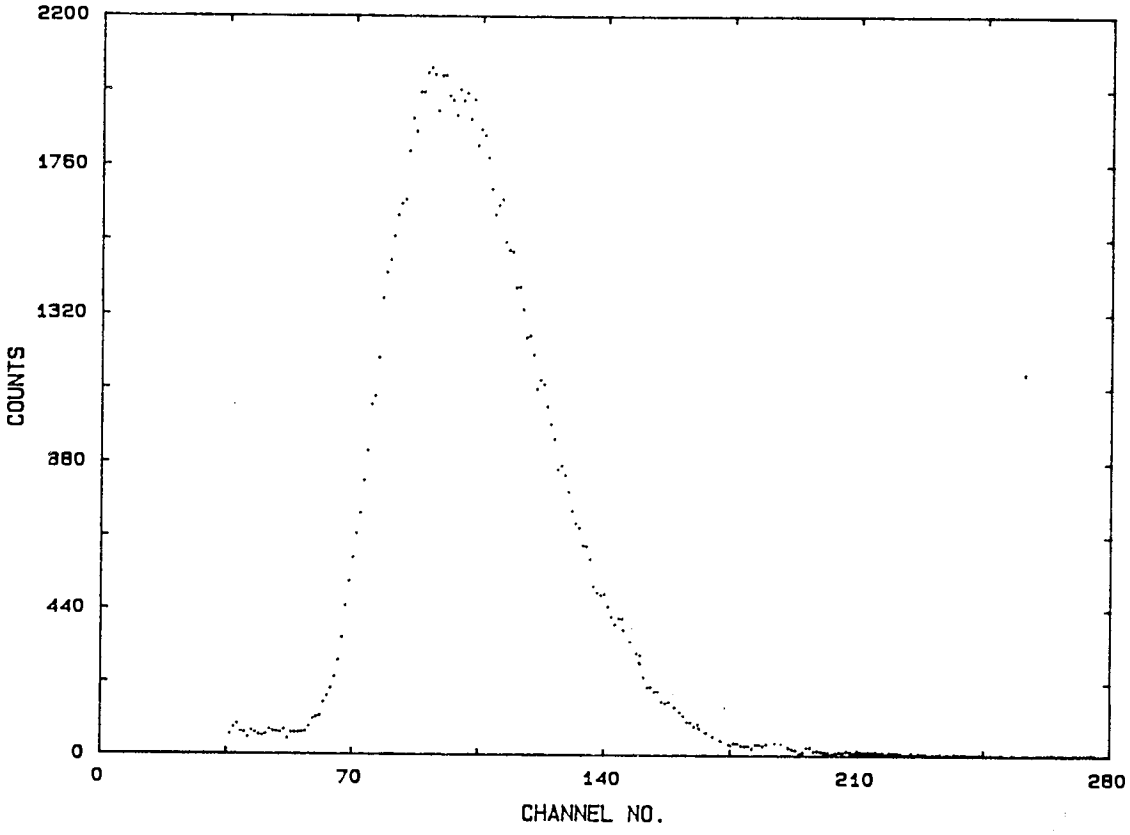

FIGURE 5.7

The spectrum of 2 μl polystyrene glue residue on Kimfol

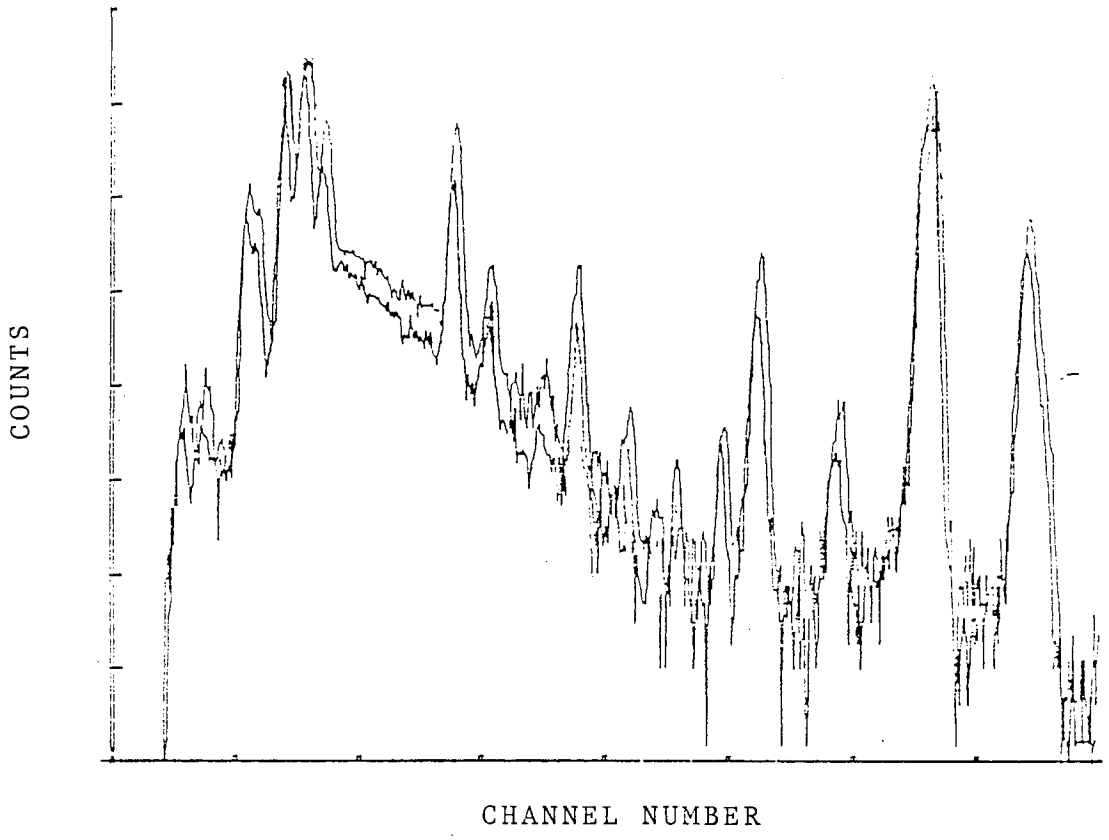

FIGURE 5.8

The spectra of amniotic fluid (AFF2) sample (a) with and (b) without glue fixation

material and due to its high solubility in water. Certain labelling elements, such as Sr may effect the sample elements like Ca owing to their somewhat similar chemical pattern, Paschoa, 1984, but no such effect for yttrium as an internal standard has been reported.

185 mg of yttrium nitrate ($Y(NO_3)_3 .3H_2O$) contains 50 mg Y. When this quantity is dissolved in distilled water and made up to 100ml it results in an yttrium concentration of 0.5mg/ml. 1ml of amniotic fluid sample was doped with 2ul of the prepared yttrium standard solution giving the required concentration of 1000 ppm. After the standard and the sample were well mixed the targets were prepared as already discussed above in sub-section 5.4.3.

5.8 Relative intensity calibration.

Before proceeding with the analysis of the actual samples, relative intensity calibration for elements of interest in amnoitic fluids were undertaken. Elements of special interest to the doctors at the Fazakley Hospital which supplied the samples were particularly Zn, Se and Cd.

Reference samples of different elements

were individually prepared using BDH (British Drug House) spectroscopy standard solutions doped with a quantity of yttrium to provide an internal standard of 1000 ppm concentration. The samples for different elements were prepared in a range of concentrations varying from 1 ppm to 1000 ppm.

Thin targets for measurements were prepared by dropping 4ul aliqouts of the reference sample onto Kimfol backing and drying in a clean desiccator as described earlier.

The targets were irradiated with a 2.5 MeV protons at a beam current of 10 nA until a statistically well defined peak for the element being measured was obtained. The irradiation time obviously depended on the sample and varied approximately between 60 seconds to 2000 seconds. Figures 5.9 and 5.10 shows typical spectra for Zn samples with 1000 ppm and 1 ppm concentrations respectively and both doped with same quantity of yttrium standard.

Figures 5.11, 5.12 and 5.13 show relative intensity calibration graphs for the elements Zn, Se and Cd. The insets in the figures represent results at lower values of concentrations.

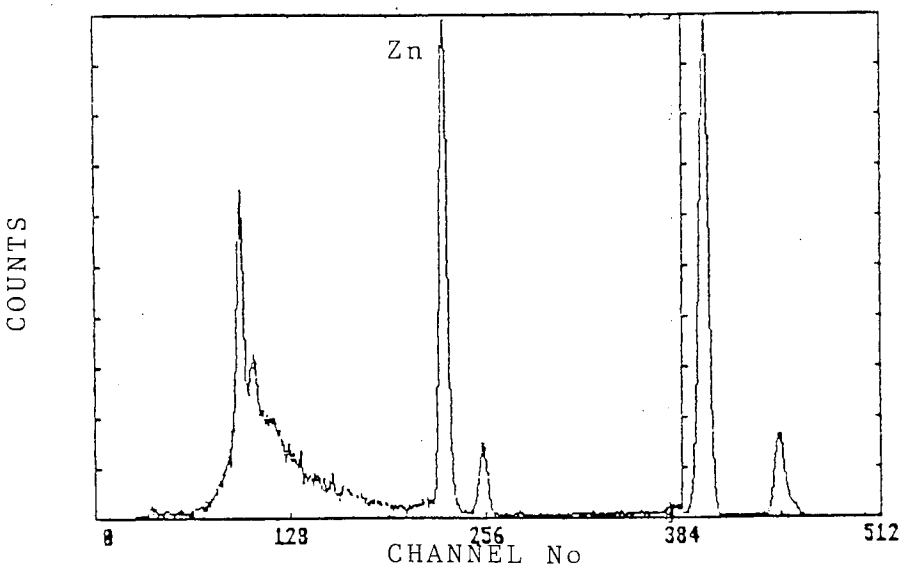

FIGURE 5.9

A typical spectrum of Zinc sample:
conc. 1000ppm

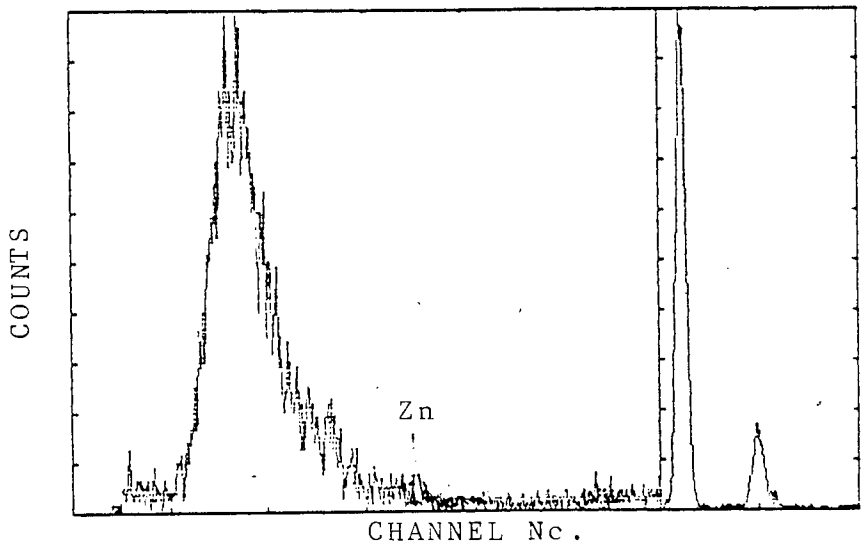

FIGURE 5.10

A typical spectrum of Zinc sample:
conc. 1ppm

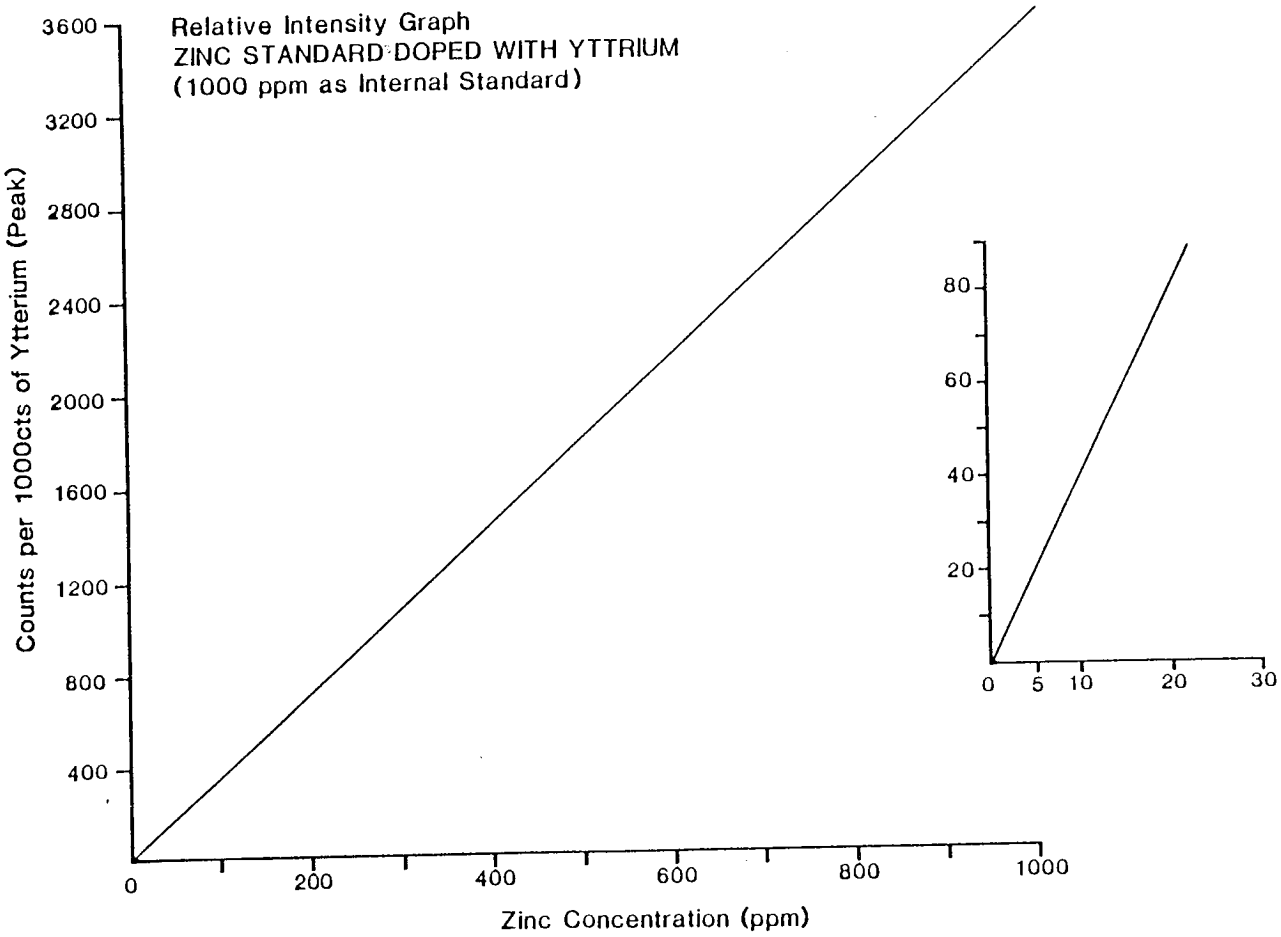
Relative Intensity Graph
ZINC STANDARD DOPED WITH YTTRIUM
(1000 ppm as Internal Standard)
Counts per 1000cts of Ytterium (Peak)
3600
3200
2800
2400
2000
1600
1200
800
400
0
200
400
600
800
1000
Zinc Concentration (ppm)
80
60
40
20
0
5
10
20
30

FIGURE 5.11

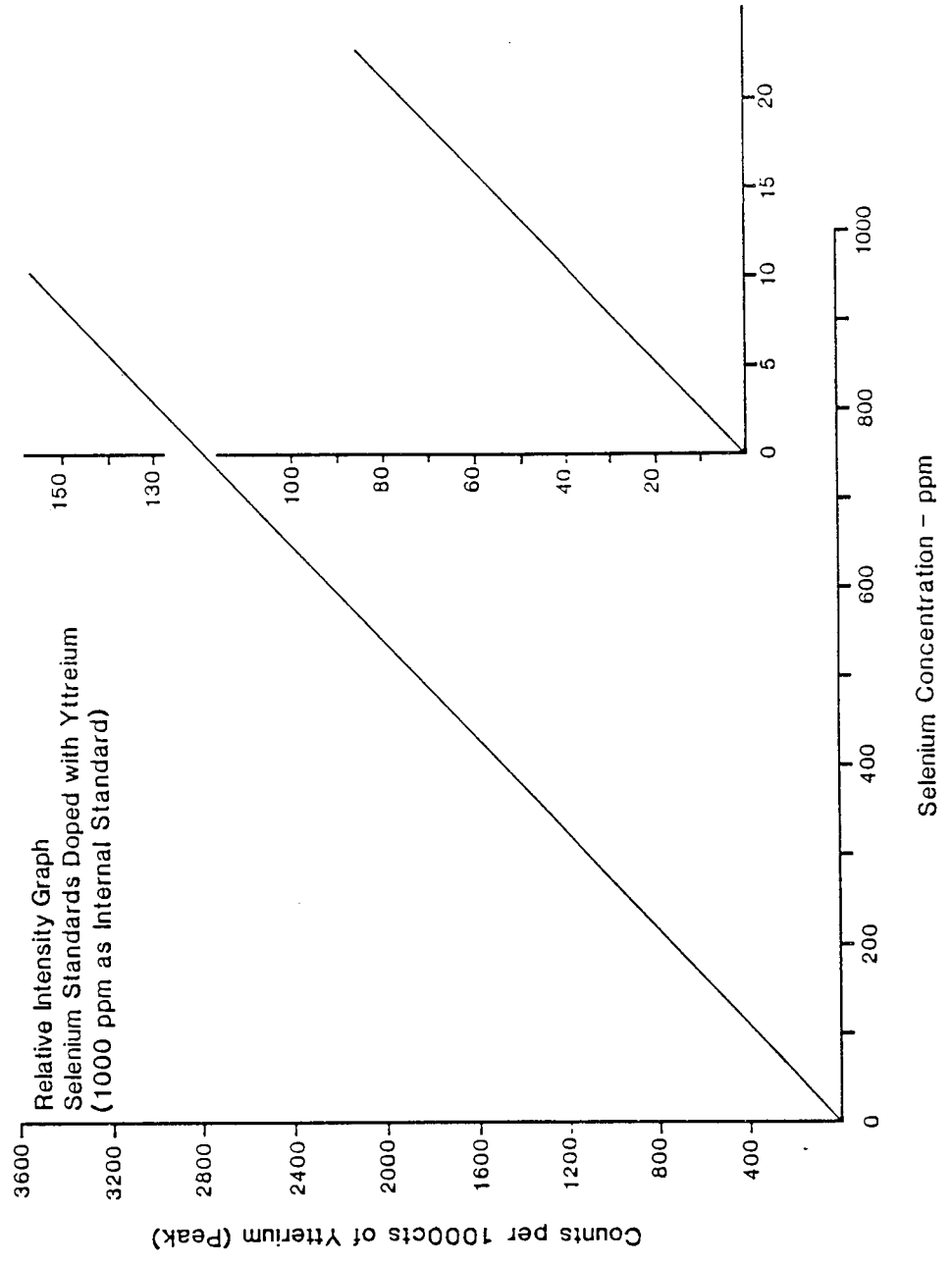
Relative Intensity Graph
Selenium Standards Doped with Yttreium
(1000 ppm as Internal Standard)
Counts per 1000cts of Yttrium (Peak)
Selenium Concentration - ppm
3600
3200
2800
2400
2000
1600
1200
800
400
0
200
400
600
800
1000
150
130
100
80
60
40
20
0
5
10
15
20

FIGURE 5.12

Relative Intensity Graph

Cadmium Standards Doped with Yttrium (1000 ppm as Internal Standard)

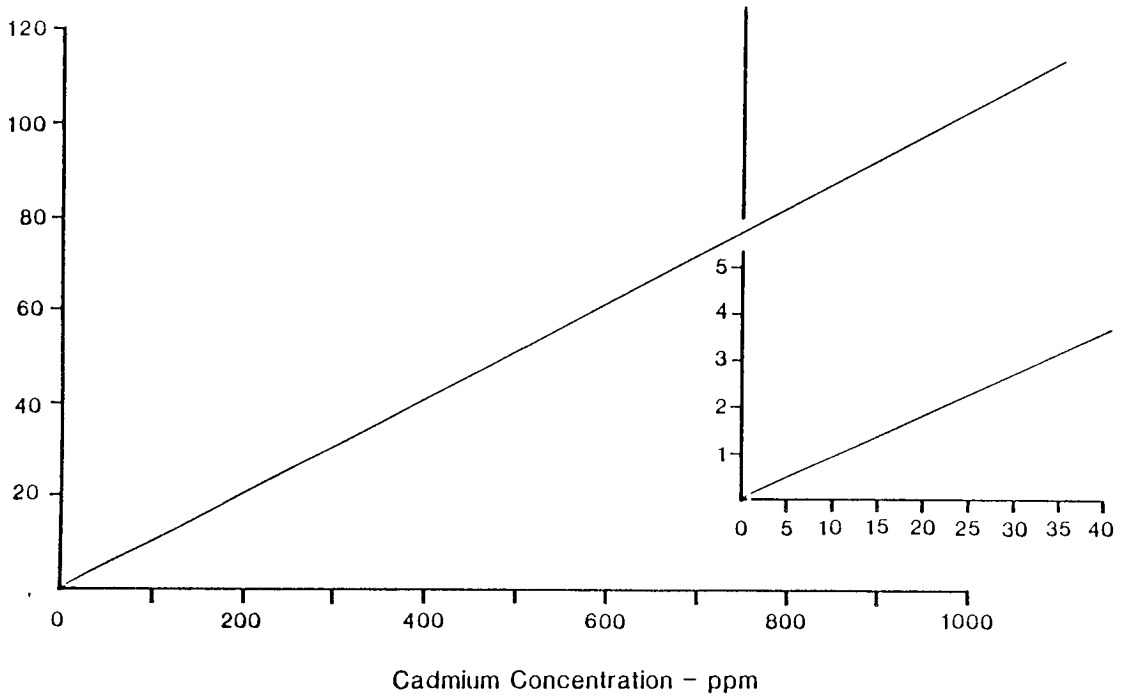

FIGURE 5.13

These graphs show that:

(i) the count rate is linear for all the concentrations used

(ii) count rate increases proportionally with the increase in the sample concentration

(iii) there is no X-axis or Y-axis offset indicating that there is no systematic error due to the experimental set up.

An interesting observation was made during relative calibration measurements. Several targets upon analysis showed zinc content far in excess of the quantities introduced. Kimguard disposable gloves, Kimberley Clarke Ltd., Kent, were worn as a precaution against contamination of the sample during thin target preparation for PIXE analysis. The gloves are normally dusted by the manufacturers with a powder before packing. This powder was the source of Zn contamination. Figures 5.14 and 5.15 show the spectra of the target handled with gloves and without gloves.

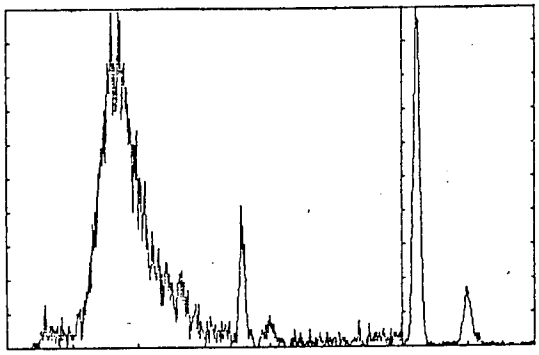

FIGURE 5.14

Spectrum of Kimfol "blank" contaminated
by Kimguard disposable gloves

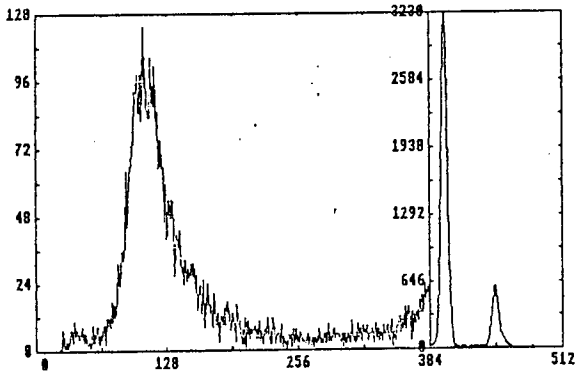

FIGURE 5.15

Spectrum of the Kimfol blank not contaminated

5.9 Amniotic Fluids - Analysis and Results.

Five thin targets from each of the ten pre-concentrated amniotic fluid samples were prepared as discussed in sub-section 5.6, and irradiated by a proton beam of 2.5 MeV energy. Beam currents of 10 to 15 nA were used and average measuring times, in which 10 μC of total integrated charge was collected, were in the region of 15 minutes.

Detector efficiency for medium Z elements of interest like Fe, Cu and Zn was improved by using 7 μm thick aluminium foil between the sample and detector. This X-ray filter absorbed some of the more intense X-ray yields produced by the light elements such as S, Cl, K and Ca present in abundance in amniotic fluids. The very large contribution from low energy X-rays makes it difficult for the medium and heavy elements present in very small amounts to be efficiently detected. The high count rate advesely affect the detector system due to the long time constants used in the amplifiers. The Al filter optimised the detection efficiency in the region of interest. Aluminium filter correction factors for different elements were computed as an integral part of the "Fxz programme" given in Appendix A.

Figures 5.16 to 5.21 show the typical pulse

FIGURE 5.17

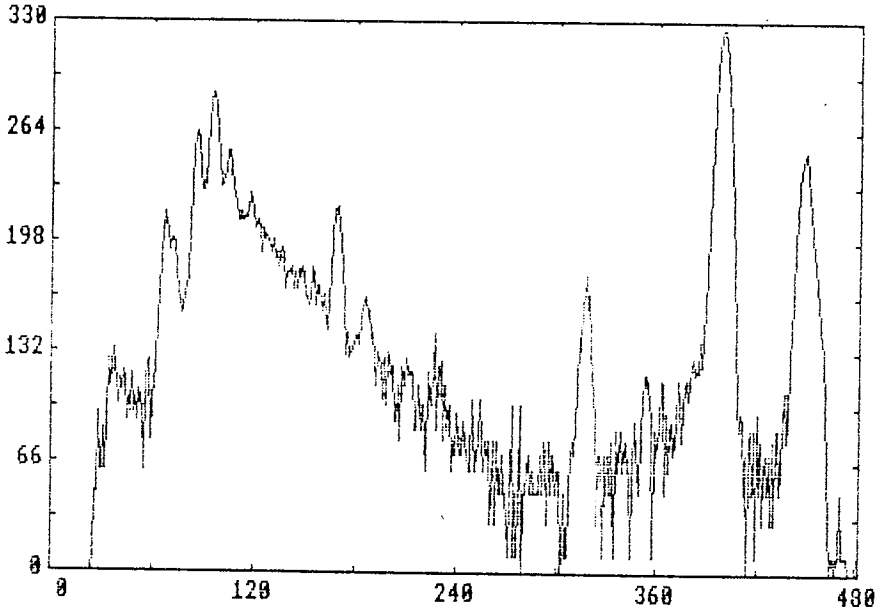

FIGURE 5.16

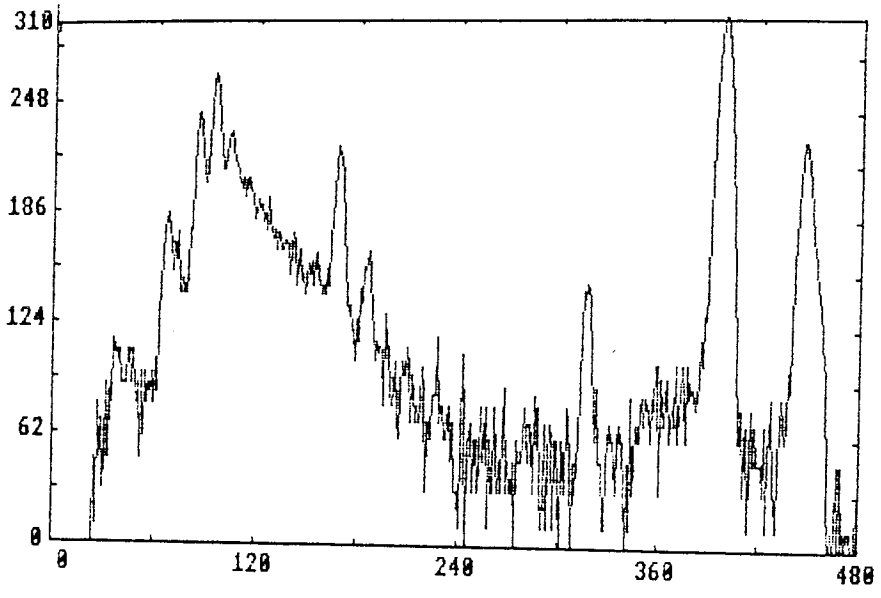

Typical pulse height spectra from the analysis of amniotic fluid samples.

FIGURE 5.18

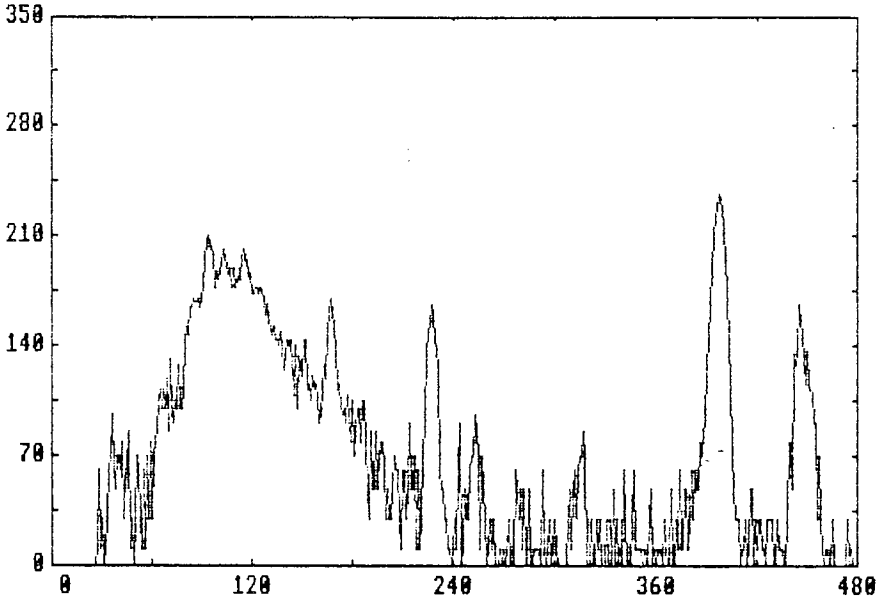

FIGURE 5.19

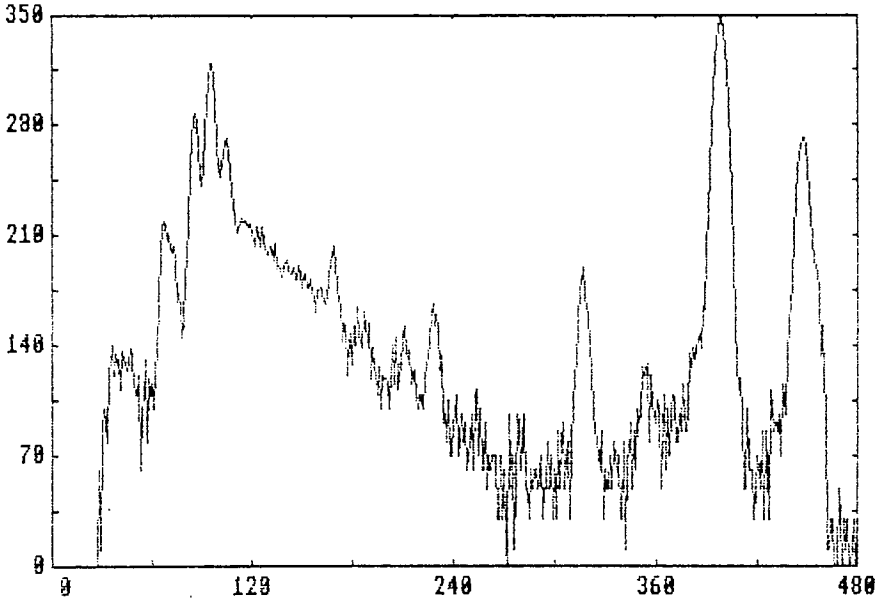

Typical pulse height spectra from the analysis of amniotic fluid samples.

FIGURE 5.20

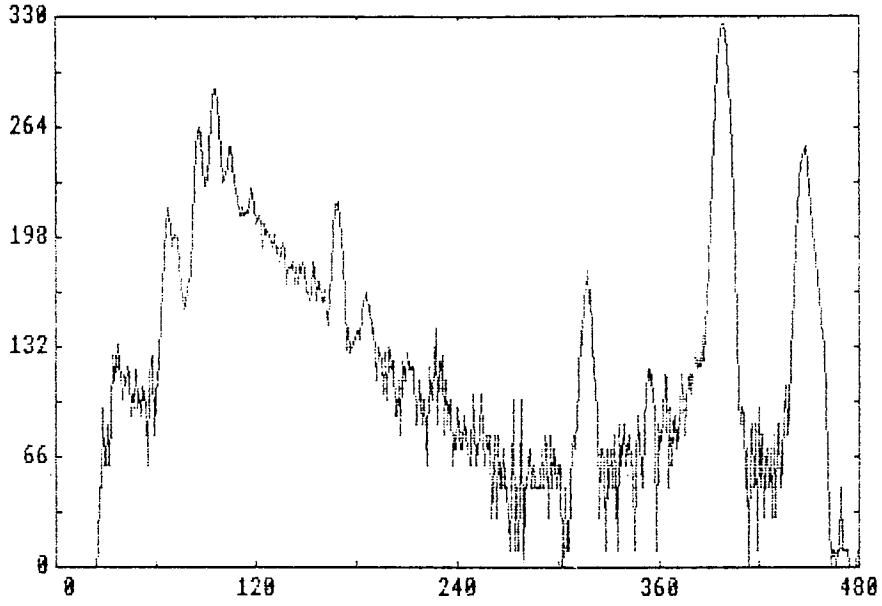

FIGURE 5.21

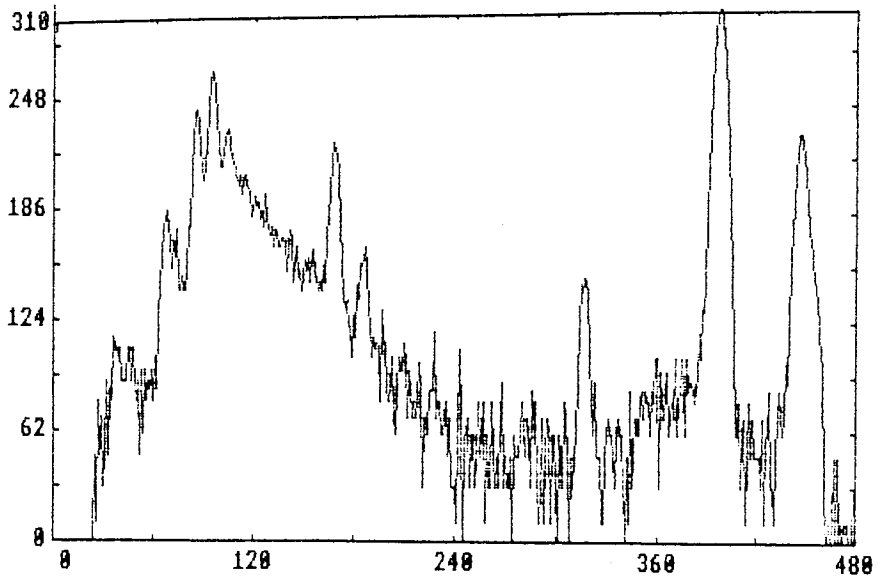

Typical pulse height spectra from the analysis of amniotic fluid samples.

height spectra from the analysis of samples AFF1, AFF4, AFP7, AFP8, AFP9 and AFP10. The vertical scales of the spectra are logarithmic, this visually enhances not only the region of low counts, but also the size of the bremsstrahlung background contribution relative to the peak amplitude. The peaks corresponding to fourteen elements ranging from Al (Z=13) to Y (Z=39) are easily identified in these spectra. The energies of the X-rays vary from about 1.5 to 15 keV.

The number of counts associated with each specified peak was obtained after subtraction of the associated background as described in Section 3.7.3. The average X-ray count from five samples prepared from each sample of amniotic fluid were used in calculating the base line elemental concentrations.

To calculate the mass of the elements in the samples, Equation 5.1 was employed with modifications to include corrections due to the X-ray absorber, 7um Al filter, and is given as :

$$Mz = Mst.(Yz/Yst).(Fst/Fz).(Calst/Calz)...5.1$$

where CalST and CalZ are the Aluminium filter correction factors for the standard and sample respectively. All other symbols are exactly the same as defined for equation 4.9.

The concentration in ppm were calculated by

rearraging equation 5.1 as :

Conc.ppm=(Mst/Mz).(Yz/Yst).(Fst/Fz).(Calst/Calz)..5.2

where Mst is expressed in ppm rather than mass of the internal standard and Mz denotes the concentration factor of the sample.

Table 5.1 shows the average concentrations obtained for the 10 samples for each of the eight elements measured. Each average is of 50 samples. The typical trend of the abundance of these elements in different samples of amniotic fluids are shown in graphical representation by Figures 5.22 to 5.31. Figure 5.32 shows the average concentration levels.

Brief comments on the elements measured and any necessary corrections in case of overlaps between the K-α and Kβ X-ray lines from neighbouring elements or interferences between K X-rays from light elements and L and M X-rays from heavier elements are given below :

Sulphur (S) : The resolution of the detector in the energy region of Kα X-ray line of S (2.307 keV) is equal to 115 eV, hence the Kβ peak of S (2.468 keV) cannot be completely separated from Kα peak. Therefore the S concentration was calculated using both the Kα and Kβ peak. Furthermore the Lα X-rays of Mo and Lβ X-rays of Nb and Mo lie in this region and may cause interference. This interference was negligible due to the relatively large quantities

TABLE 5.1

Measured elemental abundances
in amniotic fluids (ppm).

	ELEMENTS							
Sample	S	K	Ca	Fe	Cu	Zn	Se	Br
AFF1	378	134	94	1.1	0.28	0.61	0.20	8.6
AFF2	246	145	203	1.2	0.31	0.42	0.11	8.0
AFF3	428	147	196	4.8	0.42	0.62	0.13	7.2
AFF4	334	152	92	2.3	0.30	0.58	0.20	8.1
AFF5	460	168	224	1.4	0.39	0.38	ND	6.3
AFP6	180	137	180	0.8	0.12	0.12	ND	7.7
AFP7	410	105	90	3.4	0.32	0.63	0.11	8.4
AFP8	390	182	214	1.6	0.27	0.52	0.12	8.3
AFP9	387	148	192	1.5	0.29	0.81	0.12	8.7
AFP10	424	353	342	3.8	0.47	0.90	0.18	10.8
Mean	342	168	183	2.19	0.32	0.56	0.16	8.14
σ_n	128	65	73	1.30	0.10	0.20	0.04	1.10
Conc.	342	168	183	2.19	0.32	0.56	0.16	8.14
	±128	±65	±73	±1.30	±0.10	±0.20	±0.16	±8.14

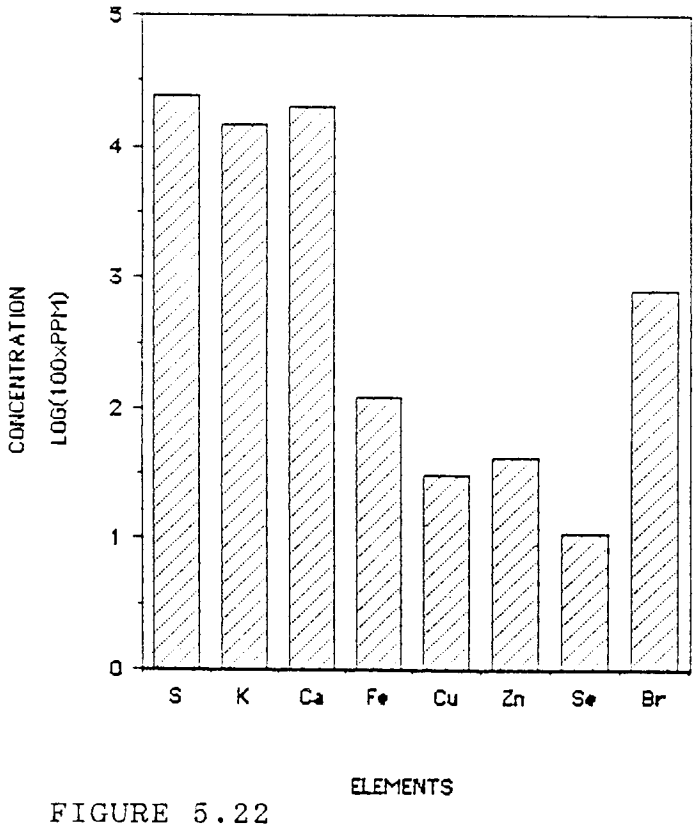

FIGURE 5.22

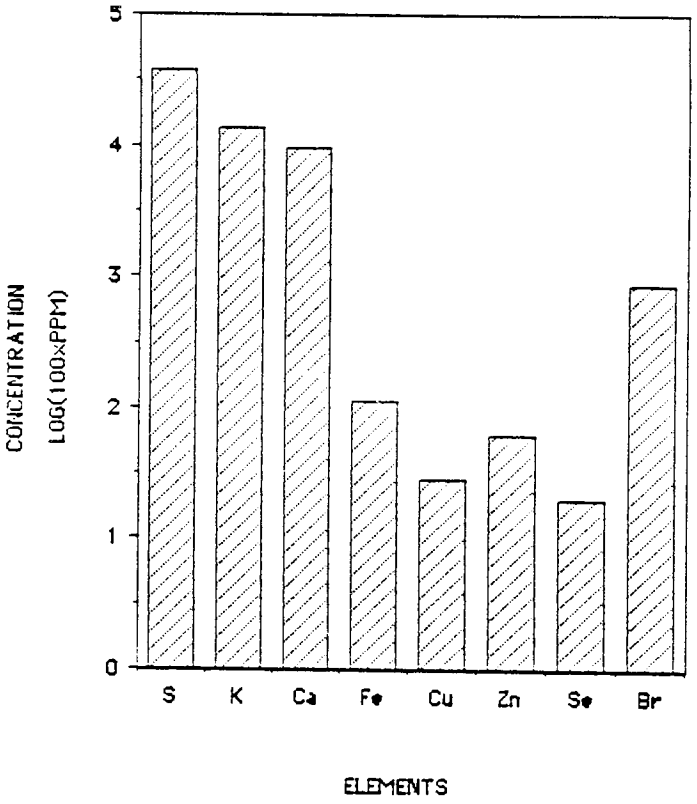

FIGURE 5.23

Typical elemental levels in the amniotic fluid samples

Typical elemental levels in the amniotic fluid samples

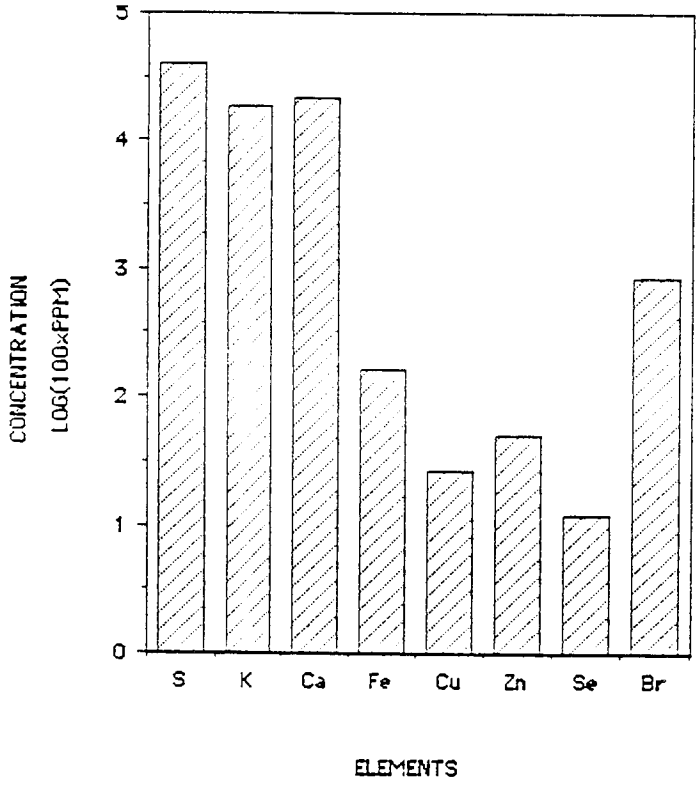

FIGURE 5.24

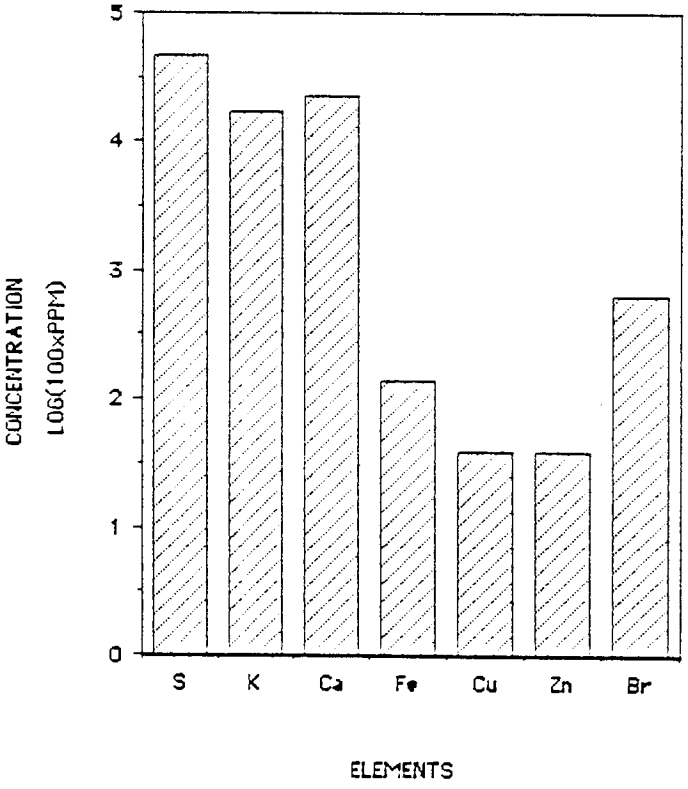

FIGURE 5.25

Typical elemental levels in the amniotic fluid samples

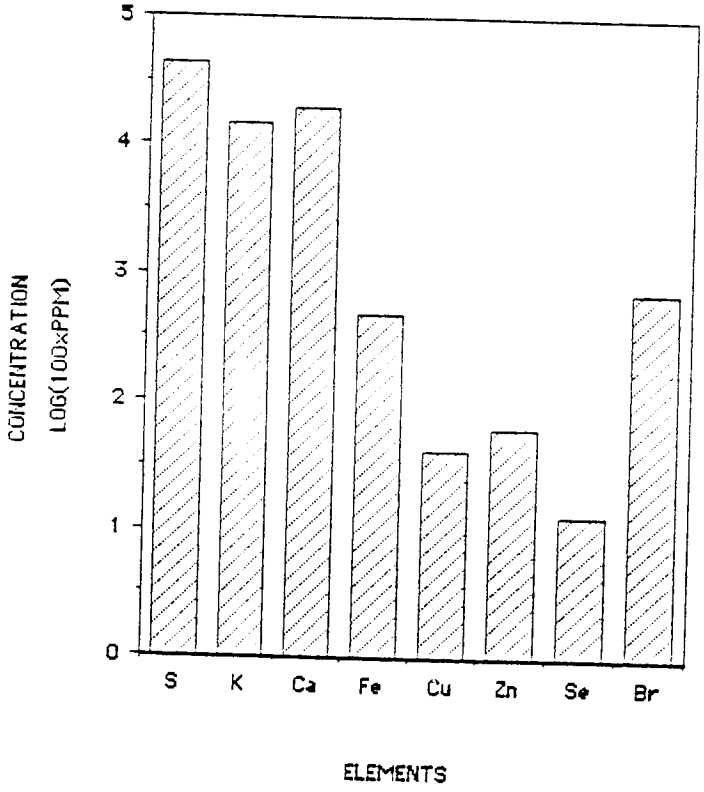

FIGURE 5.26

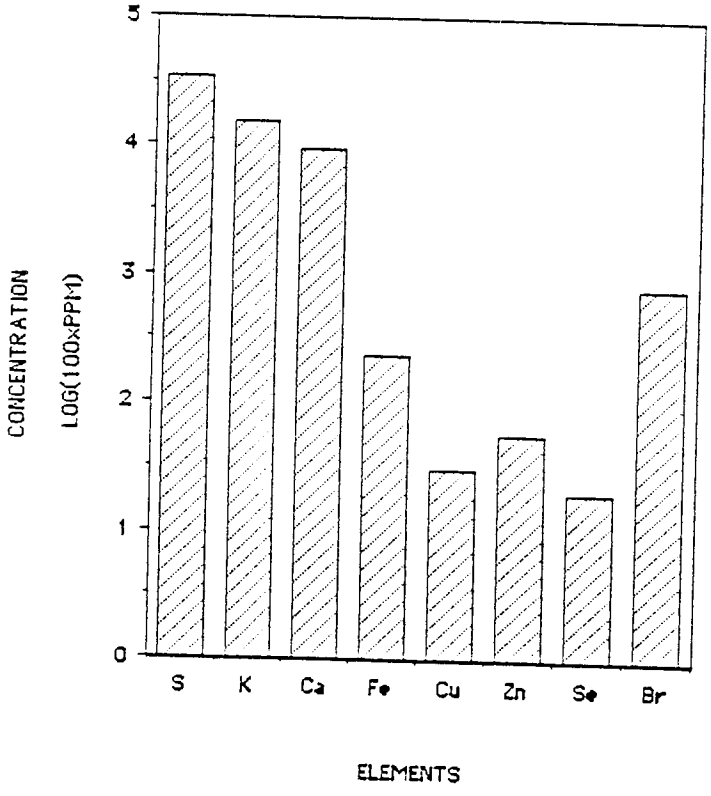

FIGURE 5.27

Typical elemental levels in the amniotic fluid samples

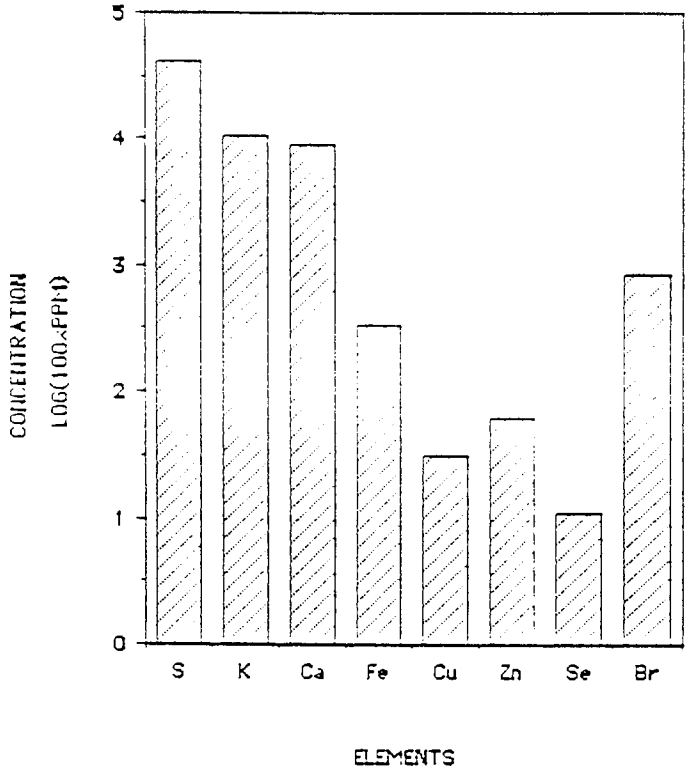

FIGURE 5.28

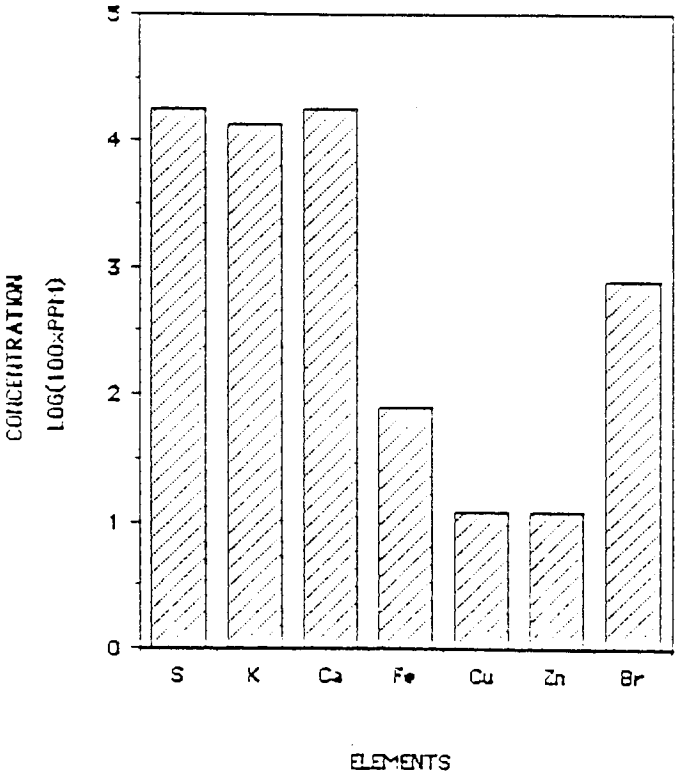

FIGURE 5.29

Typical elemental levels in the amniotic fluid samples

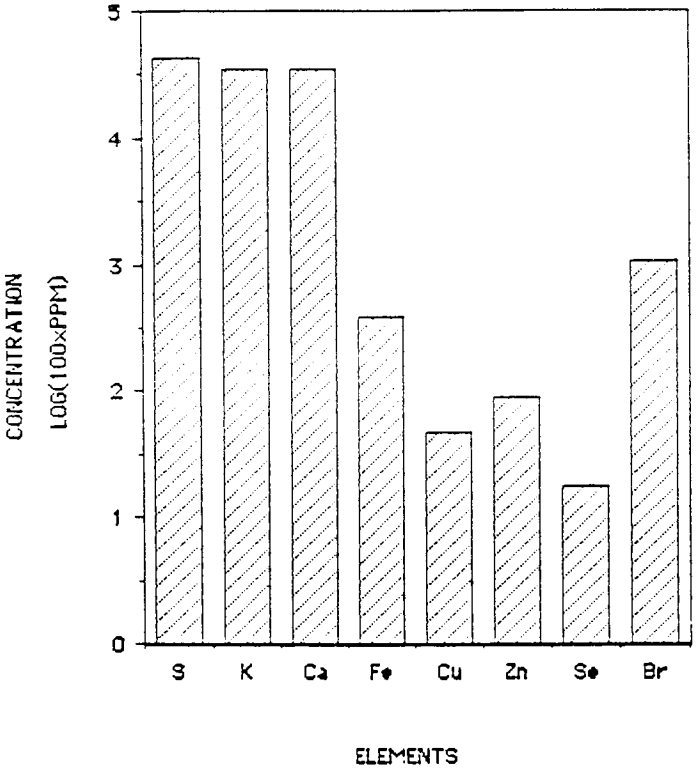

FIGURE 5.30

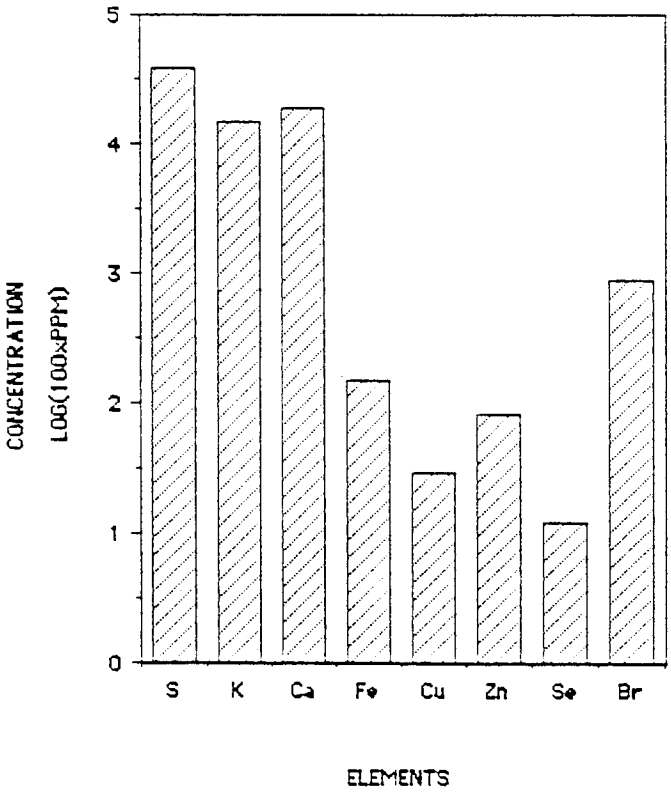

FIGURE 5.31

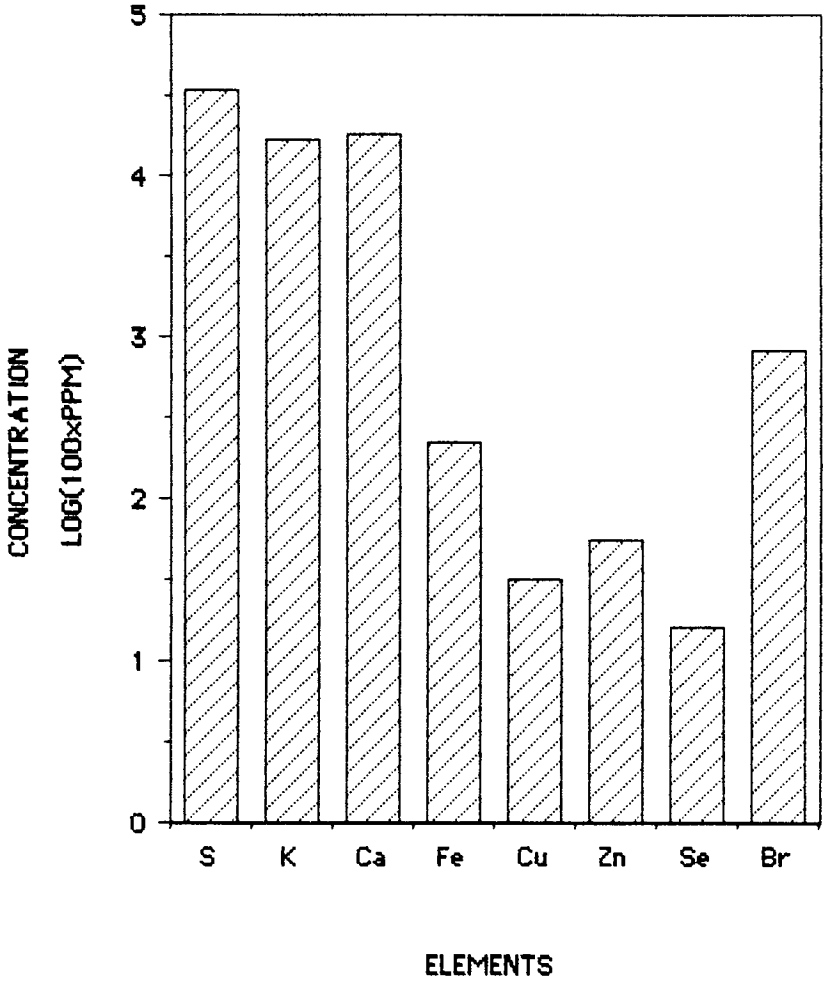

FIGURE 5.32

Mean elemental levels in the amniotic fluid samples

of S and undetectable small amounts of interfering elements present in the amniotic fluids.

Potassium (K) : Potassium Kα X-ray has an energy of 3.312 keV and its peak overlaps with any X-ray in the energy range of 3.718 to 3.442 keV, this is the region for L X-rays of elements 48<Z<52. No major interference from L X-rays were noticed.

Calcium (Ca) : The Potassium K_β peak overlaps the Ca K_α X-ray peak at 3.690 keV.The potassium K_β contribution was obtained from the published K_β / K_α ratio, Khan and Karimi 1980, and subtracted from the Ca K_α peak. No other interference was observed in this region.

Iron (Fe) : The Mn K_β X-ray line of 6.49 keV energy overlaps with Fe Kα X-ray. Since Mn was present in very small amount and detected only in 2 samples, AFP9 and AFP10, no corrections were nessary.

Nickel (Ni) and Copper (Cu) : Cu K_β at 8.907 keV interferes with Zn Kα at 8.631 keV energy. The Cu K_β contribution was calculated from the Cu K_β/K_α ratio and corrections were made to Zn Kx peak.

Selenium (Se) : No interference occurs with Se Kα X-rays at 11.210 keV.

Bromine (Br) : The only possible interference to Br Kα

X-ray at 11.907 keV is from As Kβ at 11.729 keV. As was detected only in 3 samples in very small amounts hence no interference correction was necessary.

5.9.1 Comparison of Amniotic Fluid Analysis.

The average results obtained for elemental levels are compared with the levels reported by other workers as given in Table 5.2, Hall et al, 1984, published their results representing mean concentration (ppm) for 5 elements measured in 53 samples of amniotic fluid using PIXE technique.

Ward et al, 1983, used neutron activation analysis (NAA) and a number of sample preparation techniques for different elements to analyse amniotic fluids at normal and varying gestational periods. Their results for selected elements in normal pregnancies are shown in ppm for comparison.

A literature survey of elemental concentration in amniotic fluids clearly show the scarcity of reference data, some publications report only a few elements, Chez et al, 1978, a few others have reported only the ratio of one element to another Torrisi and Forti, 1982.

TABLE 5.2

Comparison of mean elemental abundance in amniotic fluids.

Element	Hall et al 1984	Ward et al 1983	Present work
S	-	672 ± 303	342 ± 128
K	-	194 ± 82	168 ± 65
Ca	73 ± 30	164 ± 41	183 ± 78
Fe	0.4 ± 0.3	5.6 ± 2.4	2.19 ± 1.3
Cu	0.3 ± 0.1	0.37 ± 0.12	0.32 ± 0.1
Zn	0.1 ± 0.07	0.65 ± 0.24	0.56 ± 0.2
Se	-	0.1 ± 0.04	0.16 ± 0.04
Br	0.1 ± 0.1	3.69 ± 1.71	8.14 ± 1.10

The data in table 5.2, clearly indicates a reasonable agreement between the results of Ward et al, 1983, and the present work, although different analytical and sample preparation techniques were used. The results of Hall et al 1984 are lower by a factor of 2-5. A plausible explanation for this could be that the samples used by Hall et al, were of the supernatant, obtained after centrifugation in order to settle the corpuscular and cellular components of the samples. According to Rosick et al, 1983, a high proportion of elements are bound to particles, for example, for Zn the fraction is 40%. For Cu the results are in very good agreement, possibly indicating that binding of Cu to corpuscular and cellular components in amniotic fluids is very small.

The medical interpretation of the data obtained is beyond the scope of the present work. It is however being studied by the medical group at the Fazakeley Hospital, Liverpool, which supplied the samples and initiated this study.

5.9.2 Comparison of PIXE and AAS Results for Certain Elements.

All amniotic fluid samples analysed by PIXE were also measured by atomic absorption spectroscopy (AAS) for selected elements for comparison. AAS is a well

established and widely used elemental analysis technique. The samples were analysed using a Perkin-Elmer 460 atomic absorption spectrophotometer in the Geology Department at the University.

The results of the analysis for the elements measured, together with PIXE results in the present work are shown in Table 5.3 for comparison. The agreement between the results obtained from the two methods is fairly good. The only exception is Cu in which the AAS results are systematically lower than those of PIXE. Very large amount of sodium concentration is known to be present in amniotic fluid as confirmed by AAS (table 5.3), but is too low for present PIXE system.

Although restrictive detection of light elements, $Z \lesssim 14$, proved limitations of the present system, PIXE has demonstrated its powerful capabilities in analysing amniotic fluid samples. Very small amount of sample is needed, where as relatively large quantities are required for AAS. For the PIXE analysis the volume of fluid required per sample was 4ul whereas with the AAS the volume of the solution needed was as much as 1ml per element per sample. Limited amount of samples available was indeed the reason for restricting analysis to six elements using AAS. PIXE spectra of the amniotic fluid clearly shows the multi-elemental nature of the technique. It is possible to detect nearly all

TABLE 5. 3

Comparison of results
for certain elements in amniotic fluids.
(Results are quoted as average of 10 samples)

Element	AAS	PIXE
Na	3248 ±368	-
K	152 ±42	168 ±65
Ca	174 ±81	183 ±78
Fe	2.30 ±0.9	2.19 ±1.3
Zn	0.62 ±0.08	0.56 ±0.2
Cu	0.18 ±0.04	0.32 ±0.1

the elements simultaneously in amniotic fluid in the range $14<Z<39$.

Finally an accurate and reliable PIXE system developed in the present work has been successfully applied to the analysis of amniotic fluids. The results obtained agrees well with those obtained for selected elements using AAS and with the results of Ward et al, 1983. Fast, accurate, simultaneous multi-elemental PIXE technique is clearly an ideal analytical method for the analysis of body fluids such as amniotic fluids.

CHAPTER VI

6.0 CONCLUSIONS.

A proton induced X-ray emission analysis system has been developed in the present work to give cost-effective and reliable quantitative multi-elemental analysis of a large number of samples. An existing PIXE beam line at the Radiation Centre was re-designed and modified to include several entirely new features which include;

a) a large versatile vacuum chamber,
b) an automatic multi-sample system,
c) an on-demand beam pulsing facility,
d) a foil beam monitoring system,
e) an RBS spectroscopy facility.

The PIXE system as described and evaluated in Chapter III and IV respectively, has been demonstrated to provide an accurate and fast multi-elemental analytical system capable of quantitative analysis of elements in the range of $14<Z<42$. The ability to detect elements lighter than silicon ($Z=14$) is limited by the X-ray detector system used. Modern, state of the art, window less energy-dispersive Si(Li) detectors available commercially could be employed however, to detect and analyse elements as low as carbon using the

present system.

The care and attention given to design details and the installation of the PIXE beam line combining the new features is clearly reflected in the improved reproducibility and analytical capability of the present system. The improvements which eliminates some of the previously existing limitations are summarised below:

(a) A 20 fold increase in sample handling capacity without having to open the vacuum chamber to the atmosphere.

(b) An approximately 40% improvement in accelerator 'down' time resulting in more cost effective sample analysis.

(c) A provision for routine X-ray detection in the backward direction of 135° with respect to the incident proton beam giving improved signal-to-background ratio.

(d) A re-entrant tube arrangement enabling a detector to be positioned close to the target but outside the vacuum environment of the sample chamber.

(e) A virtual elimination of the photon background due to the scattered protons and X-ray fluorescence of the chamber components, thus improving the the accuracy of analytical measurements.

(f) A reliable and precise automatic sample changer capable of handling both thin and thick samples. Samples of thicknesses upto 4mm can be loaded in a standard carousel.

(g) The thick samples can be readily analysed using on-demand beam pulsing facility incorporated into the present system.

(h) Improved beam current monitoring facilities; (a) the foil ion beam monitoring, (b) the elastic backscattering from the target.

(i) An accurate and simple to operate electromechanical remote control unit for the sample changer.

(j) A provision for simultaneous PIXE and

RBS analysis.

The chamber has been constructed to accommodate an automatic multi-sample changer, beam monitoring and RBS spectroscopy facilities. It was designed especially to permit the X-ray detector to be positioned at either 90^0 or 135^0 to the incident proton beam whether in or outside the vacuum chamber. A reduction of 40% in bremsstrahlung background at 135^0 position with respect to the normal 90^0 detector position was obtained confirming work of Ishii et al, 1977 and Folkmann et al, 1984. The resulting improvement in signal-to-noise ratio at 135^0 compared to 90^0 position would be exploited in future by other workers.

The overall efficiency of the system has been improved by the use of large detector solid angles to get acceptable results in inherently low count rate situations. Another advantage of the present target chamber is that simultaneous PIXE and RBS measurements can be made. An example is the elastic backscattering from targets which has been widely used in the present work as a relative sample charge monitoring facility, described in section 3.5.6.

An automatic multi-sample changer developed in the present study has greatly improved the system. It is capable of handling a large series of thick or thin targets. Upto eighty samples can be analysed without

opening up the vacuum chamber, thus reducing accelerator "down" time which results in considerable cost savings. Over the last six years the sample changer has proved its mechanical precision and reliability. It is easy to setup and use. It is economical to run and maintain. No deterioration in position to position of sample repeatability has occurred during the present work.

The foil ion beam monitoring system, based on the work described by Mitchell et al, 1980, has been demonstrated to be more accurate than the conventional beam current integrator employed previously.Preliminary measurements with the foil ion beam monitoring indicate an accuracy of $\pm$2%, whilst the beam current integration measurements are estimated to have an uncertainty of $\pm$10% and also are often subject to large systematic uncertainties. In the present measurements, energy and angular straggling of the beam after passing through the Au foil have been neglected since beam monitoring was only used as a comparator for normalising sequential irradiations. However this could form an important study for future work if absolute measurements are needed. Mitchell et al, 1980, also reported foil thickening due to carbon deposits. No such formation was noticed in the present study after irradiation times of 3-4 hours. Here again, further work could prove useful in establishing the cleanliness of the vacuum system. This method of beam monitoring

is particularly suitable for non-conductive targets, especially where the usual electron suppression at the targets cannot be made. The main disadvantage of this technique was found to be mechanical strength and stability of the thin self-supporting foils employed. Great care had to be taken during initial pumping down of the chamber as too quick an evacuation as well as any mechanical shock led to the rupture of the foil.

The on-demand beam pulsing system has made marked improvements in the count rate handling capability. Counting rate capability of the present detection system with the main amplifier time constant of 8 μsec has been extended from normal 1000 c/s to 10000 c/s with the beam pulsing system. The spectral distortion due to pulse pile up continuum normally encountered at high count rates above 1000c/s has been eliminated.

The system has been successfully used to give quantitative multi-element analysis of elements Si, S, K, Ca, Fe, Co, Ni, Cu, Zn, As, Se, Br, Y, Mo and Cd. System calibration in terms of response functions F(x,z) values at different proton energy for the previous and the new system has been established using commercially available thin standard foils of known areal density on Nuclepore backing. These are in good agreement with the calculated calibration response functions obtained using published X-ray cross-section data. A further independent check of system calibration

at 2.5 MeV proton energy was carried out by analysing bovine liver Standard Reference Material 1577 and is found to be in good agreement with published results.

A major contribution of this work is the experimentally determined minimum detectable limits (MDL) achievable for a wide range of proton energies as a function of atomic number Z with particular reference to the light and intermediate weight elements.

This is the first time that MDL's have been experimentally measured for proton energies of 1, 1.2, 1.5, 2.0, 2.5 and 3.0 MeV for atomic numbers $14 \leqslant Z \leqslant 42$ employing the previous system. The MDL's were also determined with beam energies of 1.5, 2.0 and 2.5 MeV using new vacuum chamber at both detector positions of 90^{o} and 135^{o} with respect to the incident beam. The results obtained are similar in trend to those predicted by Folkmann et al, 1974a, 1974b.

In calculating the MDL's a statistically meaningful definition of sensitivity was used i.e $Ns=3\sqrt{(Nb)}$, where-as Folkmann et al, 1974a, 1974b employed a less rigorous definition of Ns=Nb,as discussed in section 4.4.2, which is probably the reason for the differences in the general shape of the MDL curves. The family of MDL curves for different energies provide a very useful indication regarding the experimentally achievable sensitivity of the system.

The improved sensitivity for the new system has been clearly demonstrated. The system reliability and

reproduciblity was regularly checked throughout this work by irradiating one or two standard foils, in case beam conditions or target geometry had altered with time. No noteworthy change was observed. It is therefore concluded that the system is accurate and reliable.

The PIXE analysis system was applied to the analysis of amniotic fluid samples obtained via transabdominal amniocentesis from normal pregnancies. The base line elemental concentration levels are extraordinarily scarce in the published reference data.

Amniotic fluid is not a homogeneous solution, it contains corpuscular and cellular particles suspended in the fluid. To overcome this problem of inhomogeneity 5 replicate targets were prepared from each amniotic fluid sample and analysed. The average elemental concentration in ppm from 50 samples was obtained for each element. Samples were also analysed for Na, K, Ca, Fe, Cu and Zn by atomic absorption methods to compare with the present PIXE results. Mean elemental concentrations levels in amniotic fluids as reported by Hall et al, 1984, show large systematic differences. Possible reasons for the difference highlighted by the present analysis have been discussed in section 5.9.1. Analysis of Ward et al, 1983, indicate much better agreement with our measurements.

Two computer programs were developed, the program

"Fxz" calculates theoretical F(xz) system response function values, whilst program "RBSTM" determines the areal density of thin foils using RBS measured data (Chu et al,1978).Areal densities of the standard foils supplied by Micro-Matter, Eastsound, where checked and found to be within manufacturers specification except for Ti foil.

A further development could be a totally automatic computer controlled PIXE system for on-line analysis.

Analytical capabilities of PIXE may be extended in future by coupling non-vacuum technique with a focused microbeam to study the localised concentration variations in a sample.

Nuclear reactions induced in the target by the proton beam could also be employed for analysis of elements with atomic number lower than 14 in future work.

In conclusion the test of developing and improving the quality, accuracy, sensitivity and reliability of the existing analytical system is continuous. The results of the present work are significant in that not only has a versatile PIXE system been developed, evaluated and applied to an important area of present research, but that these results will prove valuable to future workers in making

further improvements. As the demand for particular problem arises so does the improvements continue to meet this constant need for upgrading the system.

```
ST
   50 CLS
  100 PRINT"*****HELLO*****"
  110 PRINT
  150 PRINT:PRINT
  160 PRINT"FXZ VALUE CALCULATIONS"
  170 PRINT"========================="
  180 PRINT
  190 PRINT"HOW MANY THEORETICAL FXZ VALUES"
  200 PRINT"DO YOU WANT TO CALCULATE"
  210 INPUTO
  220 FOROI=1TO O
  230 PRINT"(1) ABSORPTION"
  240 PRINT"--------------"
  250 PRINT"CORRECTIONS"
  260 PRINT"-----------"
  270 PRINT"ENTER VALUE FOR INCIDENT"
  280 PRINT"X-RAY ENERGY(XE) IN KEV"
  290 INPUT XE
  300 PRINT
  310 B1=5.0311+9.2822*LN(XE)-19.1765*((LN(XE))^2)+15.1821*((LN(XE))^3)
  320 B2=-6.4213*((LN(XE))^4)+1.3724*((LN(XE))^5)-0.1162*((LN(XE))^6)
  330 UW=EXP(B1+B2)
  340 CW=EXP(-UW*1.39*0.005)
  350 PRINT"MELENEX WINDOW CORRECTION(CW)"
  360 PRINT"IS"
  370 PRINT"CW="CW
  380 PRINT
  390 R1=11.2465-14.0326*LN(XE)+15.6369*((LN(XE))^2)-10.6818*((LN(XE))^3)
  400 R2=3.80705*((LN(XE))^4)-0.6843*((LN(XE))^5)+0.048998*((LN(XE))^6)
  410 UA=EXP(R1+R2)
  420 CA=EXP(-UA*0.001205*3.2)
  430 PRINT"AIR GAP CORRECTION(CA)"
  440 PRINT"IS"
  450 PRINT"CA="CA
  460 PRINT
  470 T1=9.213-3.1837*LN(XE)-0.024204*((LN(XE))^2)+0.0002635*((LN(XE))^3)
  480 TX=EXP(T1)
  490 UB=0.06683*TX
  500 CB=EXP(-UB*0.0023)
  510 PRINT"BERYLLIUM WINDOW CORRECTION(CB)"
  520 PRINT"IS"
  530 PRINT"CB="CB
  540 PRINT
  550 SI=13.3708-2.1435*LN(XE)-0.2654*((LN(XE))^2)+0.02431*((LN(XE))^3)
  560 SX=EXP(SI)
  570 UE=0.02144*SX
  580 IFXE<=10GOTO600
  590 IFXE>10GOTO620
  600 EF=1
  610 GOTO630
  620 EF=1-EXP(-UE*2.33*0.3)
  630 PRINT"INTRINSIC EFFICIENCY(EF) OF THE"
  640 PRINT"SI(LI) DETECTOR"
  650 PRINT"IS"
  660 PRINT"EF="EF
  670 PRINT
  680 PRINT"DETECTOR SOLID ANGLE(P) IS"
  690 P=1.401E-3
  700 PRINT"P="P:PRINT
  710 AE=P*CW*CA*CB*EF
  720 PRINT"ABSOLUTE EFFICIENCY(AE) OF THE"
  730 PRINT"SI(LI) DETECTOR IS"
  740 PRINT"AE="AE:PRINT
  750 PRINT
  760 PRINT"(2) PRODUCTION CROSS-SECTION(PX)"
```

```
 720 PRINT"ABSOLUTE EFFICIENCY(AE) OF THE"
 730 PRINT"SI(LI) DETECTOR IS"
 740 PRINT"AE="AE:PRINT
 750 PRINT
 760 PRINT"(2) PRODUCTION CROSS-SECTION(PX)"
 770 PRINT"-------------------------------"
 780 PRINT"CALCULATION"
 790 PRINT"-----------":PRINT
 800 PRINT"(2A)IONIZATION CROSS-SECTION"
 810 PRINT"----------------------------"
 820 PRINT"CALCULATIONS(IX)"
 830 PRINT"-----------------"
 840 PRINT
 850 PRINT"ENTER VALUE FOR K SHELL"
 860 PRINT"BINDING ENERGY(EK)IN KEV"
 870 INPUT EK
 880 PRINT"ENTER VALUE FOR PROTON BEAM"
 890 PRINT"ENERGY(E)IN KEV"
 900 INPUT E
 910 V=E/(1836*EK)
 920 IFE<1000THEN1330
 930 IFE>3000THEN1330
 940 J=LN(V)
 950 Y=(-45.88-3.226*J-2.705*(J^2)-0.6366*(J^3)-0.0645*(J^4))
 960 IX=(EXP(Y))/(EK^2):PRINT
 970 PRINT"IONIZATION CROSS-SECTION(IX)"
 980 PRINT"IS"
 990 PRINT"IX="IX:PRINT
1000 PRINT"(2B)FLUORESCENCE YIELD(W)"
1010 PRINT"-------------------------"
1020 PRINT"CALCULATION"
1030 PRINT"-----------"
1040 PRINT
1050 PRINT"ENTER VALUE FOR ATOMIC"
1060 PRINT"NUMBER OF TARGET(ZT)"
1070 INPUTZT
1080 IFZT>50THEN1340
1090 IFZT<22THEN1340
1100 PRINT
1110 PY=0.015+0.0327*ZT-0.64E-6*(ZT^3)
1120 W=(PY^4)/(1+(PY^4))
1130 PRINT"W="W
1140 PX=IX*W
1150 PRINT"X-RAY PRODUCTION CROSS-SECTION(PX)"
1160 PRINT"IS":PRINT
1170 PRINT
1180 PRINT"PX="PX:PRINT
1190 PRINT"(4)THEORETICAL FXZ VALUE"
1200 PRINT"============================"
1210 PRINT"CALCULATION"
1220 PRINT"==========="
1230 PRINT
1240 PRINT"ENTER VALUE FOR"
1250 PRINT"ATOMIC WIEGHT(A)"
1260 INPUT A
1270 FXZ=6.022E23*P*IX*W*CW*C8*CA*EF/(A*4*PI)
1280 PRINT
1290 PRINT"FXZ="FXZ
1300 PRINT"======================="
1310 PRINT
1320 GOTO1440
1330 V$="PROTON ENERGY":GOTO1390
1340 V$="ATOMIC NUMBER":GOTO1390
1350 PRINT"NUMBER OF FREE BYTES=";FRE(0)
1360 PRINT
1370 PRINT"%%%%% THANKYOU & GOODBYE %%%%%"
```

```
1380 END
1390 CLS:PRINT
1400 PRINT""V$" NOT WITHIN LIMITS HENCE":PRINT
1410 PRINT"EXPRESSION NOT VALID":PRINT
1420 PRINT"CHECK INPUT DATA & UNITS"
1430 GOTO1380
1440 PRINT"DO YOU NEED EXPERIMENTAL FXZ"
1450 PRINT"VALUES YES=1 NO=0"
1460 INPUTEM
1470 IF EM=1GOTO1490
1480 IF EM=0:DP=0:GOTO2020
1490 PRINT"ENTER VALUE FOR KEITHLEY"
1500 PRINT"FULL SCALE DEFLECTION(SD)"
1510 PRINT"IN MICRO-AMPS"
1520 INPUTSD
1530 PRINT"ENTER VALUE FOR DIVIDING FACTOR(N2)"
1540 INPUTN2
1550 PRINT"ENTER VALUE FOR PRESET(PC)"
1560 INPUTPC
1570 BC=SD*N2*PC/1E5
1580 PRINT
1590 PRINT"PROTON BEAM CHARGE(BC) IN"
1600 PRINT"MICRO-COULOMBS IS"
1610 PRINT"BC=";BC
1620 NP=BC*1E-6/1.602E-19
1630 PRINT
1640 PRINT"NUMBER OF PROTONS(NP) PER"
1650 PRINT"";BC;"MIC-COUL"
1660 PRINT"NP=";NP
1670 PRINT
1680 PRINT"DO YOU NEED ALUMINIUM"
1690 PRINT"CORRECTION YES=1;NO=0"
1700 INPUTAN
1710 IF AN=1GOTO2180
1720 IF AN=0GOTO1730
1730 AC=1
1740 PRINT"ENTER VALUE FOR NUMBER OF"
1750 PRINT"X-RAY COUNTS(NX) PER"
1760 PRINTBC;"MICRO-COULOMB"
1770 INPUTNX
1780 XC=NX/(BC*AC)
1790 PRINT
1800 PRINT"NUMBER OF X-RAY COUNTS(NX) PER"
1810 PRINT"MICRO-COULOMB IS"
1820 PRINT"NX=";XC
1830 PRINT
1840 YE=NX/(NP*AC)
1850 PRINT"YIELD IN PHOTONS PER PROTON IS"
1860 PRINT"YIELD=";YE
1870 PRINT
1880 PRINT"ENTER VALUE FOR TARGET DENSITY(DT)"
1890 PRINT"IN GM PER CUBIC CM"
1900 INPUTDT
1910 PRINT"ENTER VALUE FOR TARGET"
1920 PRINT"THICKNESS(TT) IN CM"
1930 INPUT TT
1940 FE=YE/(DT*TT*SQR(2))
1950 PRINT
1960 LET DP=(FXZ-FE)/FXZ*100
1970 PRINT
1980 PRINT
1990 PRINT"EXPERIMENTAL"
2000 PRINT"FXZ="FE
2010 PRINT"======================"
2020 PRINT"THEORETICAL"
2030 PRINT"FXZ="FXZ
2040 PRINT"======================"
2050 PRINT"%DIFF="DP
```

```
1860 PRINT"YIELD=";YE
1870 PRINT
1880 PRINT"ENTER VALUE FOR TARGET DENSITY(DT)"
1890 PRINT"IN GM PER CUBIC CM"
1900 INPUTDT
1910 PRINT"ENTER VALUE FOR TARGET"
1920 PRINT"THICKNESS(TT) IN CM"
1930 INPUT TT
1940 FE=YE/(DT*TT*SQR(2))
1950 PRINT
1960 LET DP=(FXZ-FE)/FXZ*100
1970 PRINT
1980 PRINT
1990 PRINT"EXPERIMENTAL"
2000 PRINT"FXZ="FE
2010 PRINT"======================"
2020 PRINT"THEORETICAL"
2030 PRINT"FXZ="FXZ
2040 PRINT"======================"
2050 PRINT"%DIFF="DP
2060 PRINT"P="P
2070 PRINT"IX="IX
2080 PRINT"W="W
2090 PRINT"PX="PX
2100 PRINT"CW="CW
2110 PRINT"CA="CA
2120 PRINT"CB="CB
2130 PRINT"AC="AC;:PRINT"EF="EF
2140 PRINT"AE="AE
2150 PRINT"E="E;:PRINT"YIELD="YE
2160 NEXT
2170 GOTO1350
2180 PRINT"ALUMINIUM ABSORPTION"
2190 PRINT"--------------------"
2200 PRINT"CORRECTION (AC)"
2210 PRINT"-----------------"
2220 PRINT
2230 PRINT"ENTER THICKNESS OF ALUMINIUM"
2240 PRINT"FOIL(AT)IN CM"
2250 INPUTAT
2260 IFXE<8GOTO2280
2270 IFXE>=8GOTO2300
2280 AY=1734-35544*(XE^-1)+254856*(XE^-2)+466969*(XE^-3)
2290 GOTO2310
2300 AY=42.338-2444*(XE^-1)+48658*(XE^-2)+881703*(XE^-3)
2310 AU=0.02232*AY
2320 AC=EXP(-AU*2.7*AT)
2330 PRINT
2340 PRINT"AC="AC
2350 PRINT
2360 GOTO1740
>
```

```
ST
    5 CLS
    7 MODE0
   10 REM PROGRAM TO CALCULATE SCATTERING CROSS SECTION
   15 PRINT""
   17 PRINT""
   20 PRINT "This program will calculate the Rutherford Scattering Cross Section
"
   25 PRINT""
   30 INPUT "ENTER ATOMIC NUMBER OF THE PROJECTILE ATOM (Z1)";Z1
   35 PRINT""
   40 INPUT "ENTER THE MASS (M1) OF THE PROJECTILE";M1
   45 PRINT""
   50 INPUT "ENTER ATOMIC NUMBER OF THE TARGET ATOM (Z2)";Z2
   55 PRINT""
   60 INPUT "ENTER THE MASS (M2) OF THE TARGET ";M2
   70 PRINT " e THE ELECTRONIC CHARGE IS EQUAL TO 4.80286E-10 statC "
   80 PRINT " THEREFORE, e^2 IS 1.4398E-13 MeV cm "
   90 LET e2 = 1.4398E-13
   95 PRINT""
  100 INPUT "ENTER THE ENERGY OF THE PROJECTILE IMMEDIATELY BEFORE SCATTERING, E
 IN MeV";E
  105 PRINT""
  110 INPUT "ENTER THE SCATTERING ANGLE , THETA ",Q
  115 PRINT""
  120 PRINT" CALCULATING THE SCATTERING CROSS SECTION"
  130 Q=RAD(Q)
  140 SSQ = SIN(Q)^2
  150 R= (((Z1*Z2*e2)/(4*E))^2)*(4/(SIN(Q)^4))
  160 CMT = (((1-((M1/M2)^2)*SSQ)^0.5) + COS(Q))^2
  170 CMB = (1-((M1/M2)^2)*SSQ)^0.5
  180 CM = CMT/CMB
  190 SCS = R*CM
  192 FOR I=1 TO 5
  194 PRINT" "
  196 NEXT I
  200 PRINT "SCATTERING CROSS SECTION IS  ",SCS
  210 PRINT"DO YOU WANT TO RUN THIS PART OF THE PROGRAM AGAIN "
  220 IF GET$="Y" THEN 5
  230 PRINT""
  240 PRINT "THIS PART OF THE PROGRAM CALCULATES THE AREA DENSITY "
  250 PRINT""
  260 INPUT "ENTER THE TARGET ATOMIC MASS",A2
  265 PRINT""
  275 PRINT""
  280 INPUT " ENTER EXPERIMENTALLY MEASURED BACK SCATTERED YIELD",YB
  285 PRINT""
  290 INPUT "ENTER SSB SOLID ANGLE ",SSB
  295 PRINT""
  300 PRINT" ENTER Np, the number of incident particle with energy E "
  305 PRINT""
  310 PRINT" THE CHARGE FOR A PROTON IS 1.60E-19 C ___( 0.IuC=6.25E11 PROTONS)"
  315 PRINT""
  320 INPUT NP
  330 PRINT"SCATTERING CROSS SECTION IS  ",SCS
  335 PRINT""
  337 E=E*1000
  340 ECM = (E*M2)/(M1+M2)
  341 Z2=Z2^(4/3)
  345 F= 1 - ((0.049*Z1*Z2)/ECM)
  350 NA= 6.02205E23
  355 PRINT"ADVOGADROS NUMBER IS  ",NA
  360 PRINT" CALCULATING AREAL DENSITY "
  370 FOR I=1 TO 5
  375 PRINT""
```

```
300 PRINT  ENTER Np, the number of incident particle with energy E
305 PRINT""
310 PRINT" THE CHARGE FOR A PROTON IS 1.60E-19 C ___( 0.IuC=6.25E11 PROTONS)"
315 PRINT""
320 INPUT NP
330 PRINT"SCATTERING CROSS SECTION IS  ",SCS
335 PRINT""
337 E=E*1000
340 ECM = (E*M2)/(M1+M2)
341 Z2=Z2^(4/3)
345 F= 1 - ((0.049*Z1*Z2)/ECM)
350 NA= 6.02205E23
355 PRINT"ADVOGADROS NUMBER IS  ",NA
360 PRINT" CALCULATING AREAL DENSITY "
370 FOR I=1 TO 5
375 PRINT""
380 NEXT I
390 A=A2*YB
400 B=NA*SQR(2)
410 C=(NP*SSB*SCS)
430 RT=A/(B*C)
440 PRINT""
450 PRINT" AREAL DENSITY IS  ",RT
455 PRINT" CORRECTION FACTOR F IS ",F
460 CRT=RT*F
465 PRINT"CORRECTED AREAL DENSITY IS  ", CRT
467 PRINT"DO YOU WANT TO RUN PROGRAM AGAIN"
470 IF GET$="Y" THEN 5
480 END
>
```

REFERENCES

Alhberg, M.
Nucl. Instr. Meth. 142 (1977) 61.

Akselsson, K.R.
Nucl. Instr. Meth in Phys. Res. B3 (1984) 425.

Akselsson, K.R. and Johansson, S.A.E.
IEEE Transactions on Nuclear Science, NS26 (1979) 1358.

Alpern, W.M.
Amniotic Fluid, Physiology, Biochemistry and Clinical Chemistry. Eds Natelson, S., Scommegna, A. and Epstein, M.B. Wiley Biomedical Publication, New York, 1974.

Andersen, H.H. and Ziegler, J.F.
The Stopping and Ranges of Ions in MAtter. Vol 3. Pergamon Press, New York (1977).

Badica, T., Ciortea, C., Cojocaru, V., Ivascu, M., Petrovici, A., Popa, A., Popescu, I., Salagean, M. and Spiridon, S.
Nucl. Instr. Meth. in Phys. Res. B3 (1984) 288.

Bambynek, W; Craseman, B., Fink, R.W., Freund, H.V., Mark, H., Swift, C.D., Price, R.E. and Rao, P.V.
Rev.Mod.Phys, 44 (1972) 716.

Bang, J. and Hansteen, J.M.
Mat. Fys. Medd. Dan. Selsk. 31 (1959) No13.

Barfoot, K.M., Mitchell, I.V. and Eschbach, H.L.
Nucl. Instr. Meth. in Phys. Res. B5 (1984) 534.

Barns, B.K., Beghian, L.E., Mathur, S.C., Mittler, A. and Quinn, P.W.
Proc 3rd Conf. on Applications of Small Accelerators, Denton, Texas, 1974.

Barrette, M., Lamoureux, G., Lebel, E., Lecomte, R., Paradis, P. and Monaro, S.
Nucl. Instr. Meth. 134 (1976) 189.

Basbas, G., Brandt, W. and Laubert, R.
Phys. Rev, A7 (1973) 983.

Basbas, G., Brandt, W. and Laubert, R.
Phys. Rev, A17 (1978) 1655.

Bearse R.C., Close, D.A., Malanify, J.J. and Umbarger, C.J.
Phys. Rev. A7 (1973) 1269.

Bernstein and Lewis, H.M.
Phys. Rev. 93 (1954) 83.

Birks, L.S. and Gilfrich, C.
Anal. Chem. 48 (1976) 273R.

Birks, L.S., Seebold, R.E., Batt, A.P. and Brosso, J.S.
J. Appl. Phys. 35 (1964) 2578.

Bohgard, M. and Johansson, E.
Nucl. Instr. Meth. in Phys.Res. B3 (1984) 268.

Bothe, W. and Franz, H.
Phys. Zeits. 49 (1928) 1-26.

Bowen, H.J.M.
Trace Elements Analytical Chemistry in Medicine, Ed Bratter, P. and Schramel, P, Walter de Gruyter, New York 1980.

Brandt, W. and Lapicki, G.
Phys. Rev. A20 (1979) 465.

Brandt, W. and Lapicki, G.
Phys. Rev. A23 (1981) 1717.

Burhop, E.H.S. and Asadd, W.N.
Adv. At. Mol. Physics. (1972) 163.

Buso, G.P., Colautti, P., Moschini, G., Xusheng, H. and Stievano, B.M.
Nucl. Instr. Meth. in Phys. Res. B3 (1984) 177.

Cahill, T.A.
New Uses of Ion Accelerators. Edited by Ziegler, J.F. Plenum Press, New York 1975.

Cahill, T.A.
Nucl. Instr. Meth. 181 (1981) 473.

Campbell, J.L.
Nucl. Instr. Meth. 142 (1977) 263.

Campbell, J.L.
IEEE Trans. on Nucl. Science, NS-26 No1 (1979) 1363.

Campbell, J.L., Orr, B.H., Herman, A.W., McNelles, L.A., Thompson, J.A. and Brain, W.C.
Anal. Chem. 47 (1975) 1542.

Campbell, J.L., Russel, S,B., Faign, S., Schulte, C.W., Ollerhead, R.W. and Gingerich, R.R.
Nucl. Instr. Meth. 181 (1981) 285.

Campbell, J.L., Teesdale, W.J. and Leigh, R.G.
Nucl. Instr. Meth. in Phys. Res. B6 (1985) 551.

Cesareo, R.
X-ray Fluorescence Analysis of Thin Biological Samples in X-ray Fluorescence (XRF and PIXE) in Medicine. Field Educational Italia, Italy 1982.

Chadwick, J.
Phil. Mag. 24 (1912) 594.

Chattarji, D.
The Theory of Auger Transitions. Academic Press, London, (1976).

Chez, R.A., Henkin, R.I. and Fox, R.
Obestetrics & Gyneacology, Vol 52, No 1, July 1978.

Choi, B.H., Merzbacher, E. and Khandelwal, G.S.
At. Data Nucl. Data Tables. 20 (1977) 503.

Christenson, L.J., Khan, M.J. and Brunner, W.F.
Rev. Sci. Inst. 38 (1967) 20.

Chu, T.C., Ishii, K., Yamadera, A., Sebata, M. and Morita, S.
Nucl. Instr. Meth. 190 (1981) 395.

Chu, W.K., Mayer, J.W. and Nicolet, M.A.
Backscattering Spectrometry, Academic Press, London (1978).

Cotzias, G.C. and Foradori, A.C.
Trace Metal Metabolism in the Biological Basis of Medicine, Eds Bittor, E.E. and Bitter, N. Academic Press, New York 1969.

Cork, J.M.
Phys. Rev. 59 (1941) 957.

Currie, L.A.
Anal. Chem. 40 (1968) 586.

Davies, I.J.L.
The Clinical Significance of the Essential Biological Metals. Heinmann Medical Books Ltd (London) 1972.

Dean, H.T.
Fluorine and Dental Health. Eds Moulton F.R., Am. Assoc. Adv. Sci., Washington D.C. 1942.

Deconnick, G., Demortier, G. and Bodart, F.
At. Energy. Rev. 13 (1975) 367.

Doesthale, Y.S. and Gopalan, C.
Br. J. Nutr. 31 (1974) 351.

Dyson, N.A.
X-ray in Atomic and Nuclear Physics, Longman Group Ltd, London (1973).

Dyson, N.A.
An Introduction to Nuclear Physics with Applications in Medicine and Biology, Ellis Horwood Ltd, England, (1981).

Dyson, N.A., Simpson, A.E and Dabek, J.T.
J. Radioanal. Chem. 46 (1978) 309.

Eldred, R.A., Cahill, T.A., Ashbaugh, L.L. and Nasstron, J.S.
Nucl. Instr. Meth in Phys.Res. B3 (1984) 479.

Elliot, P.M. and Inman, W.H.W.
Lancet ii. 1961 835.

Feld, E.J. and Umbarger, C.J.
Nucl. Instr. Meth. 114 (1974) 573.

Fink, R.W., Jopson, R.C., Mark, H. and Swift, C.D.
Rev. Mod. Phys. 38 (1966) 513.

La Fleur, P.D.
J. Radioanal. Chem. 19 (1974) 227.

Flocchini, R.G., Feeney, P.J., Sommerville, R.J. and Cahill, T.A.
Nucl. Instr. Meth. 100 (1972) 397.

Folkmann, F.
J. Phys. E. 8 (1975) 429.

Folkmann, F., Gaarde, C., Huus, T. and Kemp, K.
Nucl.Instr. Meth. 116 (1974a) 487.

Folkmann, F., Borggreen, J. and Kieldgraad, A.
Nucl. Instr. Meth. 119 (1974b) 117.

Friberg, L., Nordberg, G. and Kjellstrom, T.
Cadmium in the Environment. 2nd Edn, CRC Press,
Cleveland (1971).

Galuszka, J., Jarczyk, L., Rokita, E.,
Strzalkowski, A. and Sych, M.
Nucl. Instr. Meth. in Phys. Res. B3 (1984) 141.

Garcia, J.D.
Phys. Rev. 1A (1970a) 280.

Garcia, J.D.
Phys. Rev. 1A (1970b) 1402.

Garcia, J.D., Fortner, R.J. and Kavanagh, T.M.
Rev. Mod. Phys. 45 (1973) 111.

Gardner, R.K. and Gray, T.J.
At. Data and Nucl. Data Tables. 21 (1978) 515.

Gerthsen, C. and Reusse, W.
Phys. Zeits. 33 (1933) 478.

Goclowski, M., Jaskola, M. and Luziejewski, J.
Nucl. Instr. Meth. in Phys. Res. B3 (1984) 163.

Grant, J.T.
Applied Surface Science. 13 (1982) 35.

Van Grieken, R.E., Johansson, T.B., Akselsson,
K.R., Winchester, J.W. and Chapman, K.R.
Atmospheric Environment 10 (1976) 571.

Gryzinski, M.
Phys. Rev. 138 (1965) 336.

Guy, J. and Legge, G.J.F.
Proc. of the 2nd Australian Conf. on Nucl. Tech. of
Analysis. (1978) 50.

Hall, G.S., Roach, N., Naumann, M. and Simmons, U.
Nucl. Instr. Meth. in Phys. Res. B3 (1984) 332.

Hambridge, K.M.
Analytical Chemistry in Medicine and Biology. Vol2.
1983 Walter de Gruyter & Co, Berlin.

Hansen, J.S.
Phys. Rev. A8 (1973) 822.

Hansson, H.C., Johansson, E.M. and Ekholm, A.K.
Nucl. Instr. Meth in Phys.Res. B3 (1984) 158.

Hansteen, J.M.
Adv. At. Mod. Phys. Vol II (1975).

Hansteen, J.M. and Messelt, S.
Nucl. Phys. 5 (1956) 526.

Hansteen, J.M. and Mosebekk, O.P.
Nucl. Phys. A201 (1973) 541.

Hansteen, J.M., Johnsen, O.M. and Kochbach, L.
At. Data Nucl. Data Tables. 15 (1975) 305.

Hill, C.H.
Trace Elements and Human Disease. Ed Prasad, A.S.
Vol 2 Acadeic Press, New York 1975.

Hollow, P.H.
Advances in Electronics and Electron Physics 34
(1980) 241.

Holton, J.B.
Biochemistry in Clinical Practice. Eds William,
D.L. and Marks, V. Heinemann Medical Books Ltd,
London 1983.

Ishii, K., Kamiya, M., Sera, K., Morita, S. and
Tawara, H.
Phys. Rev. A: Vol 15, No 5 (1977) 2126.

Ishii, K., Morita, S., Tawara., Chu, T.C., Kayi, H.
and Shiokawa, T.
Nucl. Instr. Meth. 126 (1975) 75.

Iyenger, G.V.
Radiochem. Radioanal. Lett. 24 (1976) 35.

Iyenger, G.V. and Sansoni, B.
Tech. Report Series No 197 (1980).

Jaklevic, J.M. and Goulding, F.S.
Trans. Nucl. Sci. NS-18, 3 (1971) 187.

Jaklevic, J.M. and Goulding, F.S.
Trans. Nucl. Sci. NS-19, 3 (1972) 384.

Johansson, E.M. and Johansson, S.A.E.
Nucl. Instr. Meth. in Phys. Res. B3 (1984) 154.

Johansson, G.I., Pallon, J., Malmqvist, K.G. and
Akselsson, K.R.
Nucl. Instr. Meth. 181 (1981) 81.

Johansson, S.A.E.
Nucl. Instr. Meth. 181 (1981).

Johansson, S.A.E.
Nucl. Instr. Meth.in Phys.Res. B3 (1984) 1.

Johansson, S.A.E. and Johansson, T.B.
Nucl. Instr. Meth. 137 (1976) 473.

Johansson, S.H. and Johansson, T.B.
Nucl. Instr. Meth. 137 (1976) 473.

Johansson, T.B., Akselsson, R. and Johansson, S.A.E.
Nucl. Instr. Meth. 84 (1970) 141.

Johansson, T.B., Akselsson, R. and Johansson, S.A.E.
Adv. in X-ray Anal.15 (1972) 373.

Johansson, T.B., Grieken, R.E., Nelson, J.W. and Winchester, J.W.
Anal. Chem. 47 (1975) 855.

Johnson, R.
Analyst 1 (Feb 1982) Kevex Corporation.

Jolly, R.K., Knae, J.R., Buckle, D.C., Randers-Pherson, G., Teoh, W. and Ceto, H.A.
Nucl. Instr. Meth. 142 (1977) 231.

Kajfosz, J.
Nucl. Instr. Meth. B3 (1984) 147.

Kaji, M., Shiokawa, T., Ishii, K., Kamiyo, M., Sera, K. and Tawara.
Nucl. Instr. Meth. 142 (1977) 21.

Katsanos, A.A.
Technical Reports Series No 197, International Atomic Energy Agency, Vienna 1980.

Katsanos, A.A., Kakanis, P.K. and Kallithrakas-Kontos, N.
Nucl. Instr. Meth. in Phys. Res. B3 (1984) 52.

Kaufmann, H.C. and Steenblik, J.
Nucl. Instr. Meth. B3 (1984) 198.

Khan, J.M., Potter, D.L. and Worley, R.D.
J. Appl. Phys. 37 (1966) 564.

Khan, M.R.
Ph.D Thesis, Aston University in Birmingham (1975).

Khan, M.R. and Crumpton, D.
CRC Critical Reviews in Analytical Chem. (1981) 103.

Khan, M.R., Hopkins, A.G. and Crumpton, D.
VIII Inter. Conf. X-ray Optics and Microanalysis. Boston, USA. (1977).

Khan, M.R., Hopkins, A.G., Crumpton, D. and Francois, P.E.
X-Ray Spectrom. 6 (1977) 140.

Khan, M.R. and Karimi, M.
X-ray Spectrometry. Vol 9 (1980) 32.

Knoll, G.F.
Radiation Detection and Measurement. John Wiley and Sons Inc. (1979).

Koening, W., Richter, F.W., Steiner, U., Stock, R., Thielmann, R. and Watjen, V.
Nucl. Instr. Meth. 142 (1977) 225.

Kossel, C.
Phys. Zeits. 18 (1917) 240

Kowasrski, S., Blair-Stanek, C.S. and Schachter, D.
Am. J. of Physiology. 226 (1974) 401.

Krause, M.O.
J. Phys. Chem. Ref. Data. 8 (1979) 307.
Kynast, G.
Analytical Chemistry in Medicine and Biology, Vol 2, Walter de Gruyter & Co. New York 1983.

Laegsgaard, E., Andersen, J.U. and Hogedal, F.
Nucl. Instr. and Meth. 169 (1980) 293.

Laegsgaard, E., Andersen, J.U. and Lund, M.
10th Inter.Conf. on the Phys.of.Elect.& At.Collison. (1978) 353.

Lecomte, R., Paradis, P., Monaro, S., Barrette, M., Lamoureuxm, G. and Menard, H.A.
Nucl. Instr. and Meth. 150 (1978) 289.

Lewis, H.M., Simmons, B.E. and Merzbacher, E.
Phys. Rev. 91 (1953) 943.

Livingstone, M.S.
Phys. Rev. 51 (1939) 839.

Madison, D.H. and Merzbacher, E.
Atomic Inner-Shell Processes , Vol.1, Ed. by
Crasemann, B., Academic Press, London (1975) 1.

Maenhaut, W., de Reu, L. Van Rinsvelt, H.A.,
Cafmayer, J. and Van Espin, P.
Nucl. Instr. Meth. 168 (1980) 557.

Maenhaut, W. and Raemdonck.
Nucl. Instr. Meth. in Phys. Res. B3 (1984) 125.

Maenhaut, W., Selen, A., Von Esplen, P., Van
Grieken, R. and Winchester, J.W.
Nucl. Instr. Meth. 181 (1981) 399.

Malmqvist, K.G., Karlsson, E. Akselsson, K.R.
Nucl. Instr. and Meth. 192 (1982) 523.

Maturu, N.R.
Tecnical Reports Series No 197, IAEA, Vienna 1980.

Merzbacher, E. and Lewis, H.M.
Hanbuck Der Physik 34 Springer-Verlag, Berlin.

Messelt, S.
Nucl. Phys. 5 (1958) 435.

Mingay, D.W., Jonker, W.D. and Smith, B.J.
At. Energy Board. Pel-259, Pretoria, South Africa
(1978).

Mitchell, I.V. and Zeigler, J.F.
Analysis 17 No 213 (1975) 311.

Mitchell, I.V. and Barfoot, K.M.
Nucl. Science Appl. B1 (1981) 99.

Mitchell, I.V., Barfoot, K.M. and Eschback, H.L.
Nucl. Instr. and Meth. 168 (1980) 233.

Mommsen, H., Sarkar, M., Starter, W. and
Schmittinger, T.
Nucl. Instr. and Meth. 166 (1979) 361.

Moseley, H.G.J.
Phil. Mag. 26 (1913) 1024.

Mousaui-Yeganeh, S., Ebrahimy-Fakhar, F. and
Enayati, F.
Nucl. Instr. Meth. in Phys. Res. B3 (1984) 364.

Mukoyoma, T. and Sarkadi, L.
Nucl. Instr. Meth. 205 (1983) 341.

Nielsen, F.H. and Ollerich, D.A.
Fed. Proc. Fed. Am. Soc. Exp. Biol. 32 (1973) 329.

Ogier, W.T., Carlson, R.D. and Knoche, J.
Phys. Rev. 142 (1966) 50.

Pakarinen, P., Pallon, J. and Akselsson, R.
Nucl. Instr. Meth. in Phys. Res. B3 (1984) 166.

Pallon, J. and Mamqvist, K.G.
Nucl. Instr. Meth. 181 (1981) 71.

Paschoa, A.S., Baptista, G.B., Mauricio, G.M.,
Barros, L., Lerner, Y.B. and Issler, P.F.
Nucl. Instr. Meth. in Phys. Res. B3 (1984) 352.

Prasad, A.S.
Trace Elements in Human Health and Disease,
Academic Press, New York.

Prasad, A.S. and Oberleas, D.
Trace Elements in Human Health and Disease,
Academic Press, New York.

Proc.of the Int.Conf. on Particle Induced X-ray
Emission and its Analytical Applications,
Nucl.Instr.and Meth. 142 (1977) 1.

Proc.of the 2nd Int.Conf. on Particle Induced X-ray
Emission and its Analytical Applications,
Nucl.Instr.and Meth. 181 (1981) 1.

Proc.of the 3rd Int.Conf. on Particle Induced X-ray
Emission, Nucl.Instr.and Meth in Phys.Res. B3
(1984) 1.

Rice, R., Basbas, G. and McDaniel, F.D.
Atomic Data and Nuclear Data Tables. 20 (1977) 503.

Richter, F.W. and Watjen, U.
Nucl. Instr. Meth. in Phys. Res. B3 (1984) 125.

Rontgen, W.C.
Ann. Physik u Chem. 64 (1898) 1.

Rosick, E., Rosick, U., Bratter, P. and Kynast, G.
Trace Elment Analytical Chemistry in Medicine and
Biology, Vol 2, 1983. Walter de Gruyter & Co,
Berlin.

Russel, S.B., Schulte, C.W. and Campbell, J.L.
Anal. Chem. 53 (1981b) 571.

Saied, S.O.
Ph.D. Thesis, University of Aston in Birmingham (1981).

Saied, S.O., Crumpton, D. and Francois, P.E.
Nucl. Instr. and Meth. 181 (1981) 53.

Sarx, B. and Bachmann, K.
Analytical Chemistry in Medicine and Biology. Vol 2, Eds Bratter, P. and Schramel, P. Publ: Walter de Gruyter, Berlin, 1983.

Schwarz, K. and Milne, D.B.
Nature (London) 239 (1972) 333.

Shakir, N.
Private Communication (1984).

Simane, C.
Letter in Czech J. Phys. 3 (1953) 175.

Smith, J., Nelissen, J. and Van Grieken, R.
Analytica Chimica Acta 111 (1979) 215.

Sokhi, R.S.
Ph.D. Thesis, University of Aston in Birmingham (1984).

Storm, E. and Israel, H.I.
Nucl. Data Tables. A7 (1970) 563.

Sundermann, J. and Williams, F.
Trace Elements in Chemical Diagnosis of Disease, Eds Brown, S.S., Mitchell, L.F. and Young, D.S. Biomedical Press, Holland 1980.

Tawara, H., Ishii, K. and Marita, S.
Nucl. Instr. and Meth. 132 (1976) 503.

Tauljberg, K. Proc.2nd.Int.Conf.on Inner Shell Ionization, Eds, Mehlhorn, W. and Brenn, R., Fieldburg, West Germany. (1976).

Tauljberg, K.
J. Phys B: At. Mol. Phys. Vol 10 No 9 (1977) L341.

Tipton, I.H. and Cook, M.J.
Health Physics 9 (1963) 103.

Torrisi, L. and Foti, G.
X-ray Fluorescence (XRF and PIXE) in Medicine. Field Educational Italia, Italy, 1982.

Trace Element Analytical Chemistry in Medicine and Biology, eds Bratter, P. and Schramel, P., Berlin, New York, Walter de Gruyter 1980.

Underwood, E.J.
Trace Elements in Human and Animal Nutrition, 4th Edn. New York, Academic Press 1977.

Valkovic, V.
Contemp. Phys. 14 (1973) 415.

Valkovic, V., Liebert, R.B., Zabel, T., Larson, H.T., Miljanic, D., Wheeler, R.M. and Phillips, G.C.
Nucl. Instr. Meth. 114 (1974) 573.

Valkovic, V.
Trace Analysis . Taylor and Francis Ltd, London (1975).

Valkovic, V.
Nucl. Instr. Meth. 142 (1977) 151.

Valkovic, V.
Analysis of Biological Material for Trace Elements Using X-ray Spectroscopy. CRC Press, Boca Raton, Florida, USA (1980).

Ward, N., Bryce-Smith, D., Minski, M., Zaaijman, J. and Pim, B.
Trace Element Analytical Chemistry in Medicine and Biology, Vol 2, 1983, Walter du Gruyter & Co, Berlin.

Walter, R.L., Willis, R.D., Gutknecht, W.F. and Joyce, J.M.
Anal. Chem. 46 No 7 (1974) 843.

Watson, R.L., Sjurseth, J.R. and Howard, R.W.
Nucl. Instr. Meth. 93 (1971) 69.

Willis, R.D. and Walter, R.L.
Nucl. Instr. Meth. 142 (1977) 231.

Woldseth, R.
X-ray Energy Spectrometry, Kevex Corporation, U.S.A (1973).

X-ray Fluorescence (XRF and PIXE) in Medicine. Ed. Cesareo, R., Field Educational Italia, Italy (1982).

Ziegler, J.F.
New Use of Ion Accelerators, Plenum Press, London (1975).

TOO LARGE TO SCAN

PLEASE REQUEST IF REQUIRED

FIGURE 3.2 Plan of Vacuum Chamber
(Drawing No.JSP/1/81)

FIGURE 3.3 Plan of Vacuum Chamber:
Re-entrant Tubes and
Special Flanges
(Drawing No. JSP/2/81)